

# Advanced Nickel Barrier Coatings: Manufacturing Process and Properties

By

MICHAEL RUMBLES



A thesis submitted in partial fulfilment of the requirements  
of Edinburgh Napier University, for the award of  
*Master by Research*

School of Engineering and the Built Environment

Edinburgh Napier University

March 2022

## **Declaration**

I hereby declare that the work presented in this thesis was solely carried out by myself at Edinburgh Napier University, Edinburgh, except where acknowledgements are made, and that it has not been submitted for any other degree.



---

Michael Rumbles (candidate)

30<sup>th</sup> June 2021 (Revised 6<sup>th</sup> December 2021)

---

(Date)

## Abstract

New-generation protective coatings should respond to mechanical or chemical damage with active corrosion inhibition, preserving coating integrity and adhesion to the substrate. Due to the implementation of legislation imposed by REACH (Restriction, Evaluation, Authorisation & restriction of Chemicals), restrictions have been placed on the use of chromium (VI) compounds, which were the main components of self-healing anti-corrosion coatings. Having similar properties, e.g. wear and corrosion resistance, nickel-phosphorous coatings might be one possible replacement for coatings containing Cr<sup>6+</sup>.

The novel work carried out during this research programme has focused on developing a process to include corrosion inhibitors within nickel-phosphorus coatings using the electroless co-deposition technique. Gelatine and sodium alginate microgels were investigated for their feasibility at this task. It was found that gelatine microgels of average diameter 2–6 µm, heat-treated at 150 °C for 15 hours exhibited the desired properties to survive the co-deposition process at 89 °C in acidic electroless nickel solutions operating at 4.9 pH.

Depositions on ISO 3574 Type CR1 steel were performed to determine the impact on the coating properties due to the inclusion of gelatine microgels. The microgels were produced without the inclusion of active corrosion inhibitors at this time. Various deposition parameters were investigated, and it was determined that the addition of small quantities, below 0.05 g/L, provided the best depositions. Above 0.1 g/L, the microgels would block the reaction sites required for the electroless deposition process which led to poor quality coatings and a reduction in deposition rate from 20 µm to 1.5 µm/hr.

The resulting novel coatings were investigated using a series of empirical and quantitative tests. The results of this study show that the coatings with gelatine microgels show increased phosphorus content, and a reduction in the surface hardness and abrasion resistance of the coatings. The corrosion studies show that the inclusion of gelatine microgels impacts the corrosion resistance of the coatings even when no additional corrosion inhibitors are included.

## **Acknowledgements**

The author wishes to express his gratitude to his Director of Studies, Dr Neil Shearer, who has provided his knowledge and time generously during this project. His support has been pivotal in the completion of the project, and I am extremely grateful of this. Special thanks also to Dr Mark Dorris, who after joining the supervision team late into the project, provided great assistance and academic support.

My thanks also to Dr Callum Wilson who provided great assistance in the laboratory and ensured that I always had access to equipment when required. Sharing his knowledge on the nuances of operating complicated laboratory equipment proved invaluable and allowed for the completion of much of the testing.

I would like to make special recognition of Dr Alicja Stankiewicz. During her time as my Director of Studies, she proved a wealth of knowledge and aided greatly in my understanding of the processes involved. She acted as the go between with Wrocław University and sourced the microgels required to make the project a reality. The academic and personal support she provided made her an extremely valued member of the team.

Finally, a special thank you to my family, whose unwavering support and encouragement through difficult times spurred me on to complete this thesis.

## List of Abbreviations and Symbols

Z	Magnitude of modulus
Ag <sup>+</sup>	Silver ion
AgCl	Silver chloride
ASTM	American Society for Testing and Materials
BS	British Standards
C	Carbon
CPE	Constant Phase Element
Cr <sup>6+</sup>	Hexavalent chromium
e <sup>-</sup>	Electron
EDXA	Energy Dispersive X-ray Analysis
EIS	Electrochemical Impedance Spectroscopy
ENP	Electroless Nickel-Phosphorus
GDOES	Glow-Discharge Optical Emission Spectroscopy
H	Hydrogen
H <sub>2</sub> PO <sub>2</sub> <sup>-</sup>	Hypophosphite anion
H <sub>5</sub> NO	Ammonium Hydroxide
HCl	Hydrochloric acid
HV	Vickers Hardness
HV <sub>0.1</sub>	Vickers microhardness scale
ISO	International Organisation for Standardization
mmol/L	Millimoles per litre
Mn	Manganese
mol/L	Moles per litre
NaCl	Sodium Chloride
Ni	Nickel
Ni <sup>0</sup>	Nickel atoms
NiP	Nickel-Phosphorus alloy
NSS	Neutral Salt Spray
P	Phosphorus
Pb <sup>2+</sup>	Lead ion
PTFE	Polytetrafluoroethylene
PVD	Physical Vapour Deposition
Ra	Arithmetical average roughness

$R_{\text{coat}}$	Resistance of coating
$R_{\text{ct}}$	Charge transfer resistance
REACH	Registration, Evaluation, Authorisation and Restriction of Chemicals
RGB	Red, Green, Blue colour additive model
$R_s$	Resistance of Solution
$R_T$	Total Resistance
SEM	Scanning Electron Microscope
SiC	Silicon Carbide
$\text{SO}_4^{2-}$	Sulfate ion
SVET	Scanning Vibrating Electrode Technique
TiN	Titanium Nitride
$\text{TiO}_2^-$	Titanium Dioxide ion
US	Ultrasound
Wt%	Weight Percent
$Z'$	Modulus real part
$Z''$	Modulus imaginary part
$\Theta$	Phase angle

# Contents

Declaration .....	i
Abstract .....	ii
Acknowledgements.....	iii
List of Abbreviations and Symbols .....	iv
1 Introduction .....	1
1.1 Background .....	1
1.2 Key Objectives.....	4
2 Literature Review .....	5
2.1 Electrochemical Deposition.....	5
2.1.1 Electrolytic Deposition .....	5
2.1.2 Electroless Deposition.....	6
2.2 Electroless Deposition of Nickel.....	9
2.2.1 History.....	9
2.2.2 Basic Composition.....	9
2.2.3 Solution Temperature.....	20
2.2.4 Solution pH.....	22
2.3 Ultrasonic Agitation.....	24
2.4 Self-Healing Coatings .....	27
2.5 Zeta Potential .....	30
2.6 Gelatine .....	31
3 Experimental Work.....	32
3.1 Introduction.....	32
3.2 Low Temperature Deposition .....	34
3.2.1 Microgels.....	34
3.2.2 Commercial 1850 Solution Variable Testing.....	39
3.2.3 Bespoke Low Temperature Solutions .....	44
3.3 High Temperature Deposition .....	49
3.3.1 Microgels.....	49
3.3.2 Gelatine Co-deposition Development .....	51
3.4 Analysis of NiP/Gelatine Composite Coatings.....	56
3.4.1 Standardised Co-deposition Procedure.....	56
3.4.2 Experimental Procedures .....	58
4 Results and Discussion – Sodium Alginate Microgel Analysis.....	68
4.1 Microgel Analysis.....	68
4.2 1850 Solution Variable Testing .....	70

4.2.1	Solution Temperature.....	70
4.2.2	Solution pH.....	71
4.2.3	Ultrasonic Agitation .....	72
4.3	Bespoke Low Temperature Depositions .....	73
5	Results and Discussion – Gelatine Co-deposition .....	78
5.1	Microgel Analysis.....	78
5.1.1	Microgel Size.....	78
5.1.2	Heat treatment .....	80
5.1.3	Zeta Potential .....	81
5.2	Deposition Results.....	83
5.2.1	Coating thickness.....	84
5.2.2	EDXA Results .....	85
5.2.3	Glow Discharge Optical Emission Spectroscopy – GDOES.....	86
5.2.4	Microscopy Analysis.....	87
5.3	Corrosion Results .....	89
5.3.1	Neutral Salt Spray – NSS.....	89
5.3.2	Scanning Vibrating Electrode Technique – SVET.....	91
5.3.3	Electrochemical Impedance Spectroscopy - EIS .....	93
5.4	Tribology Results.....	98
5.4.1	Surface Roughness.....	98
5.4.2	Coating Hardness.....	100
5.4.3	Abrasion Resistance .....	101
6	Conclusions .....	103
7	Future Work .....	105
8	References.....	106
9	Appendices .....	112
9.1	Appendix A – EDXA report of sodium alginate microgels.....	112
9.2	Appendix B – Zeta Potential Measurements .....	114
9.3	Appendix C – 1850 Variables.....	116
9.4	Appendix D – Pyrophosphate Low Temperature Solution.....	117
9.5	Appendix E – Gelatine Microgel Analysis.....	118
9.6	Appendix F – Phosphorus content in NiP/gelatine composite coatings. 119	
9.7	Appendix G – Fluorescence Microscopy Images .....	120
9.8	Appendix H – NSS Samples .....	122
9.9	Appendix I – EIS Fitting .....	123

9.10	Appendix J – Surface Roughness Data .....	124
9.11	Appendix K – Coating Hardness results .....	126
9.12	Appendix L – Abrasion Resistance Results .....	127

## Figures

Figure 1: Electroplating nickel process diagram [15].	6
Figure 2: Comparison of a) Electrolytic and b) Electroless nickel deposits [21].	7
Figure 3: Effect of nickel concentration on NiP alloy composition [29].	11
Figure 4: Effect of concentration of organic acid complexing agents on rate of deposition [29], [39].	16
Figure 5: Effect of thiourea and maleic acid concentrations on the deposition rate of the electroless nickel system [41].	17
Figure 6: Model of co-deposition process for NiP/PTFE coating [43].	18
Figure 7: The weight percentage of co-deposited dispersed PTFE particles in various concentrations of surfactant (FC) in the plating bath [43].	19
Figure 8: Effect of temperature on plating rate [29].	20
Figure 9: Effect of temperature on plating rate of pyrophosphate and citrate baths [29].	21
Figure 10: Dependence of pH value on the deposition rate of an EN bath [48].	22
Figure 11: Effect of pH on phosphorus content [29].	23
Figure 12: Effect of composition on internal stress [16].	23
Figure 13: Bubble growth and implosion in a liquid irradiated with ultrasound [51].	24
Figure 14: Schematic representation of the main effects of cavitation induced by ultrasound irradiation [51].	24
Figure 15: Effect of ultrasound on the plating rate at 50, 70 and 90 °C solution temperatures [54].	25
Figure 16: Phosphorous content of electroless nickel as a function of solution temperature, with and without the presence of ultrasound [52].	26
Figure 17: Well-dispersed TiO <sub>2</sub> particles under ultrasound conditions (lower part from substrate up to the markers > <) and nano-particle agglomeration under silent conditions (upper part) in a Ni coating [51].	26
Figure 18: (a) Recent refereed publications related to the field of self-healing materials, together with (b) their corresponding distribution of the employed key words vocabulary. All published languages were included. Statistics are available from 2000 to August 2010 inclusively [8].	27
Figure 19: Schematic representation of gelatine microcapsules and microgels [55].	28
Figure 20: Schematic display of pH-triggered opening of PSMAA nanocapsules. Change of pH to higher values increases the permeability of the capsule shell and the release of the capsule content [56].	28
Figure 21: Schematic of capsules triggered by chloride ions [57].	29
Figure 22: a) Ag-alg capsules, b) Optical image of Ag-alg capsules, c) The Ag-alginate capsule that disintegrated when exposed to chloride ions [57].	29
Figure 23: Schematic representation of the electrical double layer (EDL) and position of the slipping plane. The zeta potential is the electrical potential at the slipping plane [60].	30
Figure 24: DSC scans of calfskin gelatine heated in four different types of DSC sample pans. Y-1 DSC heat flow normalised to unit mass sample [63].	31
Figure 25: Gelatine microgel production using water-in-oil emulsion technique [55].	34

Figure 26: Sodium Alginate microgels in as received state. ....	35
Figure 27: SEM image (Cambridge Instruments Stereoscan 90) of sodium Alginate microgels used to perform EDXA. ....	37
Figure 28: Dried sodium alginate microgels in large aggregations post immersion test. Image captured at x100 magnification. ....	38
Figure 29: Example of experimental set up for producing electroless deposition using IKA hot plate with mechanical agitation. ....	40
Figure 30: Experimental set up of electroless nickel deposition using ultrasonic agitation. ....	42
Figure 31: Cross-sections prepared in epoxy resin. ....	43
Figure 32: Deposition of solution 3 using ultrasonic sonotrode. ....	46
Figure 33: Gelatine microgels a) as received, b) post heat treatment. ....	49
Figure 34: NiP/gelatine composite coating with reduced deposit thickness at edges. Coupon dimensions = 25 mm x 30 mm. ....	52
Figure 35: NiP/gelatine composite coating with large gelatine aggregations on surface post deposition. Coupon dimension = 25 mm x 30 mm. ....	53
Figure 36: High quality NiP/gelatine composite coating produced with ultrasonically processed microgels. Coupon dimension = 25 mm x 30 mm. ....	54
Figure 37: Plain mild steel S-35 Q-Panel used to confirm corrosion rate of cabinet. Area of corrosion = 60 mm x 100 mm. ....	59
Figure 38: NSS test sample with Gamry PortHole electroplating tape applied prior to test. Area of circle = 1 cm <sup>2</sup> . ....	59
Figure 39: EIS experimental set-up using Gamry Paracell and Solartron Analytical Modulab. ....	61
Figure 40: Equivalent circuit used for fitting the EIS data of NiP and NiP/gelatine composite coatings exposed to 3.5 wt% NaCl solution. ....	62
Figure 41: Surfcom Touch 50 performing coating roughness measurements on uncoated reference sample for comparison with NiP/gelatine composite coatings. ....	63
Figure 42: Example of rejected measurement due to D1 & D2 differing by greater than 5 %. ....	64
Figure 43: Example of a perforated coating due to excess abrasion test conditions. ....	66
Figure 44: EDXA results of different sodium alginate based microgels before and after 24-hour hydration in deionised water. ....	68
Figure 45: Change in Oxygen, Chlorine and Nickel constituents due to leaching. ....	69
Figure 46: Coating thickness at varying temperatures of 1850 after 30-minute deposition. ....	70
Figure 47: Coating thickness at varying solution pH of 1850 after 30-minute deposition at 89 °C. ....	71
Figure 48: Coating thickness resulting from 30-minute deposition of 1850 using mechanical and ultrasonic agitation methods at 80 °C. ....	72
Figure 49: Result of solution plating out and depositing nickel on every surface. ....	73
Figure 50: Coating thickness of glycine-based solutions using varying Metallic salt, reducer and complexor quantities. Coatings produced using 30-minute deposition. ....	74

Figure 51: Deposition rates with and without use of catalyst using varying solutions. ....	74
Figure 52: Severe delamination of nickel coating from substrate. ....	75
Figure 53: Result of solution decomposition. Solution turned turbid and produced black foam. ....	75
Figure 54: SEM image of deposition produced from pyrophosphate bath. Black spots present across surface are pores. ....	76
Figure 55: Particle size analysis of gelatine microgels as received, prior to heat treatment. ....	78
Figure 56: Particle size analysis of gelatine microgels post heat treatment. ....	79
Figure 57: Gelatine microgels imaged using optical microscope. Images a) and b) show untreated and heat-treated microgels respectively before solution temperature test. Images c) and d) show heat-treated microgels post solution temperature test with mechanical and ultrasonic agitation respectively. Each small graticule = 5 $\mu\text{m}$ . ....	80
Figure 58: Gelatine microgels adhered to the surface of NiP/gelatine microgel composite coating after 1 hour deposition at 89 $^{\circ}\text{C}$ . ....	81
Figure 59: Zeta potential of gelatine microgels in the as received state. ....	82
Figure 60: Zeta potential of gelatine microgels after heat treatment, in the ready to be co-deposited state. ....	82
Figure 61: Example of coatings analysed by visual inspection deemed to have a) Passed quality inspection, b) Failed due to surface imperfections and edge peel back, c) Failed due to coating blistering. Coupon dimensions = 25 mm x 30 mm. ....	83
Figure 62: Deposit thickness of coatings produced with varying quantities of gelatine microgel co-deposits. Microgels were mechanically agitated and added in the dry state apart from 0.025 g/L UP in which the microgels were ultrasonically processed before addition to the deposition bath. ....	84
Figure 63: Cross section of NiP+0.025 g/L Gelatine microgels. Each small graticule = 5 $\mu\text{m}$ . ....	85
Figure 64: Phosphorus content of NiP coatings with varying quantities of gelatine microgel co-deposits. ....	85
Figure 65: GDOES results for plain NiP only coating. ....	86
Figure 66: GDOES results for NiP+0.025 g/L gelatine composite coating. ....	86
Figure 67: Gelatine microgels imaged using a) RGB colour spectrum using white light, b) fluorescence using ultraviolet light. Images captured at x20 magnification with 100 $\mu\text{m}$ scale bar. ....	87
Figure 68: Fluorescent images of a) NiP+0.0125 g/L, b) NiP+0.025 g/L and c) NiP+0.05 g/L gelatine composite coatings. ....	87
Figure 69: Gelatine microgels observed a) on Surface and b) in coating defect of NiP+0.025 g/L gelatine coating. Each small graticule = 5 $\mu\text{m}$ . ....	88
Figure 70: Cross section of NiP+0.025 g/L gelatine coating with a) no acid etch and b) with acid etch. Each small graticule = 5 $\mu\text{m}$ . ....	88
Figure 71: Coating which was deemed to have failed, a) on removal from the NSS chamber, b) after light cleaning. Area of circles = 1 $\text{cm}^2$ . ....	89
Figure 72: NiP only coating Bode plot demonstrating coating failure as described by the double hump which occurs at 24 hours. ....	93
Figure 73: NiP+0.025 g/L gelatine microgel composite coating Bode plot. ....	94

Figure 74: NiP only coating Nyquist plot showing significant drop in resistance at 24-hour plot. ....	94
Figure 75: NiP+0.025 g/L gelatine microgel composite coating Nyquist plot. ...	95
Figure 76: Example of fitting accuracy achieved on NiP+0.025 g/L gelatine microgels composite coating at 12 hours. ....	95
Figure 77: Total resistance calculated from EIS fittings in relation to exposure time for plain NiP and NiP/gelatine composite coatings. ....	97
Figure 78: Surface roughness of coatings resulting from NiP/Gelatine co-deposition. ....	98
Figure 79: SEM images of a) Plain NiP, b) NiP+0.0125 g/L gelatine microgels, c) NiP+0.025 g/L gelatine microgels, d) NiP+0.05 g/L gelatine microgels. Samples show similar coating morphology with amorphous grain structure. ....	99
Figure 80: Vickers hardness results for the NiP/gelatine composite coatings in comparison with plain NiP and uncoated steel substrate. ....	100
Figure 81: Coatings abrasive wear rate for the NiP/gelatine composite coatings in comparison with plain NiP and uncoated steel substrate. ....	101
Figure 82: Plain NiP coating wear mark measured using varying imaging techniques: a) SEM imaging using scanning electrode technique, b) SEM imaging using back scatter electrode technique, c) optical microscope with integrated white light illumination, d) optical microscope with integrated white light not present. ....	102
Figure 83: EDXA report for sodium alginate microgels as received prior to immersion in deionised water. ....	112
Figure 84: Pyrophosphate solution coating showing pores. ....	117
Figure 85: Spectrum of coating showing low phosphorus content. ....	117
Figure 86: Microgel size analysis using SEM imaging. Image a) and b) are as received gelatine microgels, image c),d) & e) are post heat treatment. ....	118
Figure 87: NiP+0.0125 g/L gelatine microgels deposit surface imaged using a) RGB colour spectrum using white light, b) fluorescence using ultraviolet light, c) composite image of combined RGB and fluorescence imaging. Images captured at x20 magnification with 100 $\mu$ m scale bar. ....	120
Figure 88: NiP+0.025 g/L gelatine microgels deposit surface imaged using a) RGB colour spectrum using white light, b) fluorescence using ultraviolet light, c) composite image of combined RGB and fluorescence imaging. Images captured at x20 magnification with 100 $\mu$ m scale bar. ....	120
Figure 89: NiP+0.0125 g/L gelatine microgels deposit surface imaged using a) RGB colour spectrum using white light, b) fluorescence using ultraviolet light, c) composite image of combined RGB and fluorescence imaging. Images captured at x20 magnification with 100 $\mu$ m scale bar. ....	121

## Tables

Table 1: Components of electroless nickel baths and their functions [13].	10
Table 2: Reducing agent for EN plating [32]	12
Table 3: Stability of particles in relation to their zeta potential [61].	30
Table 4: Gelatine microgel diameters before and after heat treatment.	79
Table 5: Results of visual inspections performed at 24-hour intervals on NSS samples. Samples deemed to have failed if products of corrosion were visible.	90
Table 6: SVET scan site results from 5 to 20 hours for plain NiP deposit and for NiP+0.025 g/L gelatine composite coating.	91
Table 7: NiP only coating fitting results determined from the EIS data and equivalent circuits.	96
Table 8: NiP+0.025 g/L gelatine composite coating fitting results determined from the EIS data and equivalent circuits.	96
Table 9: Results of EDXA performed on sodium alginate microgels 1 before and after immersion in deionised water.	113
Table 10: Results from Zeta potential for sodium alginate, as received gelatine and heat-treated gelatine with outliers removed.	114
Table 11: Zeta potential results continued.	115
Table 12: Coating thickness of varying temperatures of 1850.	116
Table 13: Coating thickness of varying solution pH of 1850.	116
Table 14: Coating thickness of 1850 produced with ultrasonic agitation.	116
Table 15: Ni:P ratio as wt% for pyrophosphate deposit.	117
Table 16: EDXA results for NiP/gelatine composite coatings relating to the phosphorus content by wt%.	119
Table 17: NSS samples after test and lightly cleaned under running water using brush with no abrasive. Area of circle = 1cm <sup>2</sup> .	122
Table 18: EIS equivalent circuit at 12 hours and 24 hours exposure for Plain NiP coating and NiP/gelatine composite coating.	123
Table 19: Surface roughness measurements in x and y-axis orientations.	124
Table 20: Average surface roughness per sample.	125
Table 21: Detailed coating hardness results for NiP/Gelatine composite coatings.	126
Table 22: Abrasion resistance detailed results. This shows the difference in the wear rate for each inspection lighting environment.	127

# 1 Introduction

## 1.1 Background

Coatings are used extensively in industry to give desired properties to materials used in many applications. This is done as it is often far less expensive to produce items from steel and then tailor surface properties in a separate manufacturing process. Coatings can be used for the mechanical aspects they offer, aesthetics and for corrosion prevention.

Corrosion is a huge problem in engineering and civil projects. The global cost attributed to corrosion is valued in the trillions up to 3.4 % of global GDP in 2013 [1]. For corrosion prevention, the coatings can be barrier or sacrificial. Sacrificial protection such as zinc offers itself up instead of the steel substrate so that the act of corrosion does not damage the structure that needs protected. Some examples of this are on ships where zinc blocks are used to save the hull produced from steel. This can also be used as a barrier coating in the form of galvanising which provides both the sacrificial protection to any exposed steel, but also barrier protection by preventing any corrosive media from contacting the structure to be saved [2]. These techniques result in a high level of protection from corrosion for the structure but have some drawbacks. The resulting protection for plain zinc blocks only provides corrosion protection and is best suited to large structures, as if it were in a complex machine, each component would need its own sacrificial block. This is rectified by galvanising where each component is dipped into molten zinc to receive a barrier coating. the resulting galvanised product now exhibits a very distinctive aesthetic which may not be desired for the end use of the product. Additionally, the components mechanical properties, such as its hardness and wear resistance may be dictated by the properties of zinc which are not applicable for every use case.

Another form of coating commonly used in engineering is painting. This is a barrier coating which has many benefits. It can be used on extremely large structures, for example the Forth Bridge [3], but can also be used on smaller components in many day-to-day items, such as cars, lawnmowers and bicycles to name a few. Paints also have the benefit of aesthetics, with the ability to be tailored for its desired use. Paints also have the ability to include corrosion inhibitors which reduce corrosion in areas where the barrier coating has failed

[4]. This can happen easily due to the mechanical properties of the paint. The adhesion to the substrate is purely mechanical in most cases as the steel substrate does not bond with the paint. Some drawbacks to this technique are that the paint can be scratched easily, wear down and does not provide many mechanical properties to the steel.

Another form of coating is metallic barrier coatings. These can provide corrosion prevention using the aforementioned sacrificial method, however, are more commonly physical barriers to the corrosive media. Metallic coatings are often used for their mechanical properties, such as surface hardness for scratch resistance and abrasion resistance. Coatings such as titanium nitride (TiN) applied using PVD (physical vapour deposition) and nickel using electroless deposition and electroplating can be used on complex machinery to give both mechanical and corrosion protection. Additionally, these coatings can have additives within them to enhance the properties of the coatings. Silicon carbide (SiC) is often added and co-deposited with nickel coatings to attain depositions with harder and more abrasion resistant properties. In addition to their use providing mechanical properties, the coating aesthetics are also tailored such as with chromium or nickel.

One issue with these barrier coatings is that when they are perforated, the substrate of steel will often act sacrificially, and the production of oxides below the surface cause the coating to delaminate and expose more of the substrate to the corrosive media. This issue is prevalent in metallic barrier coatings such as electrolytic and electroless nickel deposits. Oxide inclusions and microcracks form during the deposition process which gives the coating some porosity, and residual tensile stresses can lead to the development of larger cracks within the coating [5]. The cracks propagate through the coating, exposing the substrate to the corrosive environment which can lead to accelerated disbonding of the coating [6]. One way of preventing this from occurring is to include a corrosion inhibitor within the coating so that the microcracks do not lead to substrate corrosion resulting in delamination. One such solution to this requirement, was the inclusion of chromium VI compounds in chrome plating's. Chromium VI is a corrosion inhibitor and was widely used up until recently. In 2015, the European Union publication of REACH (Registration, Evaluation, Authorisation & Restriction of Chemicals) listed chromium VI ( $\text{Cr}^{6+}$ ) as a carcinogenic compound

and restricted its use [7]. This has led to the development of other “self-healing” coatings.

Much of the research performed on self-healing coatings has applied to polymer and organic coatings containing microcapsules of corrosion inhibitors. This leaves metallic coatings with a lack of viable alternatives after the loss of chromium VI compounds. Despite this, “mechanical properties” make up almost 10 % of key vocabulary in published work relating to the subject [8]. As nickel plating’s are commonly used in the co-deposition process [9], it would be a prime candidate for investigating delivery methods of corrosion inhibiting properties. Two of the most common forms of manufacturing nickel coatings are electrodeposition, often referred to as electroplating, due to its use of electric current to deposit the nickel on the substrate; and electroless deposition, named due to its lack of electric current to perform depositions. Additionally, because of its lack of electric current, this process can be performed on non-conductive substrates and produces deposits of even coating thickness due to the lack of geometric current concentrations which occur during the electroplating process.

Electroless co-depositions have been used to successfully co-deposit both organic and inorganic second phase particles. It is often used with ceramic co-deposits, for use as a mechanical property targeted coating, but also with polymers such as PTFE as dry lubricants reducing friction [10]. Research has also been performed depositing cellulose nanofibrils within the coating to increase porosity once burned out of the coating [11]. Due to its diversity in co-deposition characteristics, it makes a suitable process for this investigation. It is also used in many applications for its mechanical properties and can be used to perform “bright” nickel deposits for similar aesthetics as chrome plating’s containing chromium VI compounds which it is aiming to supersede.

The inclusion of the second phase can be achieved by using microcapsules or microgels. The use of microgels reduces the stages required for the production by eliminating the two-step capsule production prior to filling. With a water-in-oil production method, the microgels can be produced to include corrosion inhibitors or active ingredients to produce fresh ENP (electroless nickel-phosphorus) deposits similar to the techniques used in polymer coatings. These microgels can be tailored to have different activation methods and can be produced from commonly available “green” materials such as sodium alginate

or gelatine, making them a good alternative to carcinogenic and restricted chromium VI.

This investigation will research the feasibility of using the electroless co-deposition process for the inclusion of microgels which can be used to perform self-healing, corrosion inhibiting functions. The aim is to develop a comparable technique to current electroless nickel-phosphorus deposition, including deposition rate, with the potential improvement of properties such as mechanical and barrier layer.

## 1.2 Key Objectives

- Investigate microgels developed at Wrocław University, to determine their viability to maintain structure in the electroless co-deposition technique at temperatures up to a maximum of 90 °C and pH ranging from 4–11.
- Co-deposit said particles within nickel-phosphorus coatings with two approaches:
  1. At low temperatures (< 60 °C) resulting in a more cost-effective procedure.
  2. At higher temperatures ( $\approx$  90 °C) similar to those used extensively in industry.
- Determine the impact of microgels on the deposition process by comparing the deposition rate and phosphorus content of the NiP/microgel composite coatings with similarly produced plain NiP coatings.
- Investigate the corrosion protection provided by the inclusion of microgels by comparison of NiP/microgel composite coatings with plain NiP coatings using Electrochemical Impedance Spectroscopy (EIS) and Neutral Salt Spray (NSS) testing.
- Compare the tribological properties of NiP/microgel composite coatings with plain NiP coatings using surface roughness, Vickers hardness, and micro-abrasion testing.

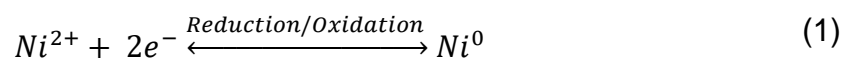
## 2 Literature Review

### 2.1 Electrochemical Depositions

Electrochemical depositions can be classified as either electrolytic or electroless deposition processes. The electrolytic method relies on an electric current which is used to dissolve a source metallic material into ions, which are transported through an electrolyte medium to the desired substrate, where they are deposited. In the case of electroless depositions, the source of the coating to be deposited is contained within a solution and uses a purely chemical reaction to deposit onto the substrate through the use of catalytic activation [12].

#### 2.1.1 Electrolytic Deposition

As briefly described, the process of electrolytic deposition or electroplating, requires the use of an electric current to deposit metal onto a substrate. The source material is connected to the circuit as the anode and the substrate is the cathode. The plating material is ionised and dissolves into the electrolytic solution which acts as the carrier. The positively charged ions are attracted to the cathode (substrate) at which point they regain their lost electrons and are deposited as atoms. The reaction for electroplating nickel can be written as a reduction/oxidation reaction as can be seen in equation (1) [13] and the process is illustrated in Figure 1.



Where:  $Ni^{2+}$  are nickel anions;  $e^{-}$  are electrons;  $Ni^0$  are nickel atoms

Some advantages of the electroplating method are that it can be performed at low temperatures which permits its use with most co-deposits. It also has a high deposition rate which can be altered by increasing or decreasing the applied current [14]. This in turn reduces the associated cost of the coating due to the time and temperature required for the process.

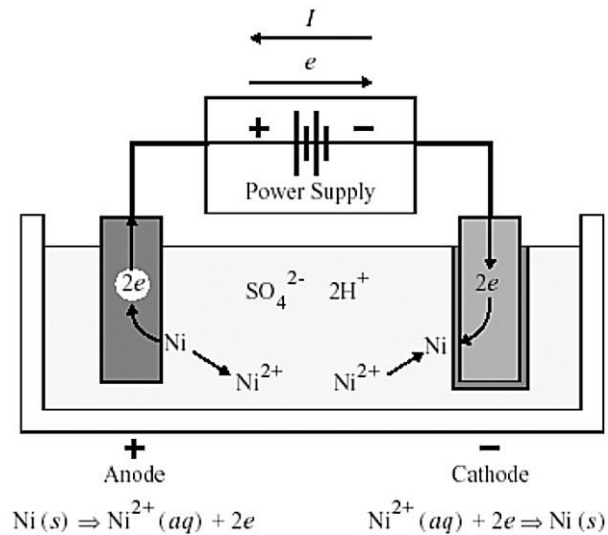


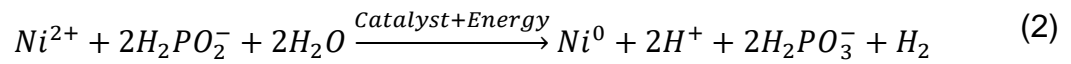
Figure 1: Electroplating nickel process diagram [15].

Some of the drawbacks associated with electroplating include the requirement of the substrate to be electrically conductive due to the mode by which the process operates. The presence of a current also leads to corner build up, where some areas of the coating are thicker. This is a result of the current concentration due to the geometry of the substrate and can limit its feasibility for some applications. Whilst the coatings produced may provide an improvement for corrosion protection, they might not be as effective as coatings produced by electroless depositions as in the case of nickel, due to the coatings crystalline structure [5]. This is due to the presence of intergranular corrosion which can occur at the grain boundaries permeating through the coating. The amorphous nature of electroless nickel-phosphorus coatings therefore negate this and provide a more effective barrier coating [16].

### 2.1.2 Electroless Deposition

The electroless deposition process is a purely chemical process which relies on chemical reactions initiated by a catalyst on the substrate to deposit metal. The process is autocatalytic in nature so once the catalyst has been obscured by the initial layer of coating, the reaction will continue. Electroless deposition solutions contain a metal salt which reacts with a reducing agent when in the presence of a catalytic site, and sufficient external energy i.e. heat.

The process for depositing nickel can be simplified and written as a reduction reaction as seen in equation (2) [17]. However, this model does not account for the deposition of phosphorus.



The benefits related to the electroless deposition process include its ability to deposit coatings onto non-conductive substrates as the process does not rely on an electric current. In addition to this, the coatings display even thickness over the entirety of the substrate as the geometry does not impact the chemical reactions that occur [18], as illustrated by Figure 2. Electroless deposition is also suitable for applying corrosion protective coatings as in the case with electroless nickel-phosphorus (ENP) plating's. ENP deposits which have a phosphorus content greater than 7 wt% are amorphous in structure which reduces the possible avenues for incursion of corrosive substances [19]. The process also operates at relatively low temperatures which permits the use of most materials for co-depositions. Additionally, the deposits poses excellent wear and abrasion resistance, in turn increasing their service life [20].

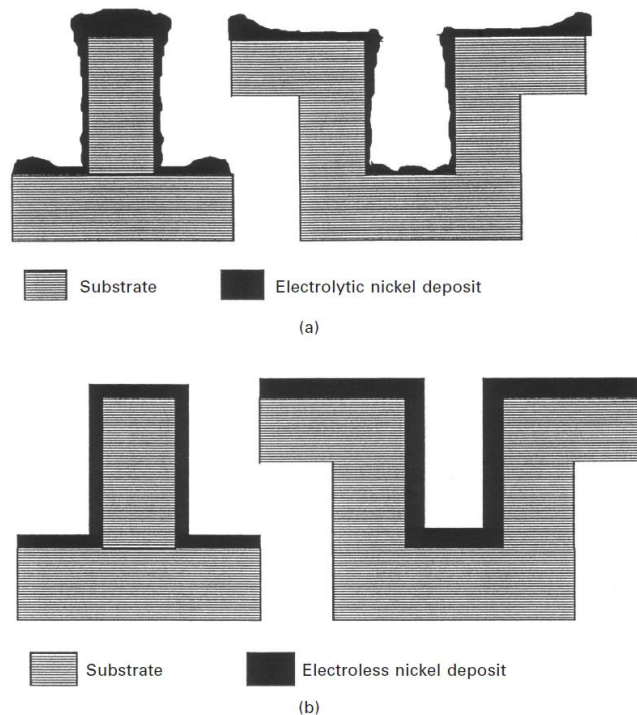


Figure 2: Comparison of a) Electrolytic and b) Electroless nickel deposits [21].

Some disadvantages of the electroless deposition process include the cost of chemicals required for depositions. The cost of electroless nickel is 2.5x the cost of electroplated nickel, purely considering the cost of nickel (~\$21/kg). With the inclusion of other chemicals such as brighteners required for electroplating, this differential in cost is reduced. In addition to the cost of chemicals, there is an associated energy cost for operating solutions at higher temperature. Operating a 200-gallon bath at 85–90 °C requires approximately 40 kW/hr compared with just 15 kW/hr at 55–65 °C required for heating comparable electroplating baths. When factoring in the additional power required for electroplating, the total operating power is approximately 60 kW/hr for a Watts nickel solution, so total power required may be similar for depositing coatings of equivalent thickness [22]. Electroless nickel exhibits a slower deposition rate than electroplated nickel, with the rate directly related to the temperature of the solution. Electroplated nickel can be deposited at 60  $\mu\text{m/hr}$  using a current density of 5  $\text{A/dm}^2$  [5], whereas most electroless nickel solutions operate at less than 20  $\mu\text{m/hr}$  [23]. This increases the cost of production in commercial uses due to the temperature and time that large baths must be operated at. The process must be monitored as the metal that is deposited is contained within the solution and requires replenishment throughout its use if plating for extended periods. As the deposition rate and coating composition are reliant on the bath chemistry, this replenishment must be carefully controlled [24].

## **2.2 Electroless Deposition of Nickel**

### **2.2.1 History**

The development of the electroless nickel deposition technique is relatively recent but has its origins back in 1844 when Wurtz [25] discovered that hypophosphite anions would reduce nickel cations. Although Wurtz had discovered the mechanism responsible for the electroless deposition of nickel, he was only able to produce a black powder deposit. The discovery that bright nickel-phosphorus could be deposited was found by Breteau in 1911 [26], and the first patent for an electroless nickel plating bath was issued to Roux in 1916 [27]. These baths were very unstable, decomposing spontaneously and were prone to plating on every surface the solution was in contact with, including the container. The process was subsequently worked on by many but the breakthrough in this plating technology was conducted by Brenner and Riddel [28], who in 1946 were the first to describe a practical procedure for the controlled deposition of electroless nickel-phosphorus [29]. In 1955, the first commercially available electroless nickel solution “Kanigen” was released by the General American Transport Corporation (GATC). Since this breakthrough, there has been much research conducted on the process with different salts, reducers and complexing agents used to produce a variety of coatings. Research continues to date on this process, finding new alloys for deposition and more efficient processes [13].

### **2.2.2 Basic Composition**

The basic composition of electroless nickel baths include nickel salts, reducing agents, complexing agents, and stabilisers. In commercial solutions, many more components are used such as surfactants and buffers however these are rarely disclosed in the data sheets provided. Some of the most common constituents of electroless nickel solutions can be found in Table 1.

Table 1: Components of electroless nickel baths and their functions [13].

Component	Function	Example
Nickel ions	Source of metal	Nickel chloride Nickel sulfate Nickel acetate
Hypophosphite ions	Reducing agent	Sodium hypophosphite Sodium borohydride Hydrazine
Complexants	Form nickel complexes, prevent excess free Ni ion concentration so stabilising solution and preventing Ni phosphite precipitation. Also act as pH buffers.	Monocarboxylic acids Dicarboxylic acids Hydroxycarboxylic acids Ammonia Alkanolamines
Accelerators	Activate hypophosphite ions and accelerate deposition. Mode of action opposes stabilisers and complexants	Anions of some mono- and di-carboxylic acids, fluorides, borates
Stabilisers	Prevent solution breakdown by shielding catalytically active nuclei	Lead, tin, arsenic, molybdenum, cadmium, thallium ions, thiourea, etc.
Buffers	For longer term pH control	Sodium salt of certain complexants. Choice depends on pH range used
pH regulators	For subsequent pH adjustment	Sulphuric and hydrochloric acids, soda, caustic soda, ammonia
Wetting agents	Increase wettability of surfaces to be coated	Ionic and non-ionic surfactants

### Nickel Salts

The most common nickel salt used for electroless nickel depositions is nickel sulfate. Nickel chloride and nickel acetate are also used but only for limited applications, such as producing high purity (99.8 wt%) electroless nickel depositions when electrical conductivity is desired. This is due to high purity nickel deposits having higher electrical conductivity than conventional nickel-phosphorus or nickel boron coatings [30]. Nickel acetate solutions can be tailored to produce similar results to nickel sulfate baths, however the increased cost associated with acetate prevents its use in most applications [31].

The nickel ion concentration found in most commercial baths is typically around 6.5 +/- 1 g/L (0.09–0.13 mol/L). At concentrations over 5 g/L (0.085 mol/L) the nickel ion concentration has no effect on the deposition rate. Figure 3 shows the phosphorus content of the deposit decreases with increasing nickel ion concentrations up to 5.8 g/L (0.1 mol/L), after which it will remain stable provided the hypophosphite content is unchanged [29].

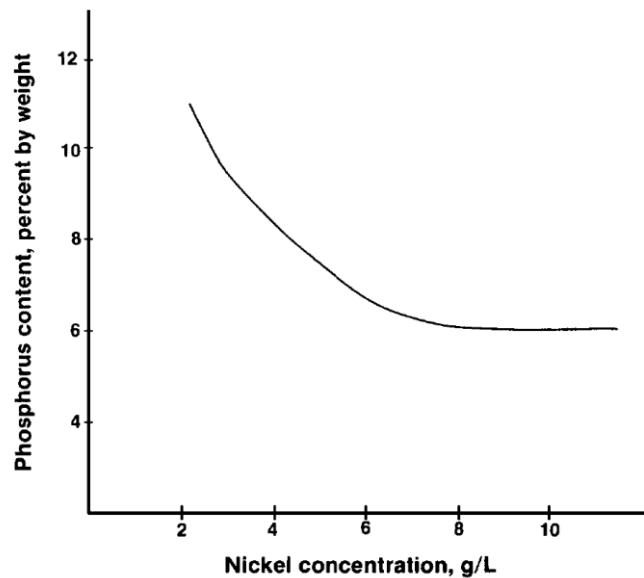


Figure 3: Effect of nickel concentration on NiP alloy composition [29].

### Reducing agents

After the nickel salt, the most important component of the solution is the reducing agent. The reducing agent determines what alloy the solution will deposit and what properties the coating will possess. The different alloys that can be deposited are nickel-phosphorus, nickel-boron or plain nickel. Table 2 shows the different reducing agents and associated deposits.

Table 2: Reducing agent for EN plating [32]

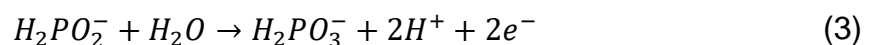
Deposit	Reducing agent	Remarks
NiP	Sodium hypophosphite (NaH <sub>2</sub> PO <sub>2</sub> )	Acid or alkaline bath (2–17 %P)
NiB	Sodium borohydride (NaBH <sub>4</sub> ) Aminoborane (DMAB)	Acid or alkaline bath Alkaline Bath (0.5–10 %B)
Only Ni	Hydrazine (NH <sub>2</sub> NH <sub>2</sub> )	Alkaline bath

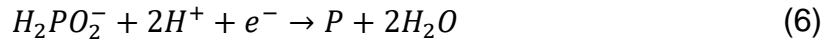
For nickel-phosphorus coatings, the optimum plating conditions are found when the ratio of Ni<sup>2+</sup>/H<sub>2</sub>PO<sub>2</sub><sup>-</sup> is between 0.3–0.45. Hypophosphite is one of the strongest reducing agents with a redox potential of -1.065 V at pH 7 and -0.882 V at pH 4.5. This value can reach up to -1.57 V in alkaline environments [13].

The process in which hypophosphite electroless deposition baths produce NiP coatings has been the subject of much research. Four models have been suggested which are either chemical or electrochemical models, where the process is divided into cathode and anode regions [33].

#### Model 1

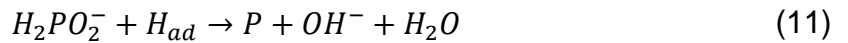
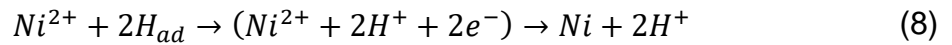
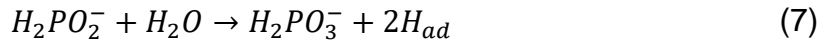
One model using only electrochemical reactions was described by Mallory and Hajdu [29]. This model uses the anodic reaction where electrons are formed by the reaction of water and hypophosphite [33].





### Model 2

Another model, described by Brenner and Riddel [28], is the reduction of nickel by atomic hydrogen, which in turn is created by the reaction of hypophosphite and water [29], [33].



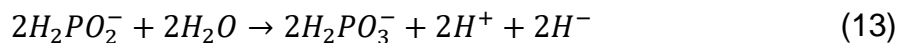
Gutzeit [34] agrees with this model but proposes a different reaction for the production of  $H_{ad}$  [33].



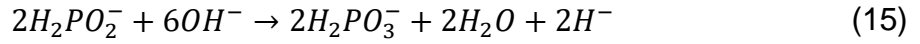
### Model 3

Put forward by Hersch [35], this model relies on the hydride transfer mechanism, where hypophosphite acts as the donor of hydride ions. This process is dependent on the solutions pH and has separate reactions for acidic and alkaline solutions [29], [33].

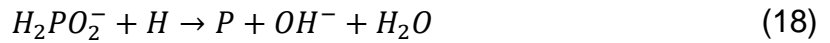
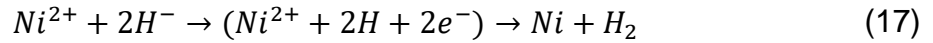
For acidic environments:



For alkaline environments:

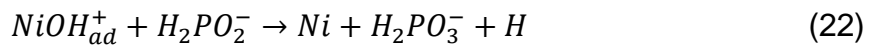
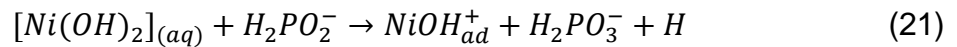
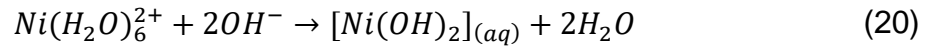


From which nickel and phosphorus are produced:

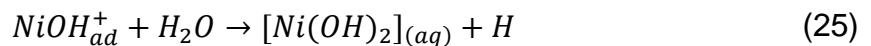
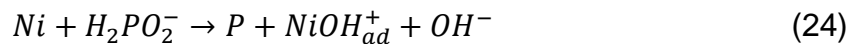


#### Model 4

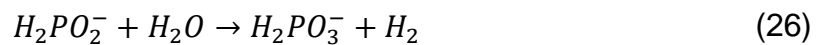
A fourth model involving the coordination of hydroxyl ions with hydrated nickel ions was proposed by Cavalotti and Salvago [36]. Dissociation of water molecules occurs on the catalytic surface, from which the Hydroxyl ions are produced, forming coordination bonds with hydrated nickel ions. The hydrolysed nickel then reacts with hypophosphite to produce atomic hydrogen [29], [33].



Hypophosphite is then reduced by reaction with metallic nickel to produce atomic phosphorus, whilst  $NiOH_{ad}^+$  adsorbate reacts with water.



Equations (21) and (25) are competing reactions. Cavalotti and Salvago [36] attribute the lamella morphology of the deposit to the adsorbed  $\text{NiOH}^+$  cations whereas Gutzeit [34] believes it is due to local differences in phosphorus content of the deposit. Gutzeit's hypothesis seems less likely as the reduction of hypophosphite (24) is only possible if the coating surface is free from ionic  $\text{NiOH}^+_{\text{ad}}$  adsorbate, hence cannot run simultaneously with reaction (22). The reaction of hypophosphite ions with water to produce hydrogen must also be included in this reaction scheme [33].



### Complexing agents

Complexing agents function by bonding with free nickel ions in the solution to create nickel complexes. This prevents the spontaneous decomposition of the plating solution by controlling reactions that occur on the catalytic surface, and buffer the solution by preventing rapid pH change due to hydrogen ions produced from the reduction reaction [37]. Complexing agents are usually organic acids or their salts such as sodium citrate. There are two notable exemptions of this: the ammonium ion which is used for controlling pH; and the organic pyrophosphate anion used exclusively in alkaline electroless solutions [38]. The deposition rate can be increased or decreased by the concentration of the complexing agent, with the optimum concentration for sodium citrate being 30 g/L [18]. Figure 4 shows the results of depositions performed by de Minjer and Brenner [39] using four organic acids for complexing agents. Small additions of complexing agent resulted with increased deposition rates. The deposition rates peaked at optimum complexing agent concentration, after which a reduction was observed [29].

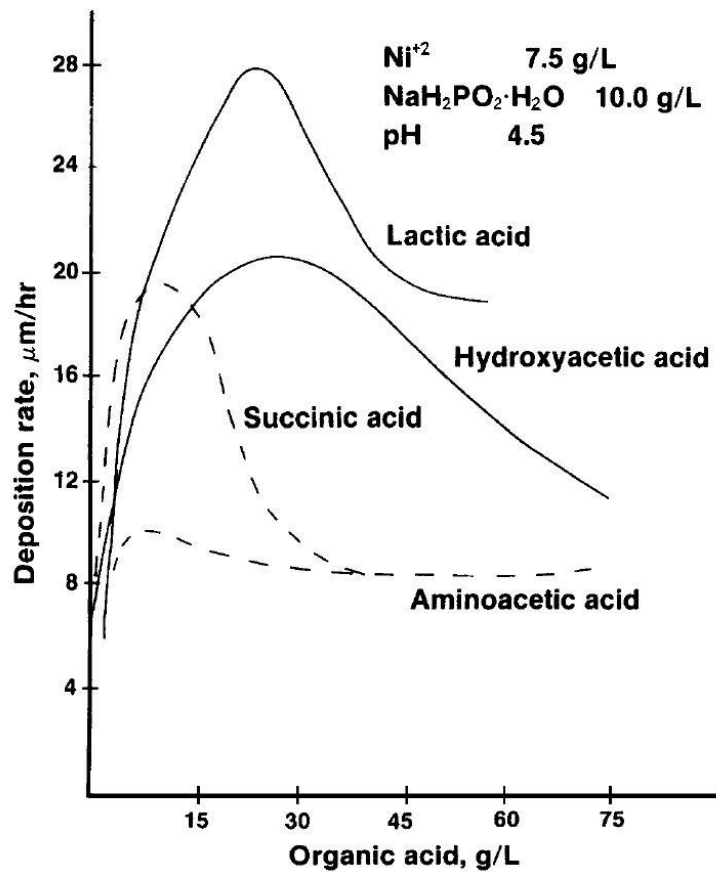


Figure 4: Effect of concentration of organic acid complexing agents on rate of deposition [29], [39].

### Stabilisers

Sometimes referred to as inhibitors, stabilisers prevent the spontaneous decomposition of electroless nickel baths. They also function to control the deposition rates of the solution over certain concentrations, which is defined as the critical concentration [40]. The three most common stabilisers used for nickel-phosphorus solutions are: sulphur compounds such as thiourea; oxy ions such as molybdates or iodates; and heavy metals including lead, bismuth and tin [5]. There are two ways in which stabilisers operate, the substitution mechanism and adsorption-poisoning mechanism. Heavy metal ions such as  $\text{Pb}^{2+}$  exhibit the substitution mechanism where they deposit onto the active metal surface through displacement reactions, preventing the random reduction of nickel. Oxy ions stabilise the solution through adsorption-poisoning, where they prevent nickel depositions by adsorbing on the catalytic sites of the metal surface [19]. Stabilizers can have multiple influences on the plating bath in addition to preventing the spontaneous decomposition of the solution or reducing the deposition rate. The concentration of stabiliser used can also

increase the deposition rate and reduce the phosphorus content of the deposit [41]. Figure 5 shows that at concentrations of 1–3 mg/L, thiourea is found to increase the deposition rate of NiP solutions due to its participation in the formation of a reactive intermediate, reducing the activation energy of the electroless nickel bath [23], [41]. Above this critical concentration, thiourea stabilises the solution through the adsorption-poisoning mechanism on the anodic reaction sites to inhibit the oxidation of hypophosphite [42].

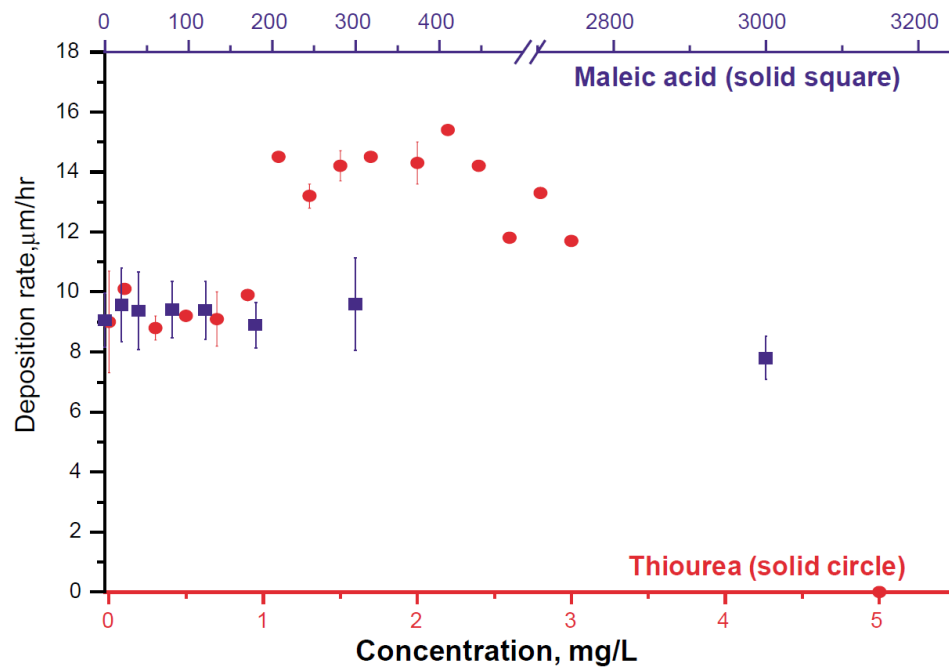


Figure 5: Effect of thiourea and maleic acid concentrations on the deposition rate of the electroless nickel system [41].

### Surfactants

Surfactants stands for Surface Active Agents and are also commonly referred to as wetting agents. Their role in an electroless nickel bath is to increase the solutions contact with the surface of the substrate, which can lead to a change in the structure of the deposit. They are often used in the co-deposition process due to the increased stability of suspension through wettability and surface charge of the suspended particles [43]. Figure 6 illustrates how surfactants are used to aid in co-deposition through forced convection. The inert particles are transferred through the diffusion layer and loosely absorbed on the substrate surface.

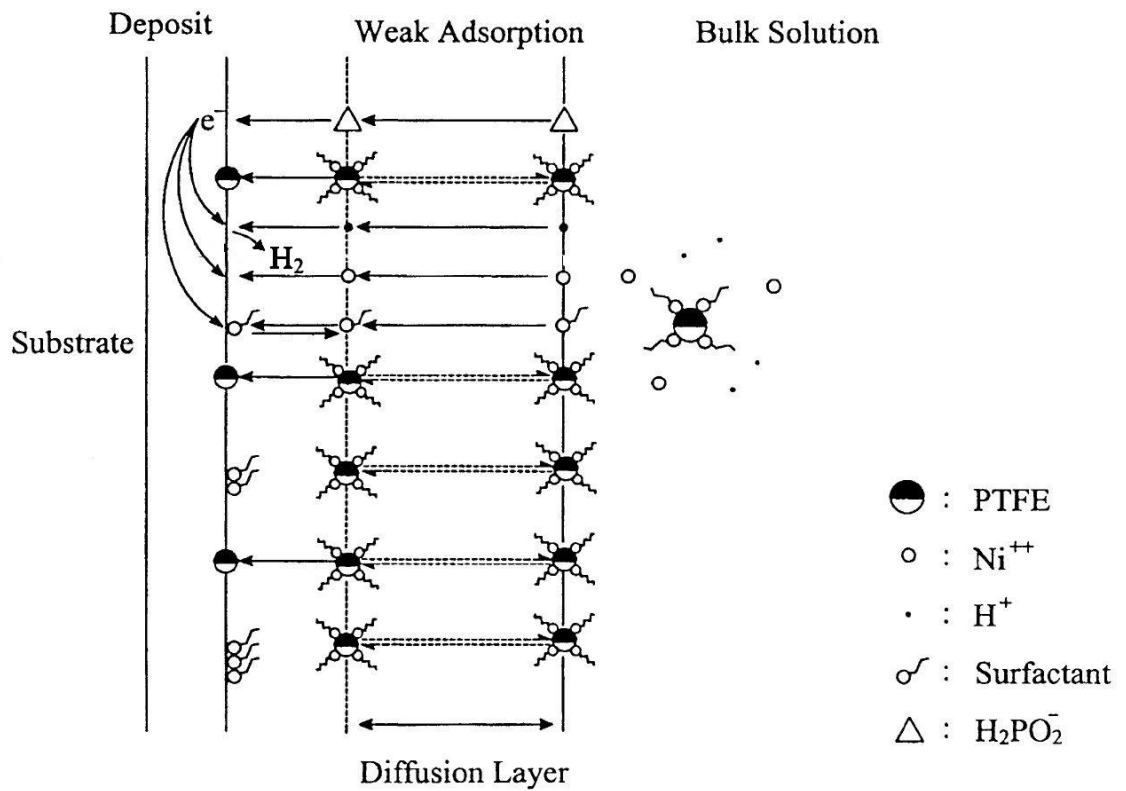


Figure 6: Model of co-deposition process for NiP/PTFE coating [43].

Figure 7 shows results from Ger and Hwang [43] which demonstrates that FC surfactant (fluorinated alkyl quaternary ammonium iodide) concentration impacts the quantity of co-deposited PTFE. Increasing the surfactant concentration resulted with increased PTFE co-deposit up to a critical point, after which, the co-deposition reduces.

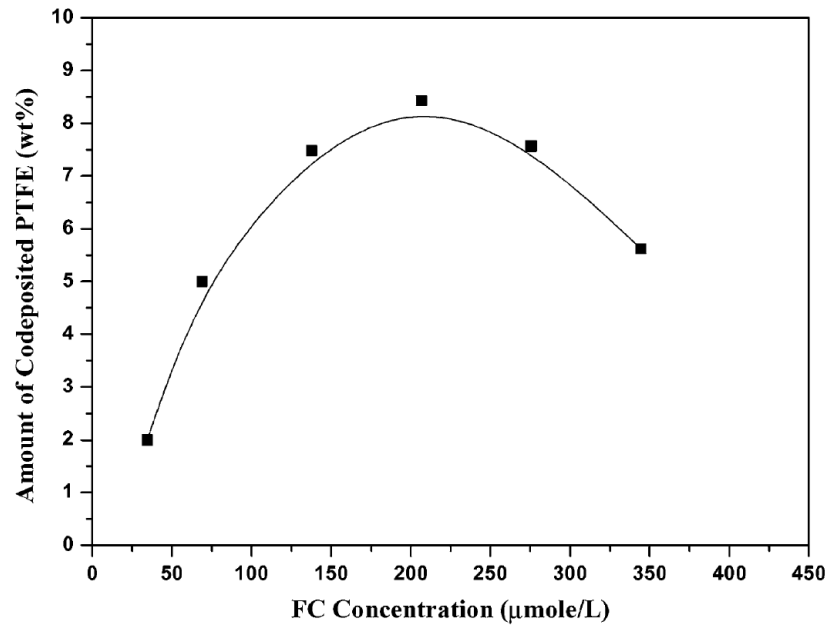


Figure 7: The weight percentage of co-deposited dispersed PTFE particles in various concentrations of surfactant (FC) in the plating bath [43].

The addition of anodic surfactants can reduce the occurrence of pitting on the deposit as the reduced surface tension of the plating solution prevents the hydrogen bubbles produced in the reaction from adhering to the substrate [14]. The inclusion of surfactants at very low concentrations between 3–6 ppm have been found to increase the deposition rate of NiP, however at higher concentrations of 0.1 g/L the resulting deposition rate was found to be significantly less [10], [44].

### 2.2.3 Solution Temperature

The temperature of the solution is the dominant factor determining the deposition rate of an electroless nickel bath. Electroless solutions typically operate with temperatures in the range of 60–90 °C with most acid hypophosphite solutions operating between 85–90 °C [45]. As the temperature of the solution is increased, the deposition rate increases exponentially, as shown in Figure 8.

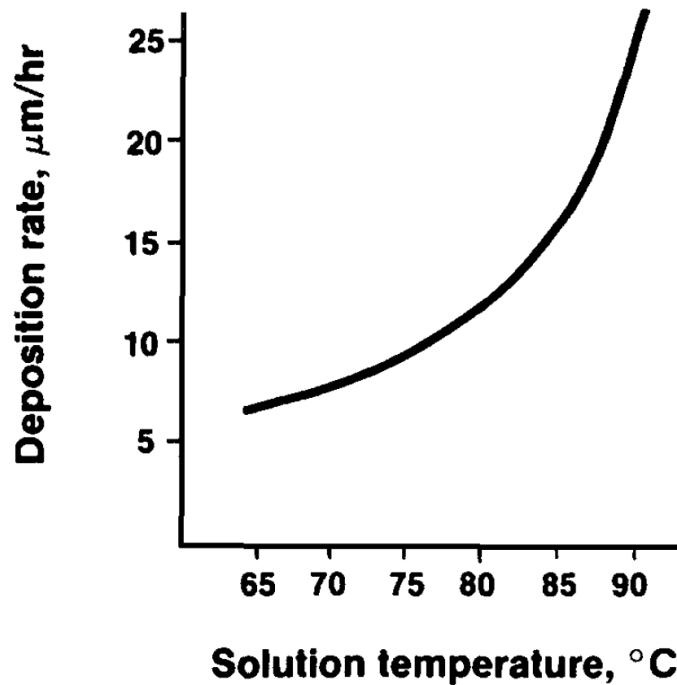


Figure 8: Effect of temperature on plating rate [29].

If the solution temperature is raised much beyond 90 °C, it can lead to plating out or complete decomposition resulting from chemical instability, rendering the solution unusable. This occurs due to the increased energy of the solution so that it no longer requires a catalytic surface for the plating reactions to occur. Baldwin and Such [46] found that when a solution was operated above its normal plating temperature range, the phosphorus content of the coating decreased.

Alkaline nickel baths can operate at lower temperatures and are often used for plating on polymer substrates. Figure 9 shows that alkaline pyrophosphate solutions have much lower activation temperatures and when operated at elevated temperatures can achieve significantly higher deposition rates than alkaline citrate baths [29].

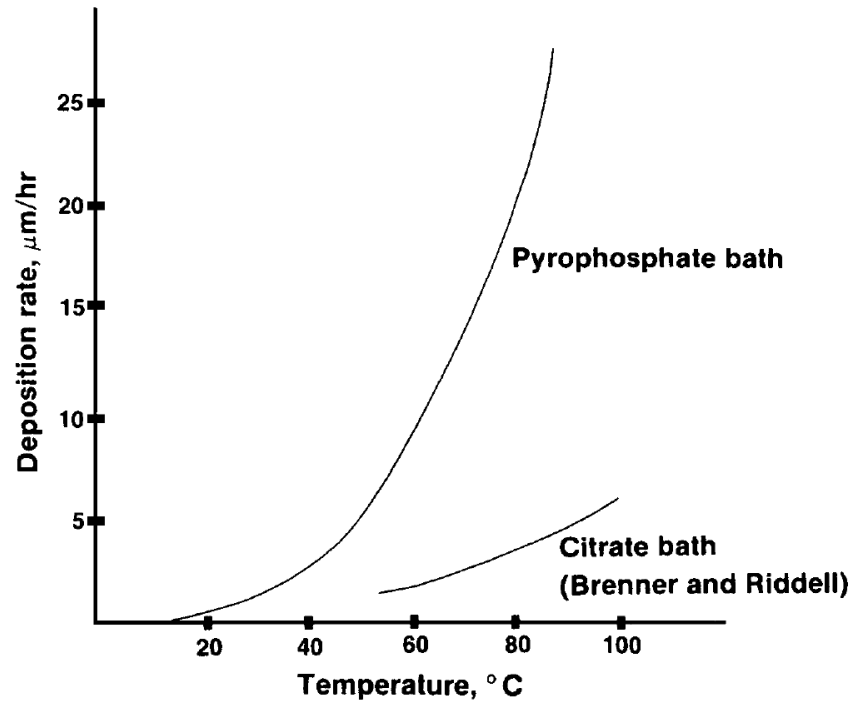


Figure 9: Effect of temperature on plating rate of pyrophosphate and citrate baths [29].

## 2.2.4 Solution pH

The pH of the solution impacts the deposition rate of both acidic and alkaline solutions. In acidic solutions, when the pH is increased from 3–6 pH, the deposition rate significantly increases when all other variables remain constant. This has also been shown to be the case with alkaline solutions, with Schwartz [47] reporting an increase in deposition rate from 20–27  $\mu\text{m/hr}$  in pyrophosphate solutions when adjusting the pH from 9–9.5 up to 10–10.5 pH [29]. Figure 10 shows the increase in deposition rate of an electroless nickel (EN) bath with increasing pH from 4–11 [48].

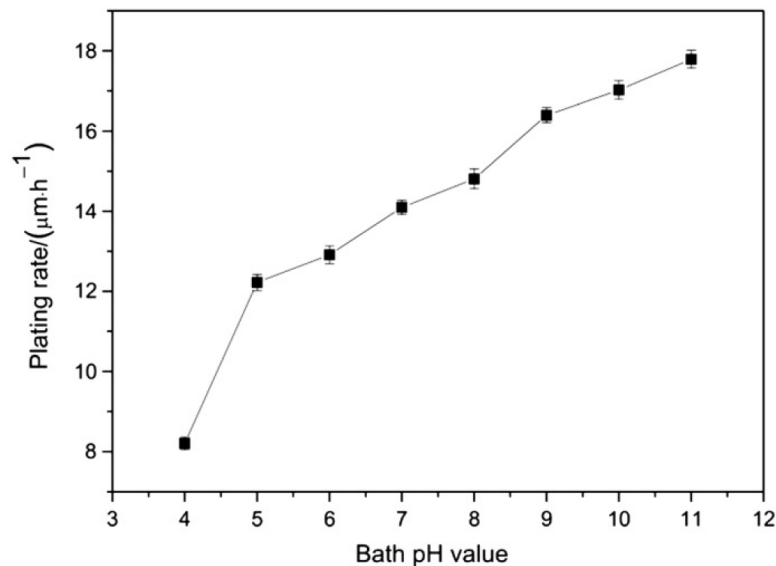


Figure 10: Dependence of pH value on the deposition rate of an EN bath [48].

The solution pH also impacts the phosphorus content of the deposit through the  $\text{H}^+$  ion concentration. Figure 11 shows that the coatings phosphorus content decreases as the solution pH increases. This effects the structure of the deposit and can determine whether the structure is crystalline or amorphous [19].

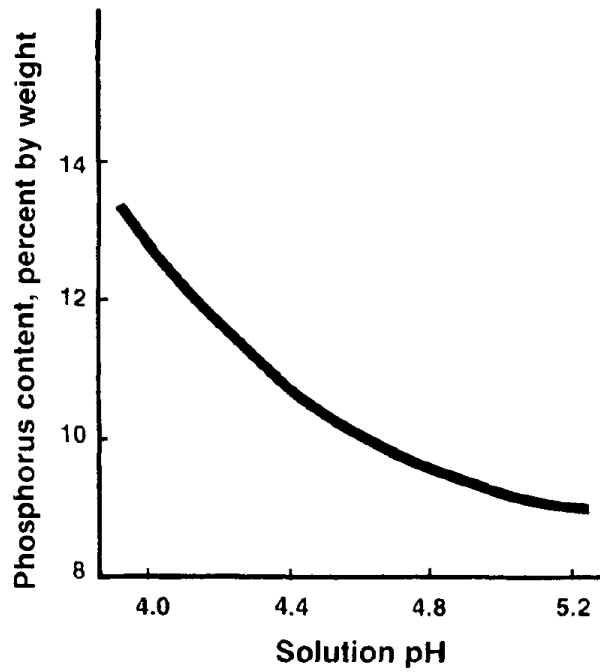


Figure 11: Effect of pH on phosphorus content [29].

This in turn impacts the intrinsic stresses within the coating, with low and high phosphorus coatings displaying compressive stresses and medium phosphorus exhibiting tensile stresses [16], shown by Figure 12.

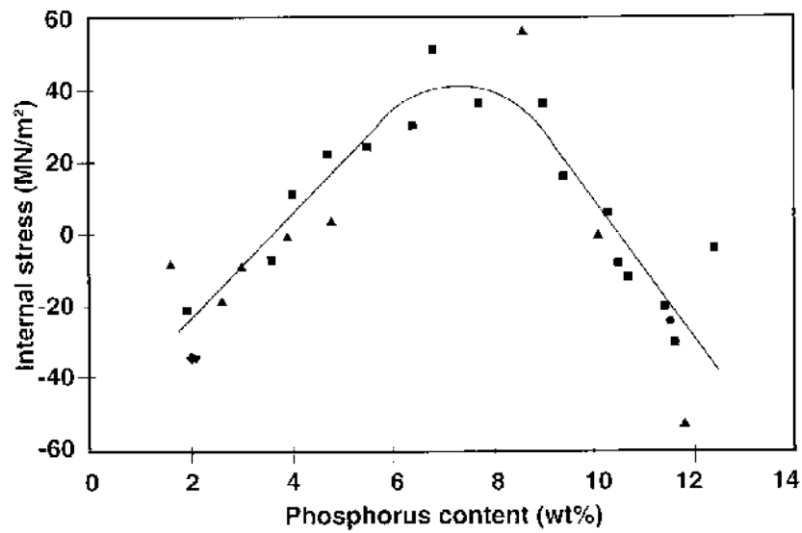


Figure 12: Effect of composition on internal stress [16].

## 2.3 Ultrasonic Agitation

Ultrasonic processing is used extensively in the electroless deposition technique to aid in the cleaning of the substrate prior to the plating phase. It has also been investigated for its use in providing agitation within the deposition bath and has been found to have a significant impact on the resulting deposit. When the ultrasonic waves are introduced to the solution, the resulting high and low pressure cycles lead to the formation of cavitation bubbles. When these cavitation bubbles collapse asymmetrically, instantaneous temperatures and pressures have been recorded as high as 10000 Kelvin and 500 atm respectively. The formation and collapse of the cavitation bubbles has been found to enhance mass transfer, thin the diffusion layer and produce localised heating [49], [50]. Figure 13 shows the formation and collapse of cavitation bubbles through successive pressure cycles.

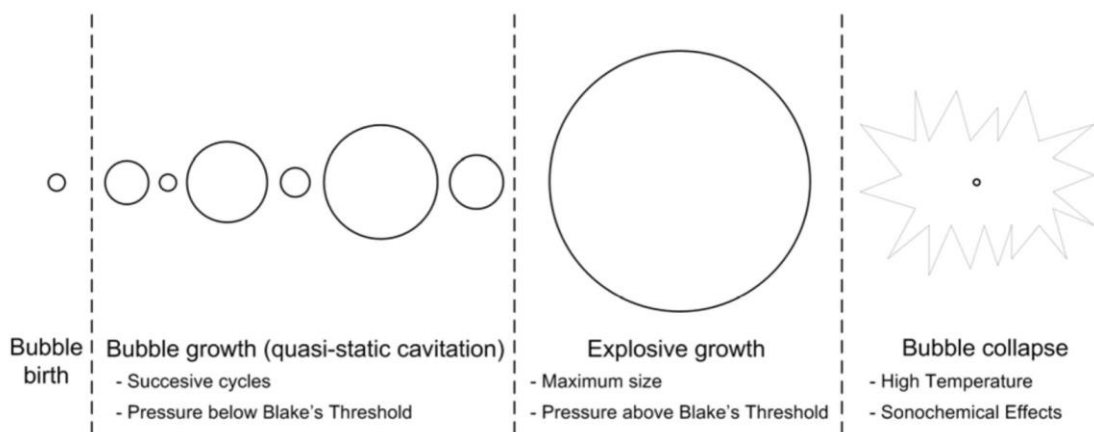


Figure 13: Bubble growth and implosion in a liquid irradiated with ultrasound [51].

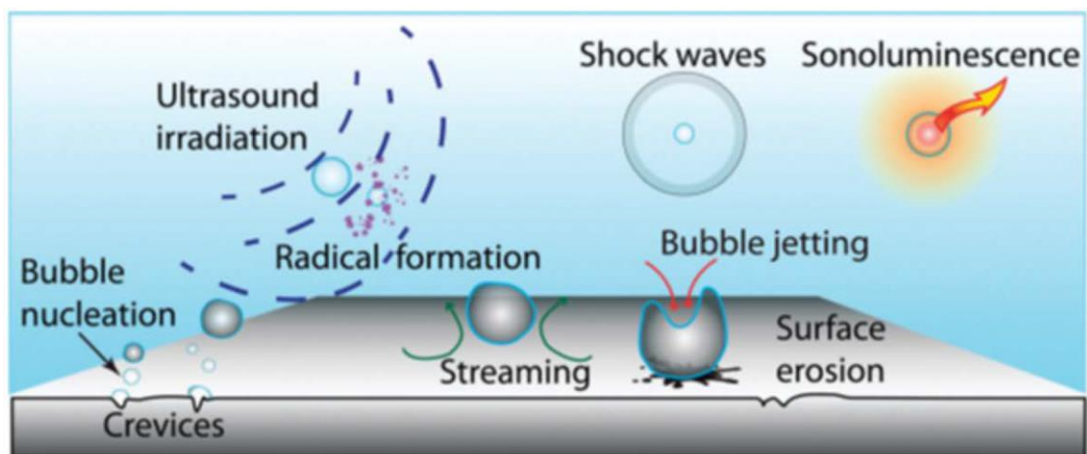


Figure 14: Schematic representation of the main effects of cavitation induced by ultrasound irradiation [51].

Low frequency ultrasound of 28 kHz has been found to increase pitting due to the impact of high energy microjets produced when the cavitation bubbles collapse. Figure 14 shows some mechanical and chemical effects of ultrasonic cavitation, such as pitting due to bubble jetting and the creation of radicals in solution. When using higher frequencies of 35–45 kHz, the pitting issue was not reported and lead to a significant increase in the deposition rate of the solution. Figure 15 shows the increase in deposition rate resulting from the presence of ultrasound at 50, 70, and 90 °C solution temperatures.

In addition to the deposition rate, the ultrasonic agitation reduces the phosphorus content of the deposit which leads to increased crystallinity and hardness, which is shown in Figure 16. This reduction is likely dependant on the solution in use, as Abyaneh et al. [52] found the discrepancy in phosphorus content to increase with temperature, whereas Cobley and Saez [53] found it to decrease with increasing temperature.

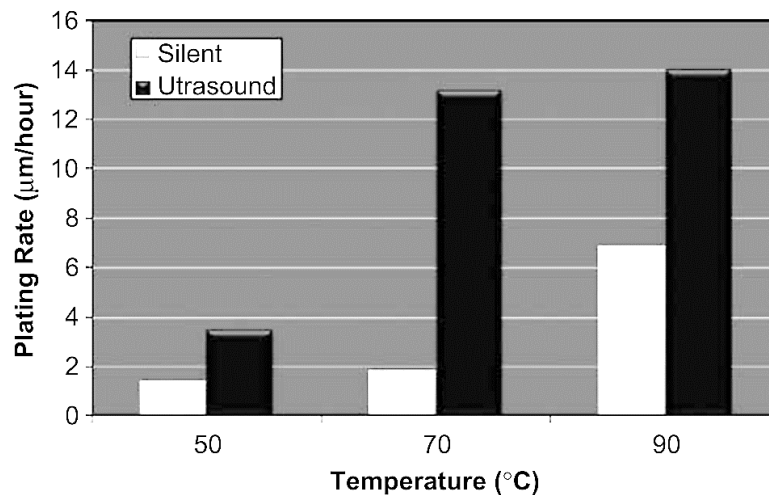


Figure 15: Effect of ultrasound on the plating rate at 50, 70 and 90 °C solution temperatures [54].

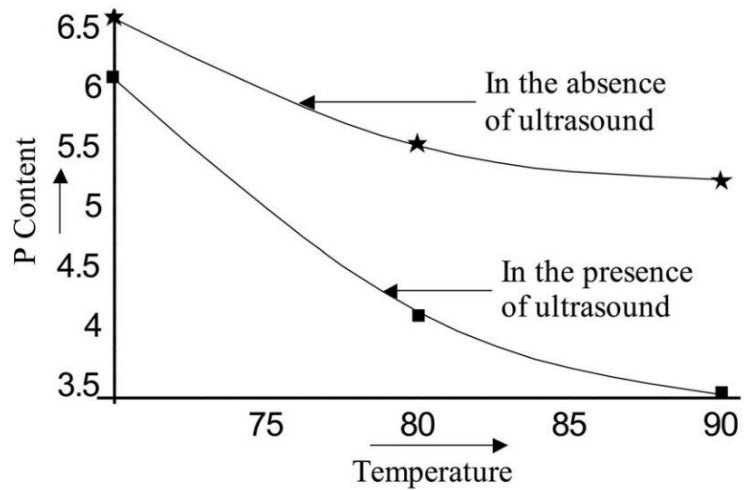


Figure 16: Phosphorous content of electroless nickel as a function of solution temperature, with and without the presence of ultrasound [52].

The agitation provided by ultrasound has been investigated for its use in the electrolytic plating process. It was found that the co-deposit was less likely to aggregate in the solution and provided an even dispersion throughout the coating, as shown in Figure 17. This resulted in the improvement of the coatings resistance to corrosion [51].

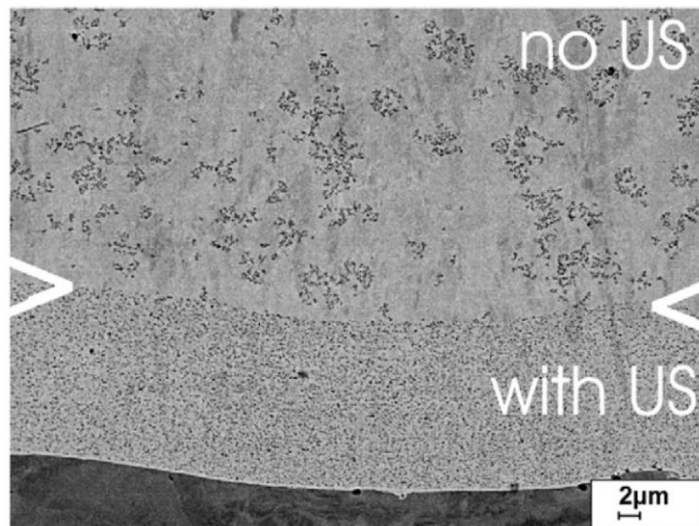


Figure 17: Well-dispersed TiO<sub>2</sub> particles under ultrasound conditions (lower part from substrate up to the markers > <) and nano-particle agglomeration under silent conditions (upper part) in a Ni coating [51].

## 2.4 Self-Healing Coatings

Self-healing coatings are the source of much interest due to the cost associated to corrosion, with the first polymeric self-healing materials proposed in 1980 [8]. Most coatings will not sacrificially protect a substrate once the corrosive substance has penetrated the barrier coating. To combat this, the inclusion of a self-healing active agent is included in the coating which can either inhibit corrosion from occurring or actively repair the damaged site. Until recently, the main components used for metallic self-healing coatings have been compounds containing hexavalent chromium ( $\text{Cr}^{6+}$ ). The introduction of legislation from REACH prevents its use due to its classification as a carcinogen [7]. New techniques for providing self-healing corrosion protection are being researched at an increasing rate. However, as can be seen from Figure 18, metallic self-healing coatings have not been developed at the same rate as polymeric coatings. This despite almost 10 % of the key vocabulary on the subject being mechanical properties, which polymeric coatings cannot provide to the same extent as metallic coatings.

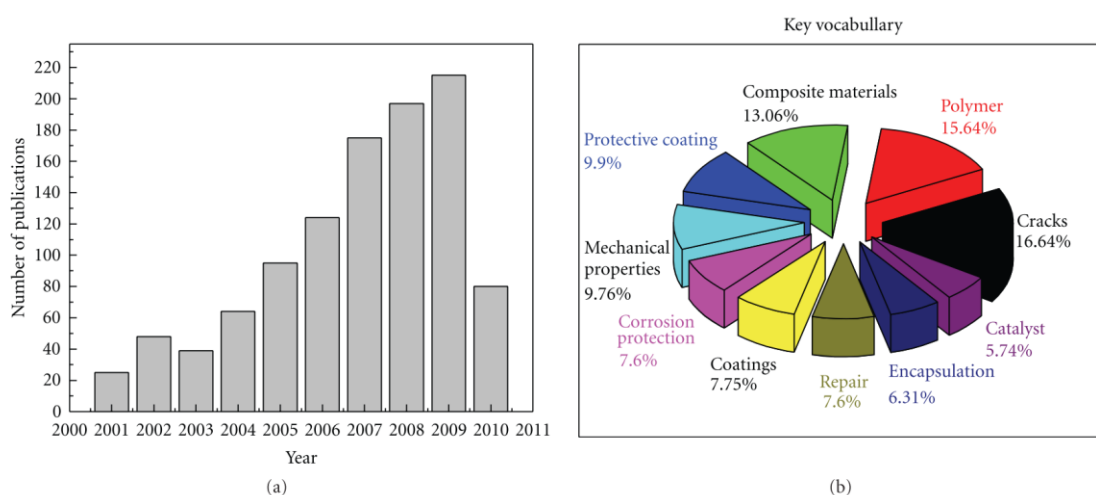


Figure 18: (a) Recent refereed publications related to the field of self-healing materials, together with (b) their corresponding distribution of the employed key words vocabulary. All published languages were included. Statistics are available from 2000 to August 2010 inclusively [8].

Methods for including the self-healing active agents include the encapsulation through microcapsules or microgels which can be included into the surface coating. The difference between the two methods is that microcapsules contain the active compound within a solid shell, whereas microgels are a single solid structure. Figure 19 shows the different structures of microgels and microcapsules.

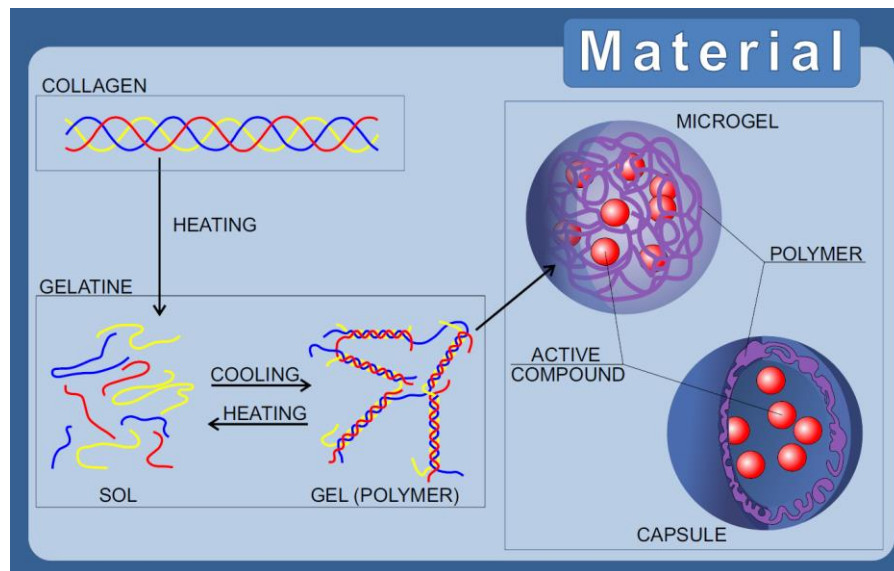


Figure 19: Schematic representation of gelatine microcapsules and microgels [55].

These microgels are typically smaller than 10  $\mu\text{m}$  in diameter and can be activated through mechanical or chemical triggers. However, the capsules must be in the tens or hundreds of  $\mu\text{m}$  in diameter to reliably rupture through a mechanical trigger and release enough active compound to activate the self-healing effect. A chemical method for triggering the release of the active compound can be pH activation, where an increase in pH leads to an increase in the permeability of the microcapsule [56], such as shown in Figure 20.

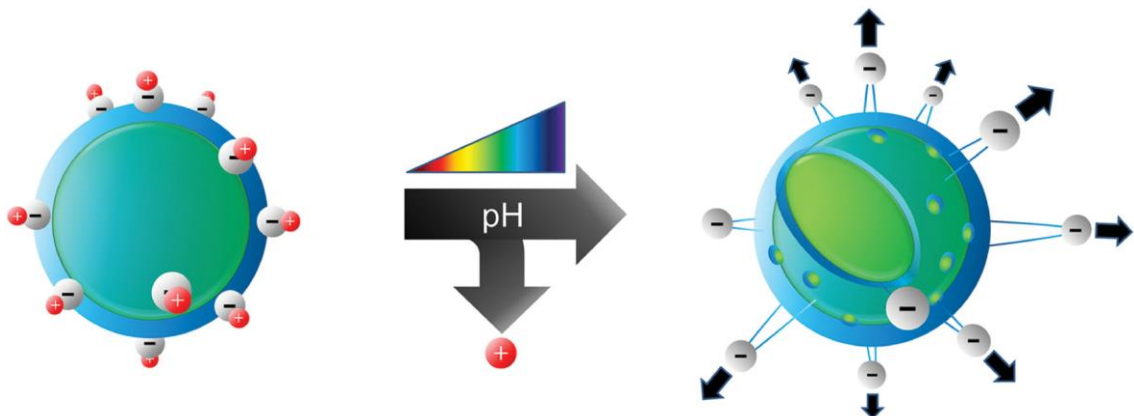


Figure 20: Schematic display of pH-triggered opening of PSMAA nanocapsules. Change of pH to higher values increases the permeability of the capsule shell and the release of the capsule content [56].

Whilst pH activation may be suitable for some applications, it may not be triggered by marine environments due to the relative neutrality of the salt water (7–8.5 pH). Figures 21 and 22 show the use of chloride ion triggers which would enable its use in the marine environment. This would trigger the release of the active compound, even if the coating had not been mechanically damaged. If the chloride ions penetrate the coating through defects or microcracks, the self-healing effect would still be triggered. If the metal ions such as  $\text{Ag}^+$ ,  $\text{Pb}^{2+}$  and  $\text{Ni}^{2+}$ , which are incorporated as crosslinking agents, contact the chloride ions of a corrosive substance, they are extracted and result in a reliable disintegration of the microgels [57].

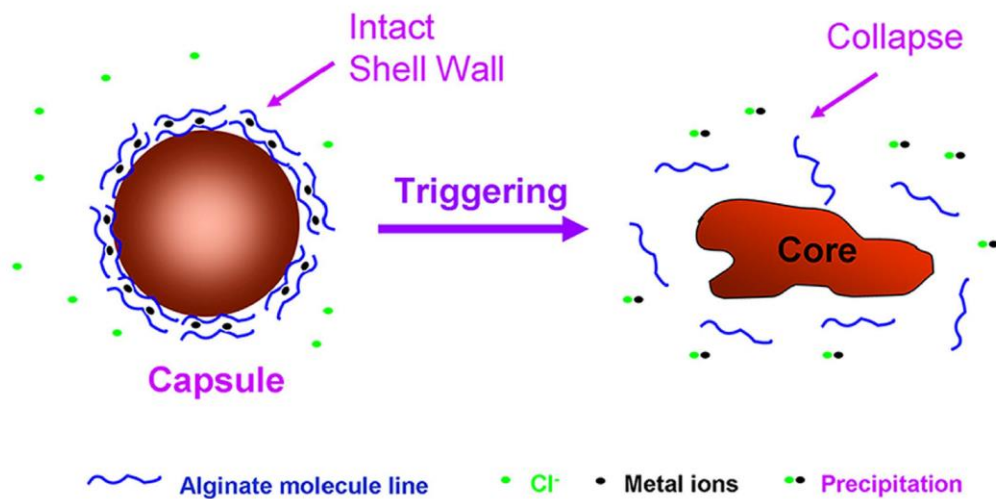


Figure 21: Schematic of capsules triggered by chloride ions [57].



Figure 22: a) Ag-alg capsules, b) Optical image of Ag-alg capsules, c) The Ag-alginate capsule that disintegrated when exposed to chloride ions [57].

## 2.5 Zeta Potential

The zeta potential is a physical property exhibited by all liquid–solid and liquid–liquid colloidal systems which refers to the charge of ions surrounding a particle. These anions and cations produce attractive and repulsive forces which lead to a diffusion with the slipping plane separating them. The zeta potential is defined by the difference in charge at the slipping plane [58][59]. Figure 23 shows a schematic representation of the slipping plane, and Table 3 shows the effect on particle stability at varying zeta potential voltages.

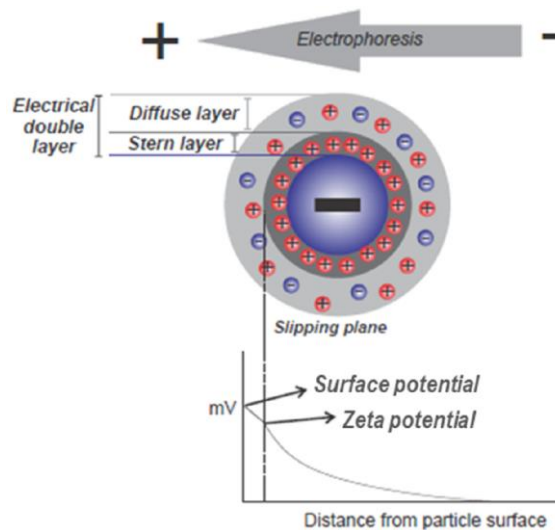


Figure 23: Schematic representation of the electrical double layer (EDL) and position of the slipping plane. The zeta potential is the electrical potential at the slipping plane [60].

Table 3: Stability of particles in relation to their zeta potential [61].

Stability Characteristics	Average Zeta potential (mV)
Maximum agglomeration and precipitation	0 to +3
Range of strong agglomeration and precipitation	+5 to -5
Threshold of agglomeration	-10 to -15
Threshold of delicate dispersion	-16 to -30
Moderate stability	-31 to -40
Fairly good stability	-41 to -60
Very good stability	-61 to -80
Extremely good stability	-81 to -100

## 2.6 Gelatine

Gelatine is a mixture of proteins and peptides produced from collagen, and is readily available due to its natural sources in domesticated animals such as cattle, chicken, and pigs. Gelatine has been used as a green corrosion inhibitor for copper, aluminium, and steel substrates. Haruna et al. [62] demonstrated that gelatine provides high corrosion inhibition efficiency on carbon steel in a 15 % HCl environment at 25 °C.

Gelatines low melting point of less than 40 °C has prevented its use with the electroless deposition technique. However, work performed by Fakirov et al. [63] has shown that when melting gelatine below its glass transition temperature, a direct crystal-glass transition occurs. This direct glass transition phase can be used to obtain highly ordered polymer glasses, increasing the temperature resistance of the gelatine [64].

This process can be demonstrated by performing a DSC (differential scanning calorimetry) on calve skin, as performed by Mukherjee et al. [63]. The resulting DSC scans are shown by Figure 24.

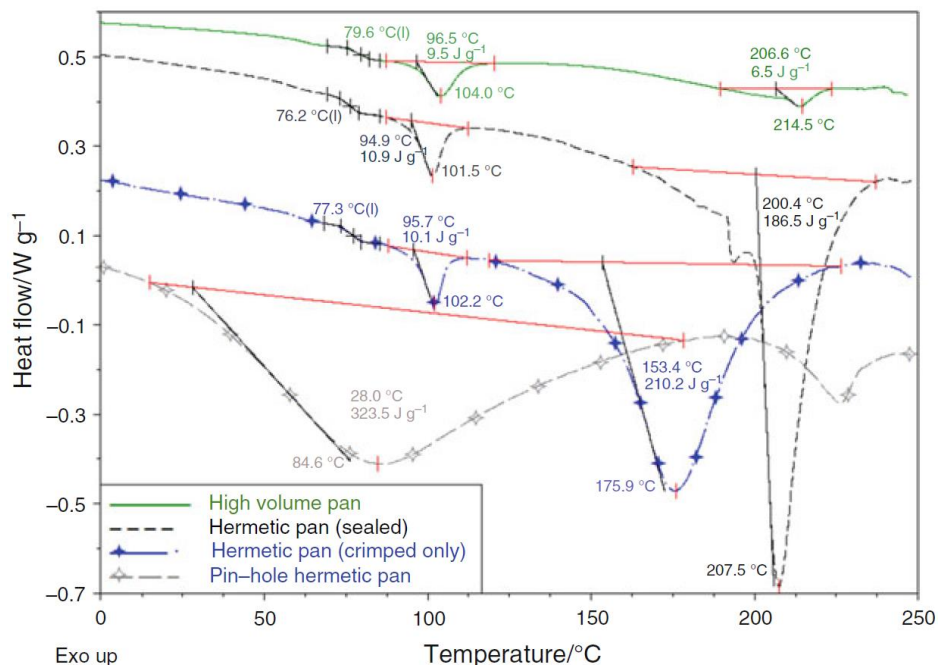


Figure 24: DSC scans of calfskin gelatine heated in four different types of DSC sample pans. Y-1 DSC heat flow normalised to unit mass sample [63].

## **3 Experimental Work**

### **3.1 Introduction**

The work carried out during this project can be separated into three phases: Low temperature depositions, High temperature depositions, and Analysis of NiP/Gelatine composite coatings.

The first phase of research focused on low temperature deposition, with the aim of co-depositing sodium alginate microgels containing active ingredients of NiP solutions. The requirement for a low temperature deposition solution was due to the limitation of sodium alginate microgels to survive at common ENP solution operating temperatures. Additionally, it would be beneficial at reducing the environmental impact associated with power requirements for heating and maintaining deposition bath temperatures. When it became apparent that this approach would require extensive research into ENP solution chemistry beyond the scope of this project, attention was pivoted to attaining high temperature depositions.

The second phase of research concentrated on high temperature co-depositions at 89 °C. Utilising heat-treated gelatine microgels enabled the use of readily available commercial ENP solutions. A procedure was developed for successfully co-depositing NiP/gelatine composite coatings. The presence of gelatine microgels within the coatings was confirmed using optical and fluorescence microscopy.

In phase three of the research project, the properties of NiP/gelatine microgel composite coatings were analysed. Coatings produced with 0.0125, 0.025 and 0.05 g/L microgel bath loadings, were compared with plain NiP samples. The impact on deposition rate and phosphorus content of the coatings was measured. Additionally, the corrosion prevention and tribological properties provided by the inclusion of gelatine microgels was analysed.

This chapter discusses the experimental procedure and apparatuses used for investigating the co-deposition of microgels with NiP and is presented in the order of operations performed.

1. Low temperature depositions.
  - 1.1. Sodium alginate microgel analysis.
  - 1.2. Commercial 1850 medium phosphorus solution variable testing.
  - 1.3. Bespoke low temperature solutions.
2. High temperature depositions.
  - 2.1. Gelatine microgel analysis.
  - 2.2. Gelatine co-deposition development.
3. Analysis of NiP/gelatine composite coatings.
  - 3.1. Standardised co-deposition procedure.
  - 3.2. Experimental Procedures for coating analysis.

## 3.2 Low Temperature Deposition

### 3.2.1 Microgels

Microgels as a delivery mechanism for corrosion inhibitors were explored in association with Wrocław University of Science and Technology. The development of microgels was being researched in Wrocław, and once the microgels were successfully produced they were received to be independently tested. Four batches of microgels were analysed to determine the viability of inclusion with nickel-phosphorus coatings produced via the electroless co-deposition process on mild steel substrates. Both investigations progressed independently, with an additional batch of microgels investigated for other applications by students at Napier University. Due to the nature of the microgel production, each batch received was novel and produced using different materials with production variables altered. Of the four batches of microgels received for investigation, three were produced from sodium alginate, and a single batch produced from gelatine. These microgels were manufactured using the water-in-oil emulsion technique (Figure 25) using corn oil with a dilute concentration of either gelatine or sodium alginate. The rate of mechanical agitation of the emulsion resulted in varying diameters of microgels. Most microgels were 2–6  $\mu\text{m}$ , however outliers smaller and larger than this range were present.

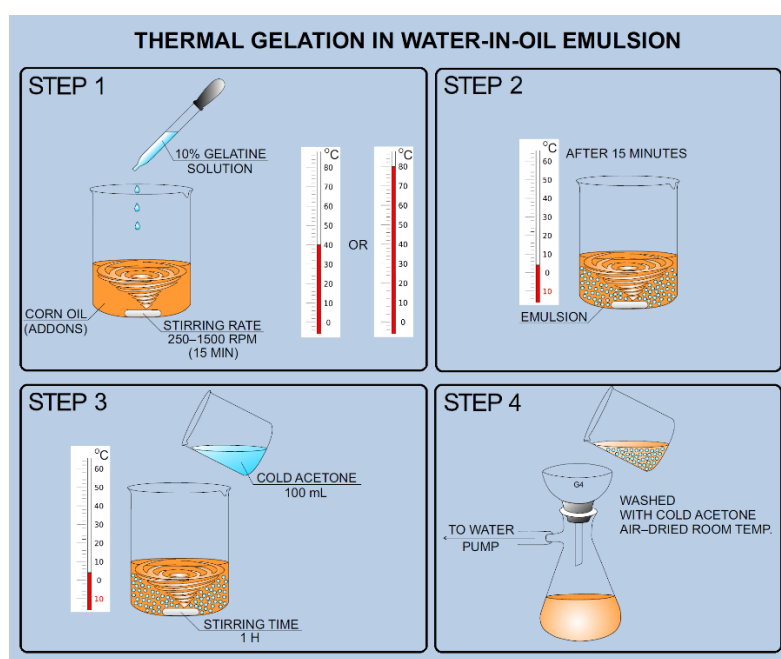


Figure 25: Gelatine microgel production using water-in-oil emulsion technique [55].

### Sodium Alginate

The sodium alginate microgels received for analysis consisted of three variants each with ~1 g dry weight. These microgels were produced to include the active reagents for electroless deposition of nickel-phosphorus, by incorporating nickel sulfate and sodium hypophosphite during the water-in-oil production method as described by Stankiewicz et al. [65]. The aim of which, was that when the coating was perforated, the microgels would break down due to exposure to salt water or other activation method and would trigger the release of the electroless nickel-phosphorus reagents. Through capillary action, the microgel reagents would travel to the extent of the crack/fissure whereby a fresh layer of electroless nickel would be deposited due to the autocatalytic nature of the electroless nickel-phosphorus reaction. With this technique it would be possible to achieve bespoke microgel manufacturing, whereby the resulting deposit of fresh NiP would match the existing Ni:P ratio of the surrounding metal matrix.



*Figure 26: Sodium Alginate microgels in as received state.*

Sodium alginate was selected as a material for microgel production as it is a suitable carrier for active corrosion inhibitors. Using sodium alginate is also less environmentally damaging than other materials which are used as microcapsules for delivery. The three variants of sodium alginate microgels (Figure 26) contained different sodium alginate sources. These were produced using synthetically manufactured alginate as well as from natural sources in the form of algae, again with focus on the environmental impact required for production.

Due to the use of sodium alginate for microgels production, this limited the use of common electroless nickel-phosphorus solutions as at temperatures above approximately 60 °C, whereby the sodium alginate would dissolve and lose structural stability.

The sodium alginate microgels were imaged optically and by Scanning electron microscope (SEM) using Leitz Aristomet Variophot and Cambridge Instruments Stereoscan 90 respectively. These microgels were in aggregations so proved difficult to image individually. The microgels were also analysed using EDXA (Energy Dispersive X-Ray Analysis) to measure the chemical composition of the microgels and the active ingredients which they incorporated. During SEM analysis, the samples experienced severe charging resulting in poor imaging and prohibiting the use of EDXA for atomic analysis. The charging was overcome by using physical vapor deposition (PVD) to give the microgels a layer of electrically conductive gold, enabling imaging using the SEM.

Microgels were imaged using a Leitz Aristomet Variophot optical microscope at 50–500x magnifications prior to the application of gold required for SEM analysis. For coating the samples with gold, a Polaron E5100 SEM coating unit sputter coating machine was used. This was operated using argon gas at voltage of 2.5 kV and current of 18–20 mA for 2 minutes. The microgels were then tested in the SEM and if the charging of the microgels continued, the process was repeated until a stable image could be captured and EDXA performed without the image and target point distorting.

The samples were then analysed using a Cambridge Instruments Stereoscan 90 (Figure 27). The scan was performed at 1340x magnification with acceleration voltage of 25 kV, working distance of 24 mm. The microgels oxygen, chlorine and nickel components were recorded for each microgels batch. The microgels carbon, hydrogen and sodium contents were rejected for analysis as due to limitations with the experimental set up providing negative percentage results.

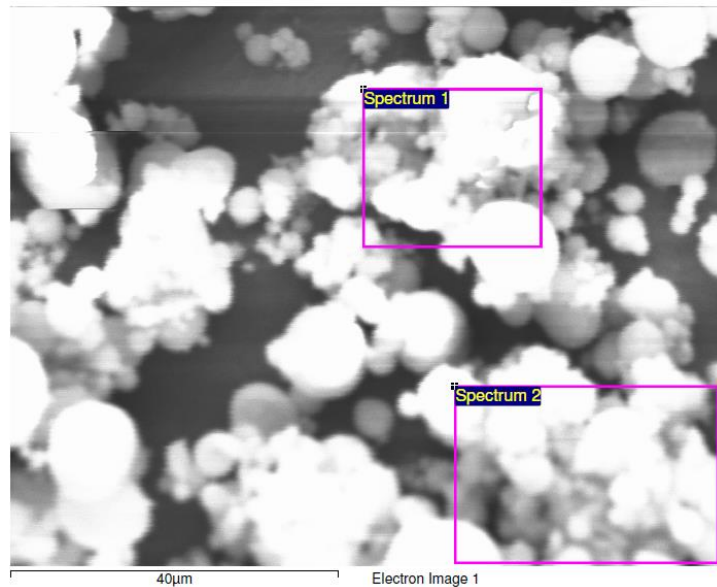


*Figure 27: SEM image (Cambridge Instruments Stereoscan 90) of sodium Alginate microgels used to perform EDXA.*

The microgels were then subject to an immersion test to determine what the impact of leaching components would have on the microgels after immersion in deionised water for 24 hours. 0.1 g of microgels were added to 20 ml deionised water in a capsule and shaken thoroughly to ensure complete immersion. The samples were then left for 24 hours at room temperature before being removed and filtered. The samples were filtered using vacuum filtration and a Büchner funnel with Gelman Laboratory Supor 200 membrane filter paper with filter size of 0.2 µm. The sodium alginate microgels were air dried over night before being collected, by scraping the recovered microgels off the filter paper onto a watch glass. The recovered microgels were imaged using optical microscopy the same as before the immersion test. The microgels were difficult to image as due to the filtering process, the microgels had aggregated into large flakes. Some samples appeared to have no identifiable microgels, with only crystalline shapes visible, others showed clear microgels however they were in larger aggregates (Figure 28).

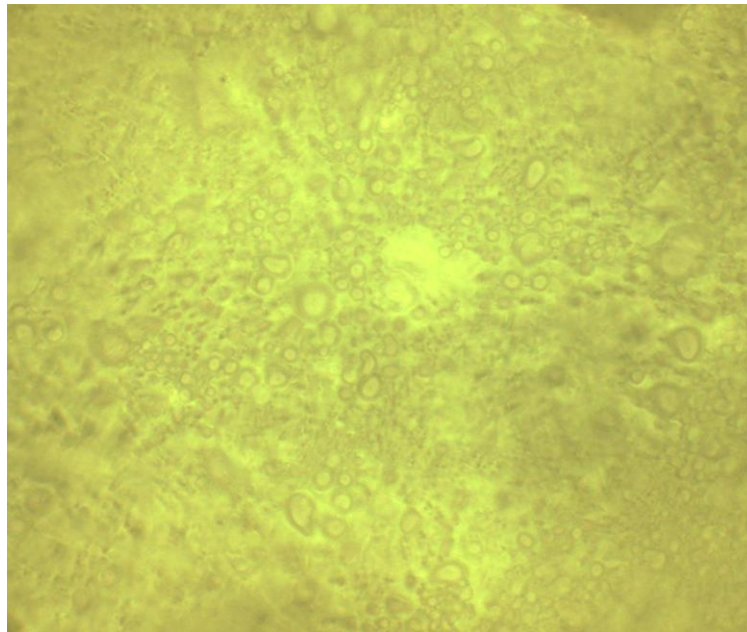


*Figure 28: Dried sodium alginate microgels in large aggregations post immersion test. Image captured at x100 magnification.*

The recovered microgels were then sputter coated using the same technique as previously described and were imaged on the SEM using as close to the same settings as could provide suitable imaging. The microgels were then analysed using EDXA to determine if the atomic constituents had changed in concentration. These results were then compared with the results from before immersion to determine, as a percentage relationship, which concentrations of the components leaked. The results of this test provided useful information regarding which microgel variant to select for trialling co-deposition. The sample with the smallest losses would likely be the most stable during the deposition process and exposure in use, however may be less likely to release the active reagents for the electroless deposition when required.

### 3.2.2 Commercial 1850 Solution Variable Testing

As the sodium alginate microgels would not survive temperatures higher than 60 °C, it was necessary to develop a technique for applying electroless nickel-phosphorus at lower temperatures. One approach to this is by altering an existing electroless nickel solution to achieve higher deposition rates, so that the deposition rates at lower temperatures would be more suitable. Schloetter Slotonip 1850 medium phosphorus electroless nickel solution was selected for analysis. This solution was selected as the author had previous experience using the solution in co-deposition applications and it produced bright, medium phosphorus deposits. The solution remained stable during depositions for up to and exceeding 1 hour which would provide a coating thickness of approximately 20 µm. The manufacturer of 1850 solution also provides clear operating parameters for the deposition process, which includes troubleshooting advice when issues occurred with the resulting coatings. This provided useful insight to how the parameters that were to be tested may impact the coating quality.

#### Temperature

The first deposition parameter investigated was temperature. As the 1850 solution included stabilisers, it would not react and produced depositions without suitable activation energy in the form of temperature. The deposition rate at temperatures less than the specified operating range were tested. This was performed at 70, 75 and 80 °C and was compared to the recommended 89 °C for control. These depositions were performed using solution produced in one batch and on mild steel samples coupons which had been prepared using pre-catalyst and catalyst.

The mild steel coupons with dimension 30 x 25 x 0.81 mm were pickled using 10 % HCl solution at 55 °C for 2 minutes. This removed any oxide layer that was present on the surface which could impact the deposition adhesion quality. Once free of any oxide layer, the samples were prepared using a two-step colloidal catalyst. The samples were first degreased using coprolite X-96 DP-B cleaner-conditioner operated at 30 °C for 5 minutes with mechanical agitation using magnetic stirrer bar. The samples were then removed and rinsed with deionised water and prepared using two-step Uniphase PHP colloidal catalyst based on palladium and tin with high catalytic activity.

Pre-catalyst solution was operated at room temperature for 2 minutes, and the catalyst solution at 35 °C for 5 minutes.

The samples were plated using the 1850 solution at 4.9 pH (manufacturer specified optimal) and temperatures of 70,75,80 and 89 °C for 30-minute depositions. The bath size was kept at 200 ml each test to ensure the same bath surface area loading between tests. The temperature was controlled using temperature feedback probe IKA ETS-D5 electronic contact thermometer, operating on IKA C-MAG HS 7 magnetic stirrer hot plate (Figure 29). To ensure the temperature of the solution was kept constant and to aid in hydrogen evolution removal, mechanical agitation was supplied using magnetic stirrer bar operating at MOT 1 which equates to 180 rpm. After the 30-minute deposition, the samples were removed from the solution and submerged in deionised water to stop the reactions, the sample was then air dried using a blower at room temperature.

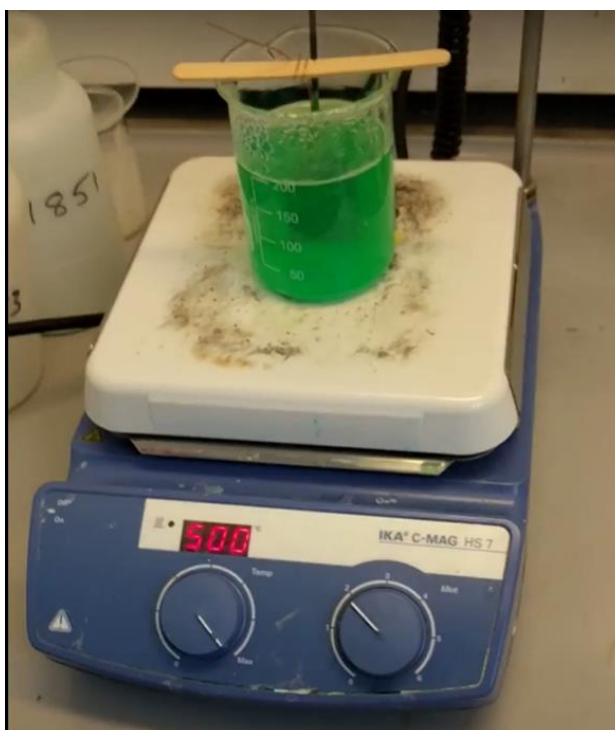


*Figure 29: Example of experimental set up for producing electroless deposition using IKA hot plate with mechanical agitation.*

### Solution pH

In addition to investigating the deposition rate at temperatures outside the manufacturers specified range, the deposition rate of solutions with altered pH were also tested. The deposition rates were measured using 1850 solution operating at pH 3.9, 5.9, 7.0, 8.0 and with the optimal 4.9 pH for control. The solutions were produced from a large batch of 1850 solution and the pH was adjusted accordingly using the specified HCl (hydrochloric acid) and H<sub>5</sub>NO (ammonium hydroxide).

The depositions followed the same plating process as for the temperature test, of 10 % HCl 2-minute pickle, pre-catalyst for 2 minutes at room temperature, catalyst at 35 °C for 5 minutes, into the 1850 solution at 89 °C for 30 minutes.

### Ultrasonic Agitation

The use of ultrasound to assist in deposition rate was also investigated. The aim was to use ultrasonic agitation to increase deposition rates and aid in co-deposit dispersion. Two experimental set ups were tested for their viability as deposition baths. The first to be tested, used a Grant Instruments XB2 ultrasonic water bath (Figure 30) operating between 30–45 kHz. 200 ml beaker of 1850 solution was suspended in the ultrasonic water bath along with a heating element which controlled the temperature of the water bath. A target of 89 °C was to be used for this test however, due to losses in the system, a maximum temperature of 82 °C was attained in the plating solution. The sample was prepared using pre-catalyst and catalyst as per the established preparation technique. After 30 minutes, the sample was removed, and coating thickness measured.

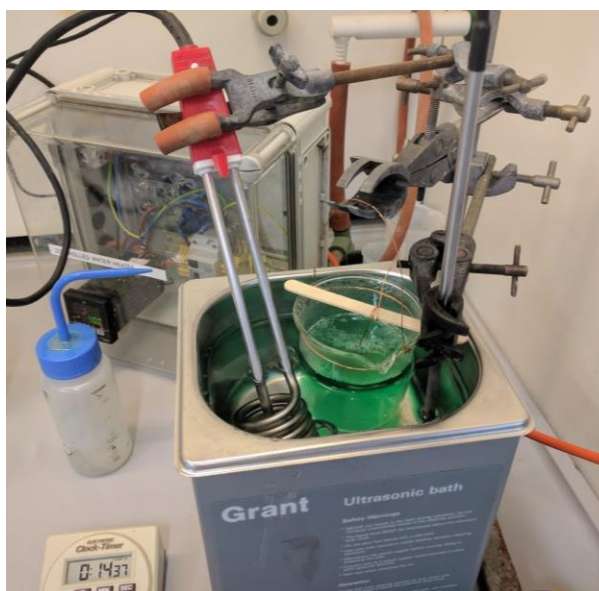


Figure 30: Experimental set up of electroless nickel deposition using ultrasonic agitation.

The samples that were produced showed dull areas on the coatings which could be due to standing waves within the ultrasonic bath. As a result, another method for applying ultrasonic agitation was investigated. This consisted of using Hielscher UP 200S with a micro tip S7 sonotrode. This operated at 24 kHz and was set to 100 % amplitude and cycle time of 1. Whilst the inclusion of ultrasound at frequency less than 28 kHz could lead to pitting [41], the test was performed as a proof of concept with the focus on deposition rate. The sample was pretreated using established catalytic preparation technique. The test was performed at 65 °C however, the coating was affected by the size of the ultrasonic cone from the sonotrode which meant it would not be feasible to plate a full sample with this experimental apparatus.

### Coating Thickness

To determine the coating thickness achieved by altering the deposition variables, both non-destructive and destructive testing were employed. An Elcometer 456 coating thickness gauge with touch probe was used to measure the coating thickness non-destructively. This probe was calibrated using 23.4  $\mu\text{m}$  and 50.0  $\mu\text{m}$  calibration foils (the thinnest available) before each sample batch. The probe would give readings  $\pm 2.5\%$ . Each sample was subject to ten readings to ensure suitable accuracy in the measurement.

As well as the non-destructive testing, the accuracy of the measurement was verified using cross-sectional analysis. One sample from each batch of coatings was selected, and the coating thickness measured at six sites to confirm uniformity of deposit thickness. To prepare the samples for cross-sectional analysis, they were cut using Struers Accutom-5 cutting machine, and the cross sections were set using Metprep two-part epoxy resin (Figure 31). Once the samples had cured, the cross-sections were ground using Struers Tegrapol-21 with Tegraforce-5 attachment.



*Figure 31: Cross-sections prepared in epoxy resin.*

The samples were prepared using MD-PIANO 120,220,600 and 1200 grit abrasive disks. Each stage was performed with water and 50 N applied force at 300 rpm for 5 minutes. Once suitable material had been removed, the surface was polished using hand pressure and 9,6, and 3  $\mu\text{m}$  diamond slurry until the previous stages score marks had been removed. Once the surface had been prepared using the finest abrasive, it was etched with Nital 2 % methanol for 30 seconds. This provided a clear separation between the ferrous substrate and the nickel coating. The samples were then imaged optically using the Leitz Aristomet Variophot microscope at 50x and 500x magnifications.

### 3.2.3 Bespoke Low Temperature Solutions

As commercial ENP solutions include stabilisers to prevent reduction reactions below the targeted operating conditions, it would be difficult to reduce the activation temperature sufficiently for sub-60 °C depositions. As a result, bespoke low temperature solutions were investigated. A series of five solution types were produced and the deposition process was evaluated for the coating quality, deposition rate, and ease of use. Each solution type was used to perform a minimum of six depositions.

#### Solution 1

Five solutions were investigated however did not produce stable reactions for depositing electroless nickel. One such solution tested was:

- Nickel sulfate hexahydrate - 0.15 mol/L (39.2 g/L)
- Sodium hypophosphite monohydrate - 0.2 mol/L (20.8 g/L)
- Tri-sodium citrate dihydrate - 0.1 mol/L (29.6 g/L)
- Solution pH - 9.0 adjusted with H<sub>5</sub>NO
- Temperature - 70 °C

This solution was tested with two sample variants, one prepared using catalyst and the other only pickled using 10 % HCl. After substrate preparation the samples were introduced to the solution at 30 °C. The solution temperature was then increased in 5 °C increments whilst observing the deposition process. Hydrogen evolution was used for identification of deposition reactions, at which point the solution temperature would be held and a deposition performed to determine deposition rate. This solution proved to be unstable, with either no hydrogen being observed, or hydrogen observed followed by rapid solution break down, in which the entire plating vessel would be plated, and the solution produced black foam.

## Solution 2

To prevent the breakdown of the solution into black foam, the complexor used in the solution was altered to determine how this would affect the deposition characteristics. Tri-sodium citrate was replaced by Glycine as a complexing agent and nine variations of the solution were tested. The base solution was:

- Nickel sulfate hexahydrate - 30 g/L  $\pm$  10 g/L
- Sodium hypophosphite monohydrate - 30 g/L  $\pm$  10 g/L
- Glycine - 30 g/L  $\pm$  10 g/L
- Solution pH - 7.5 adjusted with H<sub>5</sub>NO
- Temperature - 50 °C

Due to the autocatalytic nature of electroless nickel, and that ferrous material also activates the reaction, the samples were prepared only using HCl 10 % pickle at 55 °C for 2 minutes before being plated in the solutions at 50 °C. It was found through testing that the difference in the deposition rates between samples only pickled and those with catalytic preparation, were negligible and did not impact on the ability of the solution to produce a deposit on mild steel substrates.

To determine which variable of the solution had the greatest impact on the deposition rate, the constituent parts were tested by increasing and decreasing the solution loading by 10 g/L. The other variables were all kept constant during this testing. The depositions were performed for 30 minutes after which, coating thickness was measured using Elcometer 456 coating thickness gauge. This solution proved more stable than the previously tested citrate complexor based solution with no failures to plate and hydrogen evolution observed in the solutions.

### Solution 3

Sodium citrate was investigated again to determine if using ultrasound would produce a useful deposition rate. Using a solution described by Nwosu [61], the following solution was tested:

- Nickel sulfate hexahydrate - 15 g/L
- Sodium hypophosphite monohydrate - 12.5 g/L
- Tri-sodium citrate dihydrate - 12.5 g/L
- Ammonium sulfate - 25 g/L
- Solution pH - 9.5 adjusted with H<sub>5</sub>NO
- Temperature - 60 °C

It was found that using this solution, a stable deposition could be achieved at 60 °C. Samples with and without catalyst were tested to determine if the deposition would occur without requiring the extra steps of the catalyst process. It was found that the catalyst was not required for the deposition to occur. Using ultrasound to increase the deposition rate was investigated with this bath (Figure 32). The use of an ultrasonic probe increased the temperature of the solution, so this was controlled via air cooling the solution. By closing the fume cupboard door and increasing flow rate of air passing over the beaker of solution, it was possible to maintain a solution operating temperature of  $60 \pm 2$  °C. The depositions were performed for 1 hour using Hielscher UP200s with S7 sonotrode operating at 100 % amplitude and cycle time. The resulting coatings were visually inspected, and coating thickness measured using Elcometer 456 thickness gauge.



Figure 32: Deposition of solution 3 using ultrasonic sonotrode.

#### Solution 4

Another low temperature solution described by Khan et al. [66] was trialed, as the deposition rate at low temperatures was appealing for the role.

- Nickel sulfate hexahydrate - 30 g/L
- Sodium hypophosphite monohydrate - 40 g/L
- Tri-sodium citrate dihydrate - 40 g/L
- Solution pH - 9.0 adjusted with H<sub>5</sub>NO
- Temperature - 50 °C

Two variants of samples were plated, one with and the other without catalyst treatment. The coating produced good hydrogen evolution however after 1 hour had severe coating delamination. Variations of the plating parameters were tested, such as adjusting pH more regularly which resulted in less severe but still present delamination. Adjusting the order in which the constituent parts of the solution were added was also tested and this reduced the frequency but did not eliminate the occurrence of coating delamination. The deposits were visually inspected after deposition, but it was not possible to use coating thickness to get accurate repeatable measurements due to coating delamination.

#### Solution 5

From Mallory and Hajdu [29], a sodium pyrophosphate bath was referenced which could provide the desired deposition rate at low temperatures. The solution was:

- Nickel sulfate hexahydrate - 25 g/L
- Sodium hypophosphite monohydrate - 25 g/L
- Sodium pyrophosphate - 50 g/L
- Solution pH - 10.5 adjusted with H<sub>5</sub>NO

The solution proved unstable and would not maintain steady deposition. Five of fourteen depositions resulted in solution plating out and demonstrating run away reaction coating the entire beaker. By altering the production method of this solution, it was possible to maintain a deposition for over 30 minutes, an increase from less than 5 minutes. This was achieved by, producing the solution in the following order:

- |                                       |   |                                     |
|---------------------------------------|---|-------------------------------------|
| 1. Nickel sulfate                     | - | Salt                                |
| 2. Sodium pyrophosphate               | - | Complexor                           |
| 3. Adjust to target pH                | - | pH 10.5                             |
| 4. Sodium Hypophosphite               | - | Reducer                             |
| 5. Adjust to target pH at temperature | - | pH 10.5 at appropriate temperature. |

To ensure the optimal deposition surface, the samples were treated in pre-catalyst and catalyst prior to deposition. The resulting depositions were for 1 hour; however, the solution would often break down and plate out after 30 or 40 minutes. Additionally, the produced samples would show severe delamination on the surface after 30 minutes of deposition. The successful depositions were achieved using this technique and operating at 60 °C. By keeping the pH above 10–10.5 ensured that delamination of the coating did not occur and produced deposition rates exceeding all other solutions used. The coating was investigated and imaged using SEM and EDXA testing, however it was noted that the coatings exhibited severe porous structure when imaged using SEM. This resulted in a cease in testing using the pyrophosphate solution as the coating was to be used for corrosion prevention. Additionally, breakthroughs in the production of gelatine microgels were investigated which permitted their use in higher temperature solutions. This would provide more stable electroless solutions with proven applications could be employed in the co-deposition process.

### 3.3 High Temperature Deposition

#### 3.3.1 Microgels

An alternate form of microgel was also received which was produced from gelatine with a dry weight of ~3.5 g. Whilst the gelatine microgels did not include any active ingredients, they could be tailored at a later date if the technique for their inclusion proved viable. The gelatine microgels measured 2–6  $\mu\text{m}$  in diameter. Due to the gelatine construction, these microgels would dissolve at low temperatures and would not survive deposition in solutions of even 40 °C. The thermal resilience of the gelatine microgels were increased by heat treatment process (Figure 33). This permitted their use in solutions at elevated temperatures which would be necessary for co-depositions in common electroless nickel solutions.

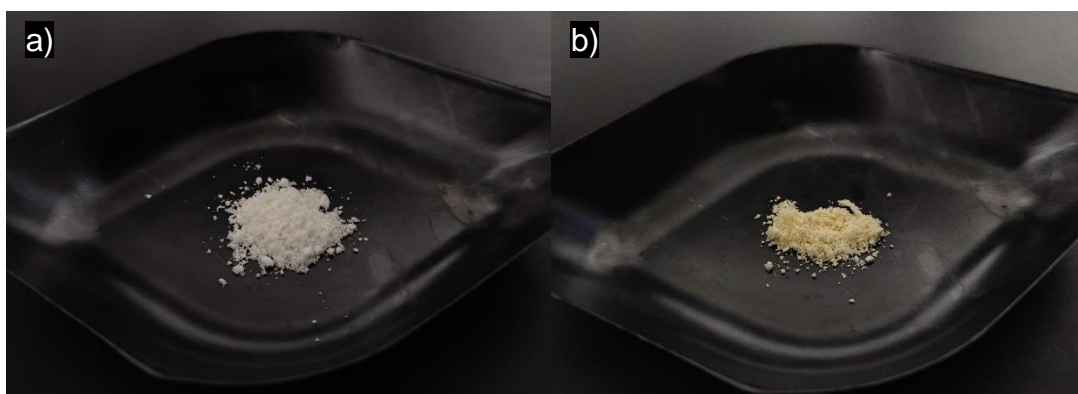


Figure 33: Gelatine microgels a) as received, b) post heat treatment.

#### Heat Treatment

To increase the gelatine microgels temperature resistance, they were heat-treated at 150 °C for 15 hours. To confirm that the heat-treatment had been successful, the microgels ability survive the deposition environment was evaluated. Gelatine microgels were imaged using Leitz Aristomet Variophot optical microscope before and after heat treatment to confirm their appearance before being subject to the test.

The microgels were then subjected to the ENP solutions at temperatures of 89 °C and 4.90 pH for 1 hour. A bath loading of 0.1 g/L was used for each test and on completion of the deposition, the solutions were filtered and imaged using same equipment to determine if any microgels had survived intact.

Four variations of this test were performed:

1. As received gelatine with mechanical agitation
2. As received gelatine with ultrasonic agitation
3. Heat-treated gelatine with mechanical agitation
4. Heat-treated gelatine with ultrasonic agitation

Mechanical agitation employed the use of a magnetic stirrer bar at 300 rpm and IKA C-MAG HS 7 hot plate. Ultrasonic agitation was provided using a beaker suspended within a Grant Instruments XB2 ultrasonic water bath with heating element.

### Microgel Size

The particle size distribution was listed as 2–6  $\mu\text{m}$  in diameter by the producer. To confirm this, the microgels analysed using a Malvern Zetasizer-nano to scan the particles when suspended in deionised water. The results of this test proved inconclusive as the zetasizer could not accurately determine the particle size. This was due to the fluorescing of the microgels, as when illuminated with the light beam they fluoresced, which the zetasizer identified as contamination on the outer case of the test cell. Fifteen repetitions of this test were performed ensuring that there were no contaminations, however the same failures continually reported, which led to the alternative method of SEM imaging for measurement being employed. It is also noted that with a size range of 2–6  $\mu\text{m}$ , the microgels were of a difficult to determine size using the available equipment. The zetasizer nano would be best suited to smaller particles as the specifications for the device allow for samples from 0.3 nm to 10  $\mu\text{m}$ . However, due to the lab-based production of the microgels, and the presence of aggregations, some outliers were larger than 10  $\mu\text{m}$  and would cause inaccurate readings when measuring size.

To counter this and ensure that the microgels were of the correct size, they were investigated using a Tescan Vega 3 scanning electron microscope. To prevent charging, the microgels were first coated with gold using Polartron E5100 sputter coater. The size of microgels before and after heat treatment was determined by analysing the SEM images and recording 160 individual measurements.

### Zeta Potential

The zeta potential of both as received and heat-treated microgels were investigated using Malvern Zetasizer-nano. Due to gelatines low temperature survivability, a larger range of pH was investigated with non-heat-treated gelatine. 3 g/L microgels were added to deionised water and ultrasonically agitated using a Hielscher UP 200S with a micro tip S7 sonotrode for 30 seconds. The pH of the microgel solution was altered with hydrochloric acid and ammonium hydroxide to achieve test pH of 4.1, 5.1, 7.4 and 10.0. These pH ranges may be required to achieve suitable depositions at low temperatures. The zeta potential measurement was repeated for each pH level twenty-five times.

For the heat-treated gelatine microgels, a narrower pH range as investigated as the microgels were to be used with 1850 ENP solution operating at 4.9 pH. Following the same preparation procedure as non-heat-treated microgels, a minimum of ten zeta potential measurements were recorded for solution pH of 4.4, 4.9, 7.0 with microgel concentration of 2.2, 3.0 and 6.0 g/L respectively.

### **3.3.2 Gelatine Co-deposition Development**

As the gelatine was heat treated, enabling its use in higher temperature solutions, 1850 medium phosphorus solution was selected for the co-deposition. This solution was selected as it proved extremely stable when altering the solution variables, with no solution breaking down or plating-out like the alternate solutions tested. Additionally, the solution provides a bright nickel medium phosphorus deposit which aids in coating analysis, as the morphology of the surface makes irregularities due to the inclusion of microgels more readily identifiable.

To begin the co-deposition process, the microgels were heat treated in large batches to reduce any variance in preparation. Co-depositions were performed using techniques known to work for SiC co-depositions carried out by the author in previous laboratory work. 200 ml of 1850 solution were operated at 89 °C with a pH of 4.9, within the optimal settings as described on the data sheet for the solution. 1 g/L was first tested, by adding 0.2 g microgels to the solution 1 minute prior to the sample being added. The samples were prepared using

pickle only, as 1850 solution has no issues depositing on plain mild steel. Once at 89 °C, the microgels were added slowly to the solution. The rpm was set to MOT 2 = 465 rpm using magnetic stirrer bar, as the microgels would float on the surface of the solution and aggregate without sufficient stirrer rpm.

The samples would fail to be coated when microgels were present in the solution prior to the addition of the substrate. To counter this, the samples were plated for 15 minutes in the plain 1850 to achieve a nickel base layer of 5 µm before the microgels were added. This ensured the electroless deposition was in an active state and was functioning correctly. The resulting coating showed aggregations on the surface and lower than expected deposition rates. The samples also showed a reduction in the coating at the edges of the sample which should not occur in normal plain 1850 deposition (Figure 34).



*Figure 34: NiP/gelatine composite coating with reduced deposit thickness at edges. Coupon dimensions = 25 mm x 30 mm.*

To increase the deposition rate, ultrasonic agitation was employed. This was performed using the Grant XB2 ultrasonic bath with similar experimental set up as previously tested. The resulting plating's failed to deposit coatings on the samples, even after the samples had 5 µm nickel base coat. This was likely due to insufficient agitation as microgels were observed on the surface of the deposition solution. A lower bath loading of 0.5 g/L heat treated gelatine microgels was then attempted. The samples were plated at 89 °C for 20 minutes using IKA hotplate before transferring for use in ultrasonic baths, this test was repeated four times using variations on the solution loading of 0.5 and 0.25 g/L.

Some success was had using lower microgels concentrations as well as ultrasonically processing the microgels in deionised water before adding the microgels suspension to the deposition bath.

To get suitable, higher deposition rate co-depositions, the concentration of microgels was reduced. These depositions were performed using 1850 at 89 °C for 1 hour and pH 4.9. The substrates were prepared without the use of catalyst and a 15-minute base coating was performed before the deposition. Reducing the microgel concentration resulted in increased deposition rates. However, the microgels were not evenly distributed and aggregations were present on the surface of the samples leaving pits where they had inhibited the reaction sites and prevented deposition (Figure 35).

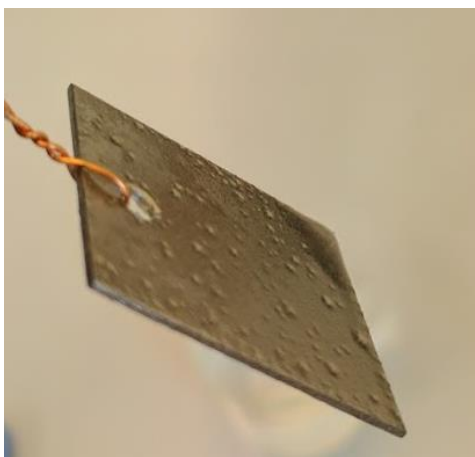


*Figure 35: NiP/gelatine composite coating with large gelatine aggregations on surface post deposition.  
Coupon dimension = 25 mm x 30 mm.*

To negate this, the microgels were ultrasonically processed in deionised water. The required quantity of microgels were added to 20 ml of deionised water, and ultrasonically processed using a Hielscher UP 200S with a micro tip S7 sonotrode. This was performed at room temperature for 5 minutes prior to deposition and for 30 seconds before each addition to the plating solution. The microgels were added at 15-minute intervals, in 5 ml batches, ensuring that no aggregations were present. This resulted in coatings without aggregations, that experience deposition rates higher than without ultrasonically processed microgels (Figure 36). 5 ml of microgel solution was added in 15-minute intervals which replenished the solution of losses due to evaporation.

The coating deposition rate was measured using Elcometer 456 coating thickness gauge and was confirmed with cross-sectional analysis performed on one coating per deposition type across six sites. Coating composition was also measured using EDXA to determine what effect the gelatine microgels had on the nickel to phosphorus ratio.



*Figure 36: High quality NiP/gelatine composite coating produced with ultrasonically processed microgels.  
Coupon dimension = 25 mm x 30 mm.*

### Fluorescence Microscopy

To confirm that heat-treated gelatine microgels survived the deposition process, the surface of the coatings was investigated using fluorescence microscopy using an Olympus BX53M microscope. To ensure the heat-treated gelatine microgels would fluoresce, dry microgels were imaged both with visible and 400 nm ultraviolet light. Once this had been confirmed, the NiP/gelatine composite coatings with bath loadings 0.0125, 0.025 and 0.05 g/L gelatine were imaged. Three samples for each coating variation were inspected at x5, x10 and x20 magnifications using white light for colour (RGB), and ultraviolet light for fluorescence images. The images were then composited using Olympus cellSens software to confirm the objects fluorescing matched the location of microgels observed on the coating surface.

In addition to confirming that microgels survived the plating process and were present on the surface of the coating, issues with depositions were also investigated. During the deposition process, microgels would aggregate and would adhere to the surface of the coating. This would block the reaction sites and prevent the reduction reaction from occurring, leaving depressions in the coating surface and avenues for corrosion to permeate. Images captured using Leitz Aristomet Variophot optical microscope with white light were compared with similar images captured on Olympus BX53M fluorescent microscope to confirm the presence of microgels within these depressions.

### **3.4 Analysis of NiP/Gelatine Composite Coatings**

#### **3.4.1 Standardised Co-deposition Procedure**

##### Plating solution

Commercial electroless nickel solution was chosen to carry forward testing of the co-deposition technique. Schloetter Electroless Nickel SLOTONIP 1850 is a bright, medium phosphorus self pH regulating electroless nickel solution. The solution employs sodium hypophosphite as a reducer and as such produces a nickel-phosphorus content of 6–9 wt% P. With the optimum operating conditions of 89 °C and 4.9 pH, the solution has a plating rate of 20 µm/hr.

##### Substrate Preparation

The substrates used for the depositions were coupons of mild steel. These coupons were cut from larger Q-panels which consisted of ISO 3574 steel comprising of 0.60 % Mn, 0.15 % C, 0.035 % S and 0.030 % P. The dimensions of the coupons were 30 mm x 25 mm x 0.81 mm for plating with NiP/Gelatine composite coatings.

To prepare the substrates for the deposition process, the coupons were degreased using an acetone rub. This ensured the surface was free from any contaminants. After this stage, the coupons were pickled using 10 % hydrochloric acid at 55 °C. The coupons were placed in the acid for 2 minutes to remove any oxidation on the surface and prime the sample for deposition.

As steel is catalytic to the electroless nickel deposition process, the surfaces did not need to be sensitised by using a catalyst. Instead, the coupons were rinsed in deionised water after the acid pickle and placed straight into the electroless nickel plating solution.

### Electroless deposition

To plate the coupons, deposition baths containing 200 ml of 1850 solution were used operating at 89 °C and with a pH of 4.9. To plate the plain nickel-phosphorus samples, the deposition was performed for 1 hour. For the co-deposition procedure, the samples were plated in plain NiP solution for 15 minutes to ensure an even base coating of 5 µm thickness.

After 15 minutes, the microgels were added to the solution to begin the co-deposition process. This was achieved by adding 5 ml of gelatine microgels suspended in deionised water dropwise at 15-minute intervals. This ensured that the addition of the microgels did not overload the substrate and inhibit the reaction sites.

### Microgel Preparation

Gelatine microgels were heat treated at 150 °C for 15 hours to increase their resilience to elevated temperatures of the electroless deposition process. These microgels, measuring from 2–6 µm, were suspended in 20 ml of deionised water and ultrasonically processed. This ensured that there were no aggregations of microgels that would attach to the substrate surface and inhibit deposition. For the co-deposition, the appropriate quantity of microgels for 200 ml of plating solution were ultrasonically processed before addition to the deposition bath. This was done incrementally to ensure the solution was not overloaded, preventing reduction reactions. The microgels were ultrasonically processed for 5 minutes to ensure the removal of aggregates and aid in even co-deposit dispersion. Ultrasonic processing was performed using Heilscher UP200S and S7 sonotrode. The processor was operated with pulse and amplitude settings of 0.75 and 90 % respectively. The microgel suspension was again processed for 30 seconds prior to each subsequent addition.

### 3.4.2 Experimental Procedures

#### Neutral Salt Spray

Samples were produced for corrosion analysis using a neutral salt spray test. This test was performed over the course of 96 hours and was performed on twelve samples total. Four varieties of coating were subject to this test to determine the effectiveness of the co-deposited gelatine microgels in aiding in resistance to corrosion. The coatings used for this test were plain NiP for a control, NiP+0.0125 g/L gelatine, NiP+0.025 g/L gelatine and NiP+0.05 g/L gelatine microgel co-deposit.

The test was performed in accordance with ISO 9227:2017 Corrosion tests in artificial atmospheres – Salt spray tests. The salt spray solution used for this test was at a concentration of 50 g/L NaCl dissolved in deionised water. The test was performed CW SF/200/CCT Cyclic Corrosion Test Cabinet. To prepare the chamber for the test, it first had to be calibrated to ensure that it was operating to the desired standard. To ensure that the correct flow rate was used for the spray, the mist inside the chamber was collected and measured. This was performed using two funnels of 80 cm<sup>2</sup> located separately within the chamber which would record the quantity of spray for the associated flow rate, which was set to 0.025 L/hr. The chamber was run over night and the resulting quantity of spray was measured and compared with guidelines specified in the standard. The target collection for the period of 19 hours in which the test was performed was 28.5 ml ± 9.5 ml. The actual recorded collection was 26 ml for the funnel in the centre of the cabinet and 27 ml for the corner of the cabinet. This proved that the chamber was operating at the correct mist levels.

To confirm the correct corrosivity of the cabinet, uncoated S-35 Q-Panels with dimensions 0.81x76x127 mm were tested for 48 hours in the chamber. The edges of the Q-Panels were masked with epoxy leaving 60 cm<sup>2</sup> (60x100 mm) area exposed for corrosion test (Figure 37). After 48 hours, the corroded samples were removed from the chamber and the corrosion was removed using an abrasive slurry of 20 % by volume SiC in deionised water and a brush. The resulting change in mass before and after the corrosion had been removed was calculated as an average for surface area. The results of this confirmed that the corrosion rate was 65.82 g/m<sup>2</sup> which again was within standard.



*Figure 37: Plain mild steel S-35 Q-Panel used to confirm corrosion rate of cabinet. Area of corrosion = 60 mm x 100 mm.*

To ensure an even area of coating was exposed to the salt spray, Gamry 990-00254 PortHole electroplating tape was used which fully enclosed the samples, leaving only 1 cm<sup>2</sup> circles of coating exposed (Figure 38). The test was run for 96 hours, with the samples being inspected at 24-hour intervals. Notes were taken on the appearance of the coatings during the test, and when corrosion of the substrate was identified it was noted so that an approximate failure time could be recorded. The samples were not disturbed during inspection and were only removed at the end of the test.

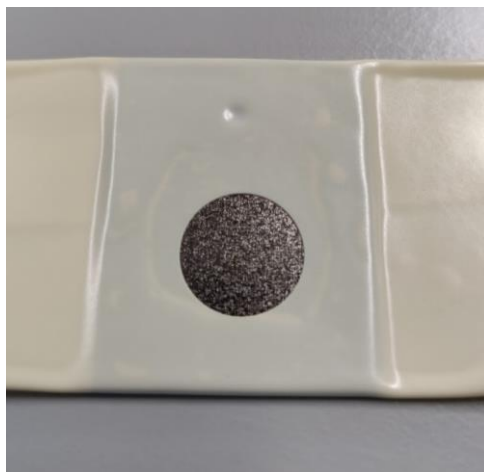


*Figure 38: NSS test sample with Gamry PortHole electroplating tape applied prior to test. Area of circle = 1 cm<sup>2</sup>.*

On completion of the test, the samples were inspected and cleaned. The surface of the coatings were visually inspected using optical microscope and SEM. EDXA was performed to confirm if iron could be detected from the substrate.

#### Scanning Vibrating Electrode Technique – SVET

To determine what form of electrochemical reactions were occurring on the surface, scanning vibrating electrode technique was employed. SVET visualises the electrochemical processes occurring on a target site by measuring whether there is anodic or cathodic reaction sites present.

Due to limitations with the availability of equipment, this test was outsourced and performed at The University of Manchester. Whilst the test was conducted by the team at Manchester University, the results were sent back to Edinburgh Napier University where they were analysed as part of this investigation.

The test was performed using a Uniscan M370 Electrochemical workstation. The probe used was a platinum-iridium wire at 100  $\mu\text{m}$  from the surface of the samples. The Probe vibration operated at 30  $\mu\text{m}$  amplitude, at 80 Hz using steps of 100  $\mu\text{m}$ . The electrolyte used was 50 mmol/L aqueous NaCl at room temperature, and readings were recorded at 5 h, 12 h, 18 h and 20 h.

#### Glow Discharge Optical Emission Spectroscopy – GDOES

Glow discharge optical emission spectroscopy was used to measure the coating composition throughout the depth of the coating from surface to substrate.

Again, due to limitations in the availability of equipment, this test was outsourced to be performed in Manchester where the relevant equipment was located. The test was performed using a 30 second burst to etch through the coating. Due to the thickness of the of the coatings, this process was repeated 12–13 times. Each etch produced a crater of 2.2  $\mu\text{m}$  depth, so  $0.1 \text{ s} = 0.007333 \mu\text{m}$ . After thirteen repetitions, the coating depth analysed was 28.6  $\mu\text{m}$ .

The data from this test was then sent back to Edinburgh Napier University in raw form .txt files where it was extracted, and analysis performed. Each signal was normalised to show weaker signals, as these can otherwise be lost in the noise of more prominent signals. The signals were then compared to determine what impact the inclusion of the gelatine microgels had on the coating composition.

### Electrochemical Impedance Spectroscopy – EIS

The corrosion protection of the coatings was investigated using electrochemical impedance spectroscopy. This was performed using a Solartron Analytical Modulab with Gamry Paracell (Figure 39). The experiment was controlled using Modulab XM ECS software to define the parameters of the test and record the impedance of the coating over time.



Figure 39: EIS experimental set-up using Gamry Paracell and Solartron Analytical Modulab.

The analysis was performed on one sample each of plain NiP and NiP+0.025 g/L gelatine composite for comparison. The samples were exposed to 450 ml of 3.5 wt% NaCl solution using Gamry 990-00254 Porthole electroplating tape to ensure 1 cm<sup>2</sup> of coating was exposed. A graphite counter electrode was used with 2.55 cm<sup>2</sup> exposed to the solution, and a Ag/AgCl reference electrode used. An open circuit was run when the sample was introduced to the solution, and the impedance was recorded at 3, 6, 12, 18 and 24 hours after exposure. The measurements were recorded using a frequency sweep starting at 10 kHz to 0.008 Hz with the amplitude set to 10 mV absolute.

Once the test was complete, the resulting data was presented in Bode and Nyquist plots. The resulting plots were analysed using fitting software with the following equivalent circuit employed (Figure 40), where:

$R_s$  = Solution Resistance

$R_{coat}$  = Coating Resistance

$R_{ct}$  = Charge Transfer Resistance

$R_t$  = Total Resistance

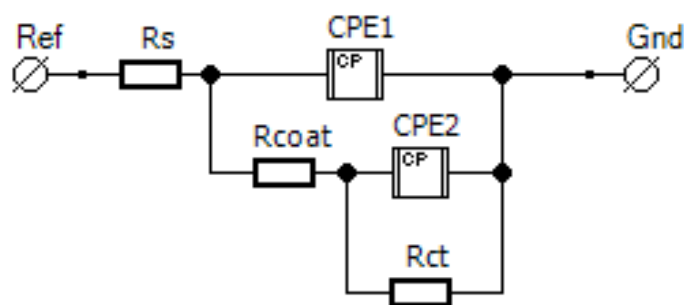


Figure 40: Equivalent circuit used for fitting the EIS data of NiP and NiP/gelatine composite coatings exposed to 3.5 wt% NaCl solution.

### Surface Roughness

To determine what impact the inclusion of gelatine microgels had on the resulting coating, the surface roughness was measured. As the 1850 medium phosphorus solution was designed to produce bright coatings, the surface was relatively smooth, and the amorphous nature of the medium phosphorus did not exhibit the cauliflower heads which can be found in other amorphous nickel coatings.

The coatings were measured using an Accrettech Surfcom Touch 50 surface measuring device (Figure 41). The surface roughness of the plain steel substrate and plain nickel-phosphorus coatings were measured in addition to the three gelatine co-deposited coatings of 0.0125 g/L, 0.025 g/L and 0.05 g/L bath concentrations. As the test was non-destructive, the test was performed prior to other destructive testing which could lead to false results. The samples surface roughness was measured in three sections along the x-axis and the y-axis of the coating. This was to ensure that any impact of the plating procedure such as rising hydrogen bubbles along the face of the samples resulting from the reduction reaction, did not influence the surface roughness.



*Figure 41: Surfcom Touch 50 performing coating roughness measurements on uncoated reference sample for comparison with NiP/gelatine composite coatings.*

Three samples for each coating were measured so that each coatings roughness results were calculated as an average of eighteen measurements. The procedure selected on the Surfcom Touch 50 calculated the Ra values for the coating using the ISO 1997/2009 standard procedure. These results were then compared to determine what impact the gelatine was having on the deposit coating roughness.

### Coating Hardness

As the gelatine microgel particles were soft when compared with the nickel-phosphorus deposit, it was important to determine what impact this had on the coating as a whole. The coatings microhardness was measured using a Vickers microhardness test. This was performed on the surface of the samples and the resulting indentation was measured, from which the coatings hardness was calculated.

The test was performed on a Buehler Wilson® VH1202 microhardness tester using both the Knoop microhardness and Vickers microhardness testing. The testing parameters for each test were that a 100 g mass would be applied for 10 seconds. The resulting indentation was then measured using a 50x magnification microscope built into the tester, and graticules were placed at each side of the indentation so that it could be measured.

The Knoop indenter consisted of a diamond tipped right pyramid with rhomboid base, and the Vickers indenter used a right pyramid with a square base. Due to the surface roughness of the coatings, many of the indentations resulting from the Knoop microhardness did not pass the test, as the difference in length of indentation on each side differed outside the specified range. Due to this the Vickers microhardness test was performed. With the coating thickness at least 1.4x the size of the indentation, this allowed for the Vickers microhardness to be used. As the coatings had surface hardness of over 300 HV, a test force of 0.981 N was used for a test condition of HV<sub>0.1</sub>. The Buehler Wilson® VH1202 performs the calculations to ASTM and ISO standards, which provided immediate feedback when the resulting indentation did not satisfy the testing standards (Figure 42). As a result, this ensured that the tests that were included in the calculations, all met the correct standards to give accurate results.



Figure 42: Example of rejected measurement due to D1 & D2 differing by greater than 5 %.

### Abrasion Resistance

The coatings abrasion resistance was measured to determine what impact the microgels had on the coating. Different inclusions can result in increased wear resistance due to a lubricating effect in some cases. The test was performed on Phoenix Tribology TE66 Micro-Scale Abrasion Tester with BS ISO 28080:2011 “Hardmetals — Abrasion tests for hardmetals” for guidance. The testing also used BS EN ISO 26424:2016 “Fine ceramics (advanced ceramics, advanced technical ceramics) — Determination of the abrasion resistance of coatings by a microscale abrasion test”, to ensure the correct slurry concentration for promoting the correct wear type.

To ensure an even wear pattern, a slurry which promotes rolling wear was selected. This consisted of 20 % by volume silicon carbide in deionised water. Ideally, a cylindrical rolling wear would be performed on the coatings, however due to limitations with the accessible equipment, that could not be performed. As a result, the rolling wear using spherical ball would be closest to simulating the testing standards, and as the testing was a comparative study, would provide meaningful results. To attain the 20 % by volume SiC abrasive slurry, 80 g of SiC with an average diameter 3  $\mu\text{m}$  and density 3.2  $\text{g}/\text{cm}^3$  was added to 100 ml of deionised water. This slurry was then mechanically agitated so that a uniform suspension of SiC was achieved.

The slurry was then pumped and added dropwise automatically to the rotating 25 mm steel ball used for the abrasion. The load selected for the test was 20 g and the speed set to 80 rpm. 200, 300, 400, 500 and 2000 revolution tests were performed to determine what number of revolutions would produce the best crater for measuring the wear rate of a plain NiP coating. Too few revolutions and the crater would not be deep enough, so the outer edge of the crater would be ill defined. Too many revolutions and the coating would be perforated, and the substrates wear rate would also impact the results (Figure 43).

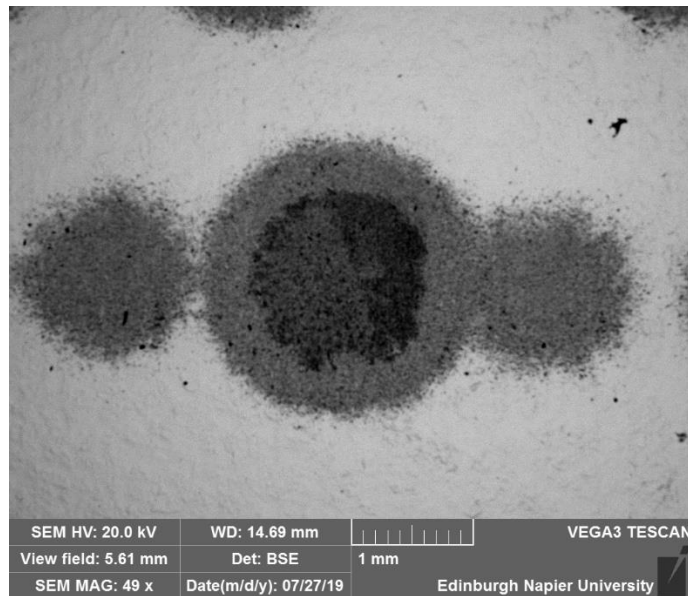


Figure 43: Example of a perforated coating due to excess abrasion test conditions.

The resulting wear marks were analysed using optical microscope and scanning electron microscope. From these results, it was determined that operating the test at 80 rpm for 300 revolutions with a load of 20 g would produce the optimal wear marks for analysis.

The test was performed on three separate coatings of plain NiP, NiP+0.0125 g/L, NiP+0.025 g/L and NiP+0.05 g/L gelatine, with each sample subject to three abrasion tests. These results were compared to determine what impact the gelatine co-deposit had on wear rate.

The resulting wear rates were measured using optical and scanning electron microscopes. The diameter of the wear mark was measured parallel and perpendicular to the rotation of the ball. If the diameter of each axis differed by greater than 10 %, the measurement was not used in the calculations, and the test was repeated to produce a useable wear mark. Once the diameters of the wear marks were recorded, the following equations were used to determine the abrasive wear rate for the coating.

The volume of wear,  $V$ , when the depth of the crater is less than the radius of the ball is given by:

$$V = \pi \frac{b^4}{64R}$$

Where:

- R is the radius of the ball (m)  
b is the crater diameter (m)

The Archard wear equation relates the volume of wear to the normal load and distance slid by the ball as:

$$V = K_c SN$$

Where:

- N is the normal load (N)  
S is the distance slid by the ball (m)  
 $K_c$  is the abrasive wear rate of the coating ( $\text{m}^3 \cdot \text{N}^{-1} \cdot \text{m}^{-1} \times 10^{-13}$ )

So:

$$K_c = \pi \frac{b^4}{64RSN}$$

## 4 Results and Discussion – Sodium Alginate Microgel Analysis

The results discussed in this chapter relate to phase one of the research project with analysis performed on sodium alginate microgels and the development of low temperature electroless nickel solutions, as discussed in section 3.2.

### 4.1 Microgel Analysis.

The results from the Energy Dispersive X-Ray Analysis (EDXA) performed on the sodium alginate microgels before and after 24-hour immersion showed differences in the levels of leaching experienced by each microgels type (Figures 44, 45).

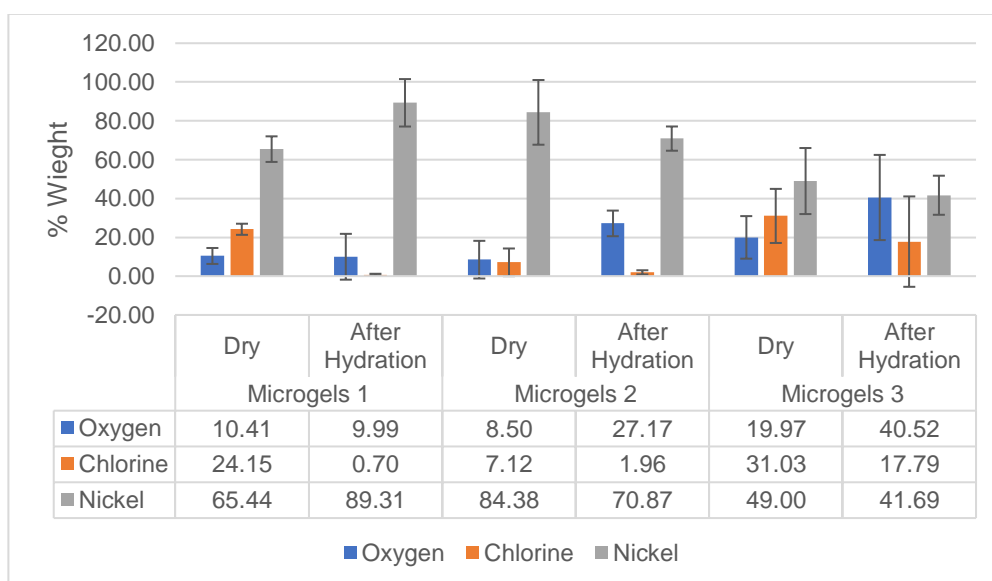


Figure 44: EDXA results of different sodium alginate based microgels before and after 24-hour hydration in deionised water.

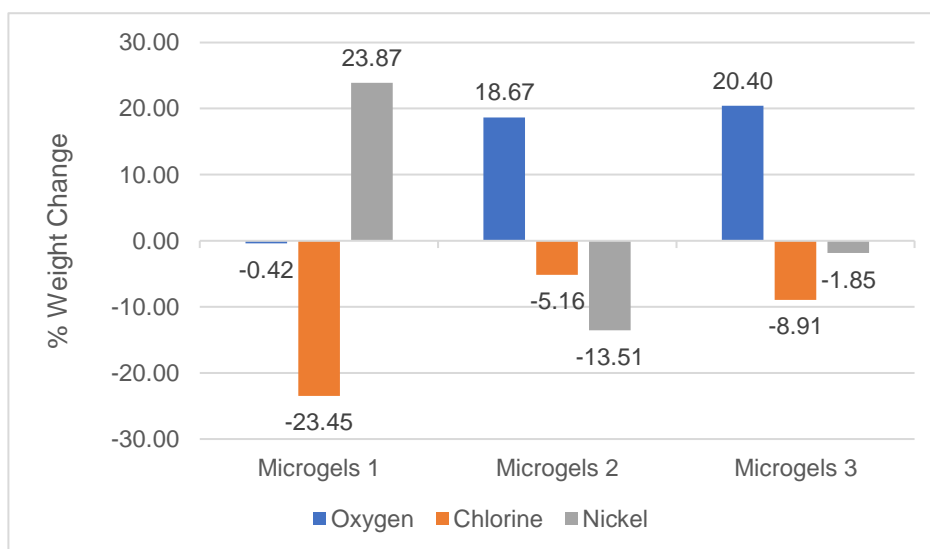


Figure 45: Change in Oxygen, Chlorine and Nickel constituents due to leaching.

The results from the leaching test shows that the difference in the origin of the sodium alginate has an influence on the microgels resilience when in deionised water. The results shown in Figure 45, clearly show that microgels 1, which is synthetic based, experienced different levels of leaching when compared to microgels 2 and 3, which were both formed from sodium alginate produced from natural sources (algae). The EDXA measured the respective ratios of the microgels oxygen, chlorine, and nickel. Both of the “natural” microgels saw a reduction in the total wt% of both chlorine and nickel, with an increase in the quantity of oxygen. This could be due to leaching of the nickel salt within the microgels or could be due to an increase in the oxygen content due to hydration of the compounds within the microgels. Microgels 1 did not exhibit the same characteristics, with an increase in nickel content, a reduction in chlorine, and little change in oxygen. This indicates leaching of the chloride ions, as the nickel increase cannot be due to a net gain of nickel present in the microgel.

The zeta potential of the sodium alginate microgel 1 was measured as 12.80 mV with standard deviation 0.77 mV at pH 7.0. This suggests that the microgels would not create a stable suspension due to the surface charge being in the region of the threshold of agglomeration (Table 3) [61]. To successfully incorporate these microgels into a coating, some form of surface modification would be required such as the introduction of surfactants. However, the use of surfactants could lead to the premature activation of the microgels which would break down and release its components before incorporation within the nickel-phosphorus matrix.

## 4.2 1850 Solution Variable Testing

### 4.2.1 Solution Temperature

The increase in the operating temperature of the solution resulted in a corresponding increase in the deposition rate achieved. The relationship between temperature and deposition rate follow the trends observed by Mallory et al. and Brenner et al. [29], [67]. Using 30-minute depositions, at varying temperatures, the exponential increase in deposition rate with increase in temperature was demonstrated (Figure 46). 85 °C was not tested as this temperature falls within the specified operating temperature provided by the manufacturer. Below 70 °C was not deemed necessary as hydrogen evolution was not visible at solution temperatures less than 70 °C, and deposition rates are too low for the co-deposition of microgels.

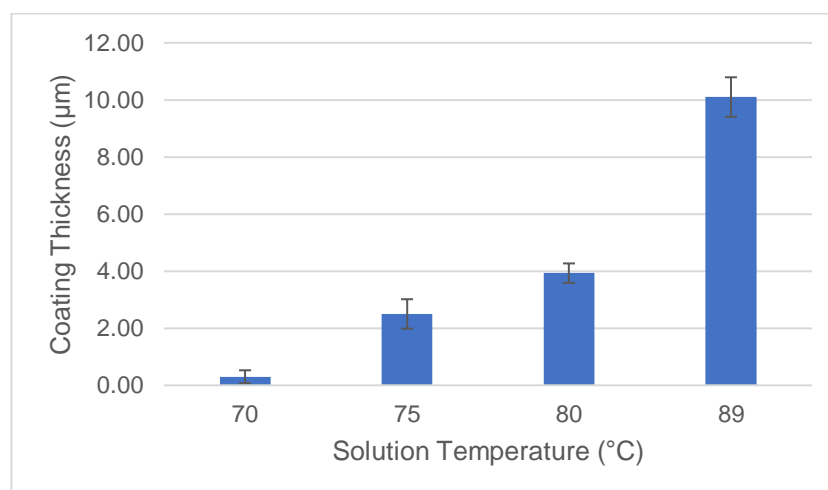


Figure 46: Coating thickness at varying temperatures of 1850 after 30-minute deposition.

#### 4.2.2 Solution pH

The results for the pH testing demonstrated that as the pH of the 1850 electroless nickel solution increased from acidic to alkaline, the deposition rate increased. This follows the trends in other ENP solutions observed by Mallory et al. and Hu et al. [29], [48]. The specified solution pH for 1850 is 4.6–5.2 pH so all depositions other than 4.9 were outside the manufacture’s specifications. The solutions deposition rates increased drastically with an increase in pH, with pH 8.0, producing almost 20  $\mu\text{m}$  in only 30 minutes, double the optimal deposition rate (Figure 47). It should be noted that the solution colour at pH 8.0 had turned from the normal green to blue, indicating that the octahedral hexaqua nickel had been replaced with a nickel ammonia complex [61]. None of the solutions broke down or spontaneously plated out like other bespoke solutions, proving the resilience of this solution and practicality of use. As the depositions were only performed for 30 minutes, it is possible that the solution would not maintain this deposition rate for periods of close to 1 hour without replenishment. Additionally, only the coating thickness of the resulting deposits were investigated so the quality or porosity of the coating is not known, however under visual inspection, no major defects were noted.

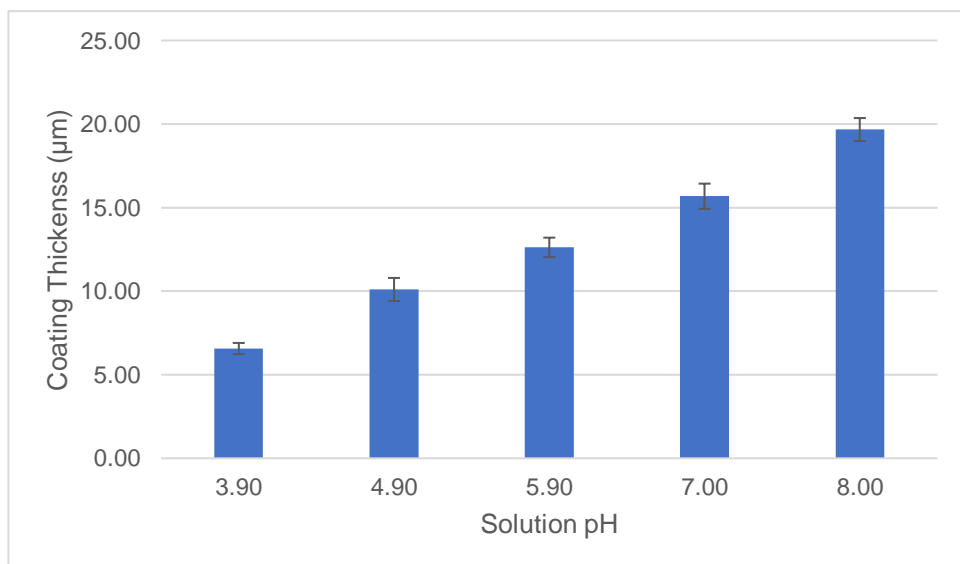


Figure 47: Coating thickness at varying solution pH of 1850 after 30-minute deposition at 89 °C.

### 4.2.3 Ultrasonic Agitation

The results of the ultrasonically agitated depositions show an increase in the deposition rate when compared with mechanically agitated solutions operated at the same temperature (Figure 48). Similar results have been described by Park et al., Mason et al. and Cobley et al. [49], [50], [54]. The increase in deposition rate was significant and could prove to be a useful benefit to the inclusion of microgels. However, the implementation used for this project was not the optimal set up. Due to the losses associated with heating the ultrasonic apparatus, it was not possible to raise the temperature to the optimal 89 °C for testing. The experimental set up also required constant supervision as there were many ways that unintended variables could be added to the system, such as the beaker tipping over within the water bath, or the heating element boiling the water and splashing the deposition process. Altering the experimental set up to employ an ultrasonic processor or heated ultrasonic water bath could prove to be an efficient deposition procedure.

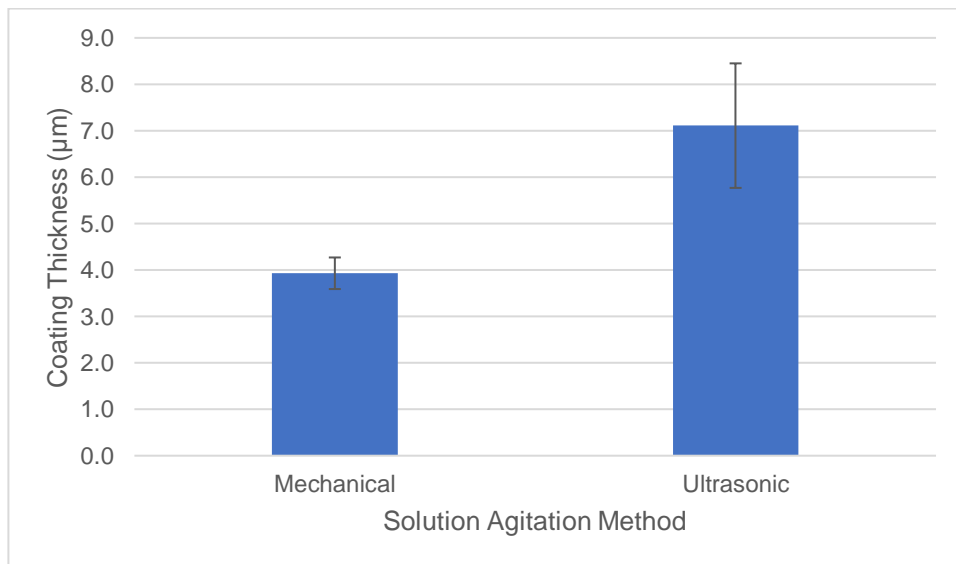


Figure 48: Coating thickness resulting from 30-minute deposition of 1850 using mechanical and ultrasonic agitation methods at 80 °C.

### 4.3 Bespoke Low Temperature Depositions

#### Solution 1

This solution proved difficult to successfully deposit nickel coatings. The solution did not readily deposit on surfaces of mild steel or those prepared with tin-palladium catalyst. If the solution did begin to deposit, it would break down and plate out within 5 minutes of deposition commencing (Figure 49). No successful depositions were achieved with this solution. As such, coating quality and deposition rates could not be quantified.



*Figure 49: Result of solution plating out and depositing nickel on every surface.*

#### Solution 2

The glycine complexed solutions were tested using different concentrations for evaluating the highest deposition rate. This solution was stable during operation and proved to be resilient to the alterations made to the solution ratios. The coating quality was good under visual inspection, with bright nickel deposits and no obvious defects. The deposition rates were achieved using 30-minute depositions, however when extrapolated for 1 hour, fail to achieve sufficient deposition rates of the ideal 15  $\mu\text{m/hr}$  (Figure 50).

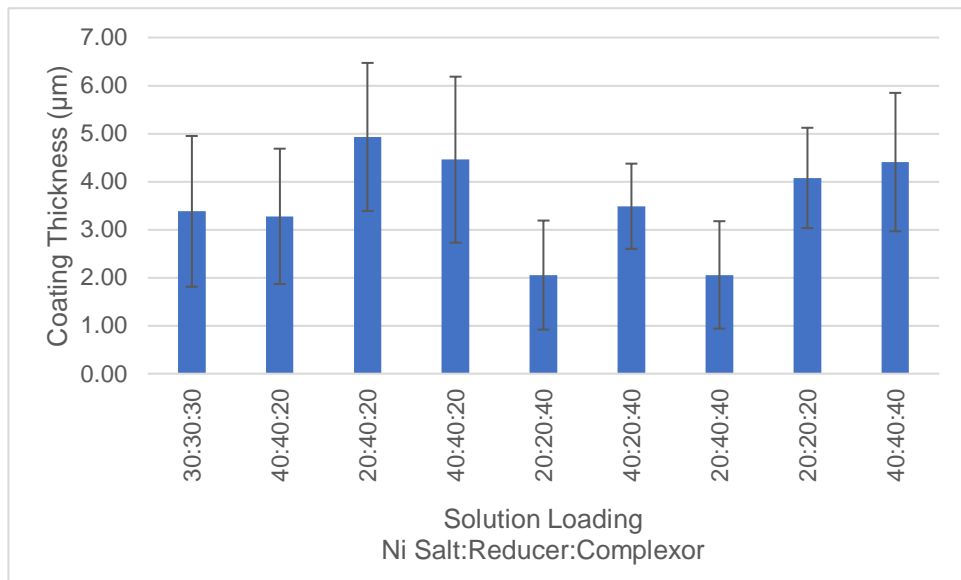


Figure 50: Coating thickness of glycine-based solutions using varying Metallic salt, reducer and complexor quantities. Coatings produced using 30-minute deposition.

### Solution 3

This solution proved stable at 60 °C and was also used to confirm that tin-palladium catalyst was not necessary for the deposition on steel substrates. The samples with catalyst did show increased deposition rates (Figure 51), however this difference was deemed not significant enough to require the extra steps of preparation which increase the complexity and operating cost of production.

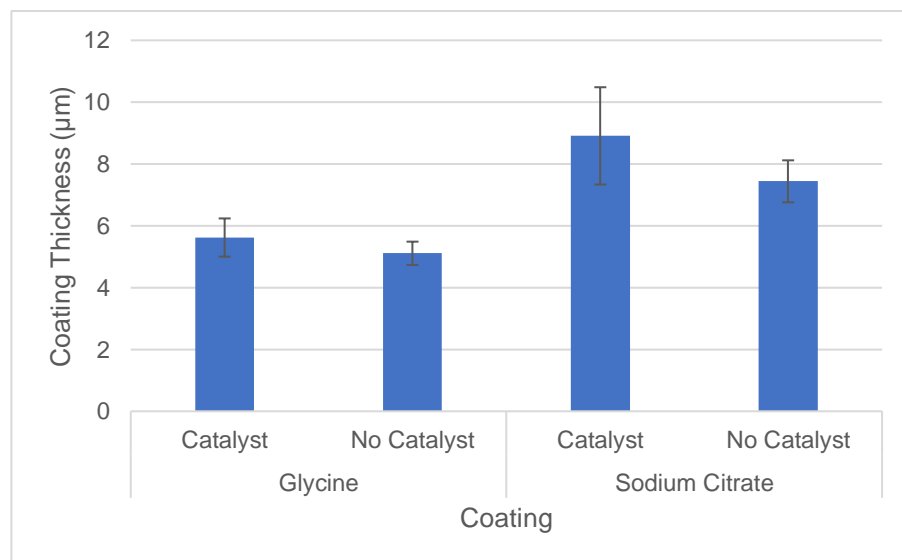


Figure 51: Deposition rates with and without use of catalyst using varying solutions.

#### Solution 4

The resulting deposits from this solution exhibited severe delamination (Figure 52) which occurred in all but one deposition. Six iterations were attempted but this issue could not be overcome. The coating thickness of the sample was not measured as the deposition of a uniform coating was not achieved.



*Figure 52: Severe delamination of nickel coating from substrate.*

#### Solution 5

From Mallory and Hajdu [29], the pyrophosphate-based solution showed promise in literature, however, was troubling when depositing in practice. If the solution ingredients were not methodically added, the solution would break down and produce black foam within 5 minutes of deposition commencing (Figure 53).



*Figure 53: Result of solution decomposition. Solution turned turbid and produced black foam.*

By altering the production of the solution, more stable depositions were achieved, however it would break down after 30 or 40 minutes of deposition. The resulting coatings would exhibit severe delamination when removed from the solution. By being vigilant with keeping the pH above 10–10.5, the delamination was reduced however at the elevated temperatures, the  $H_5NO$  used for pH adjustment would boil off rapidly. A successful plating was produced however was determined to be porous under SEM inspection (Figure 54). As this solution was very labour intensive to produce a coating, it was deemed not practical and not investigated further.

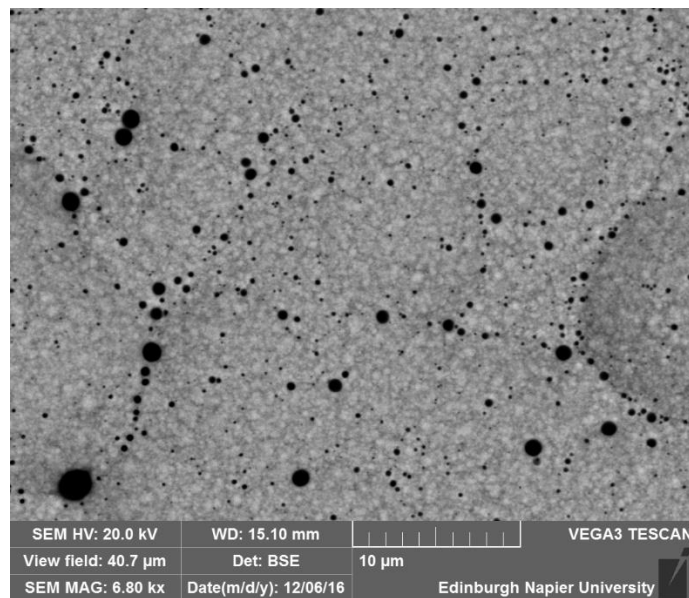


*Figure 54: SEM image of deposition produced from pyrophosphate bath. Black spots present across surface are pores.*

### Summary

The solutions reviewed in this section were tailored towards low temperature depositions with the aim of high deposition rates, above 15  $\mu\text{m/hr}$ . This proved to cause unstable solutions which could not maintain useful deposition rates for long enough to achieve sufficient deposit thickness required to fully incorporate a minimum of two layers of 6  $\mu\text{m}$  microgels. The delamination experienced with seven of the coatings only occurred after 30 minutes or more of deposition time which indicates that the substrate preparation was not the cause of failure. Instead, it is postulated that unbalanced internal stresses due to varying solution pH was the cause. This issue may have been resolved with more attempts, however as it was known that gelatine could be heat treated to survive in high temperature electroless depositions, the focus of work pivoted to this aspect, and the high temperature medium phosphorus 1850 solution which had proved stable in testing was chosen to perform the co-depositions.

## 5 Results and Discussion – Gelatine Co-deposition

This chapter discusses the results obtained during phase two and three of the research project relating to the development and analysis of gelatine co-deposition with electroless nickel-phosphorus, as described in sections 3.3 and 3.4.

### 5.1 Microgel Analysis

#### 5.1.1 Microgel Size

To confirm the particle size distribution of 2–6  $\mu\text{m}$  in diameter specified by the manufacturer, zetasizer and SEM analysis was performed. The results from the zetasizer proved inconclusive as accurate particle size could not be determined. This is likely due to issues with either microgel fluorescence or the size distribution being too great for accurate analysis using this method.

The results from the SEM analysis demonstrated that there was a large variation in the particle size, however the majority of microgels did fall within the prescribed range of 2–6  $\mu\text{m}$  (Table 4). The variation in microgel size is present both before and after the heat treatment process and can easily be identified in the SEM imaging (Figures 55, 56).

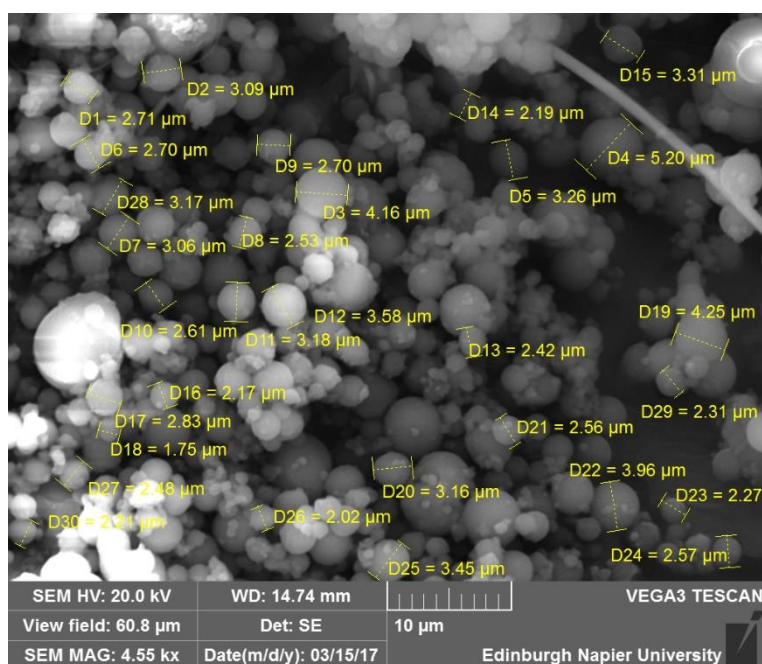


Figure 55: Particle size analysis of gelatine microgels as received, prior to heat treatment.

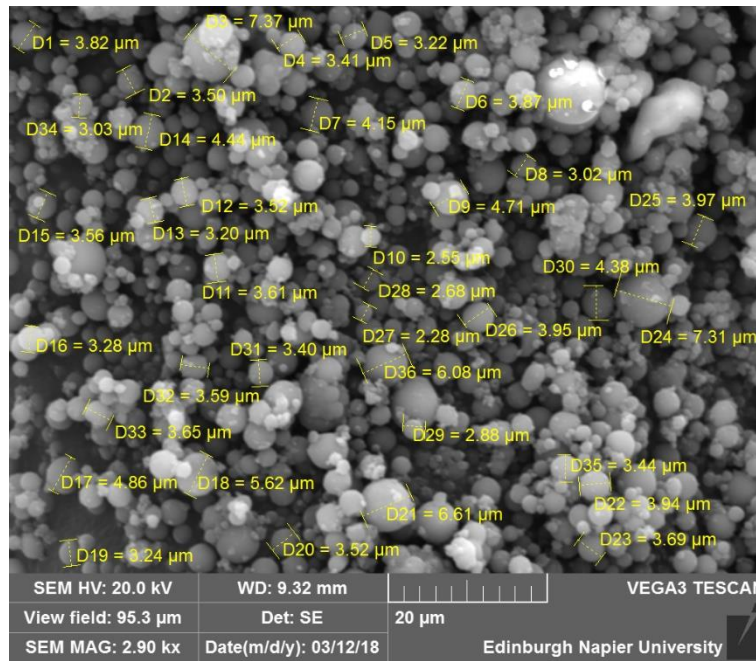


Figure 56: Particle size analysis of gelatine microgels post heat treatment.

Table 4: Gelatine microgel diameters before and after heat treatment.

Microgel Type	Objects counted	Min. value (μm)	Max. value (μm)	Mean value (μm)	Std. dev. (μm)
As Received	49	1.50	5.20	2.82	0.76
Heat Treated	111	2.16	7.49	3.77	1.11

### 5.1.2 Heat treatment

The results of the elevated solution temperature test (section 3.3.1 – Heat Treatment) demonstrated that microgels were able to survive the deposition environment post heat treatment. No microgels from the untreated gelatine was observed after solution temperature testing, however deposits were found of both the mechanically and ultrasonically agitated heat-treated samples (Figure 57).

The ultrasonically agitated microgels appeared to have changed visually, being less defined under the same microscope conditions. This result, in addition to the difficulties with preparing the apparatus for the ultrasonic deposition, led to the decision to use mechanical agitation for the depositions for further investigations.

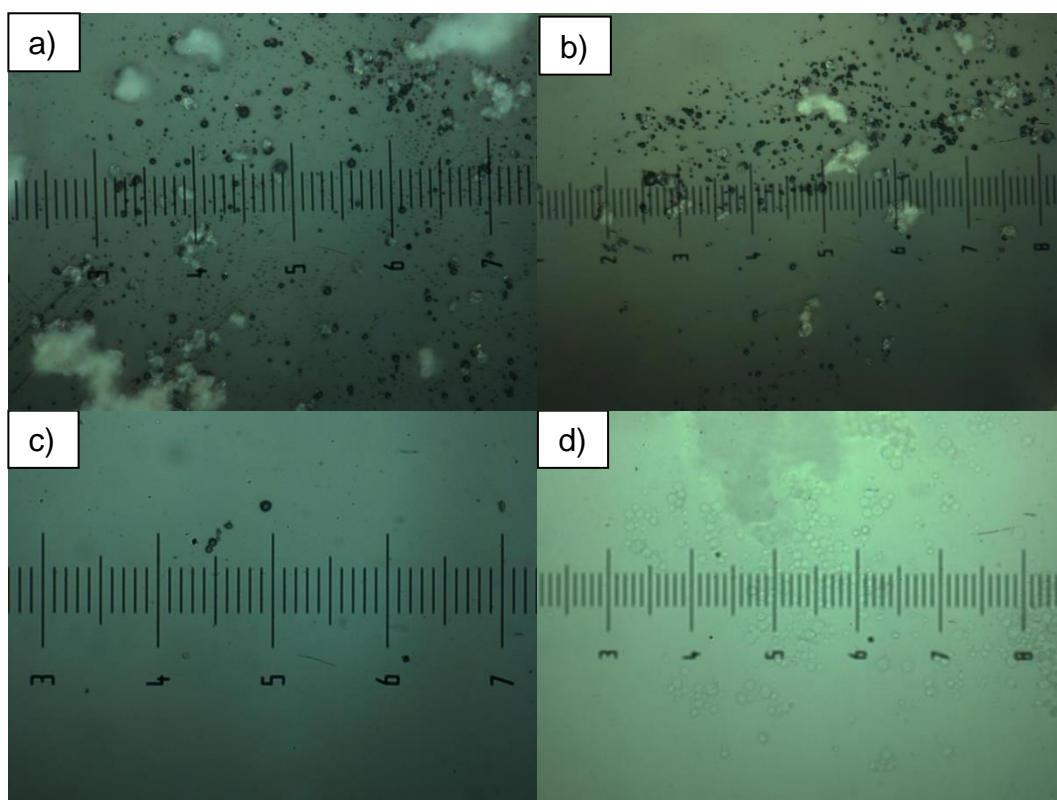


*Figure 57: Gelatine microgels imaged using optical microscope. Images a) and b) show untreated and heat-treated microgels respectively before solution temperature test. Images c) and d) show heat-treated microgels post solution temperature test with mechanical and ultrasonic agitation respectively.*

*Each small graticule = 5  $\mu$ m.*

SEM imaging of the surface of the NiP/microgel composite coatings showed gelatine microgels adhered to the surface (Figure 58). These microgels were measured, and confirmed that they were within the expected size, as well as maintaining the spherical structure. These microgels have survived being ultrasonically agitated in deionised water and co-deposited using mechanical agitation at 89 °C with pH 4.9. As the microgels were added in 15-minute increments, the microgels imaged could have been present in the deposition solution for 15,30,45 or 60 minutes.

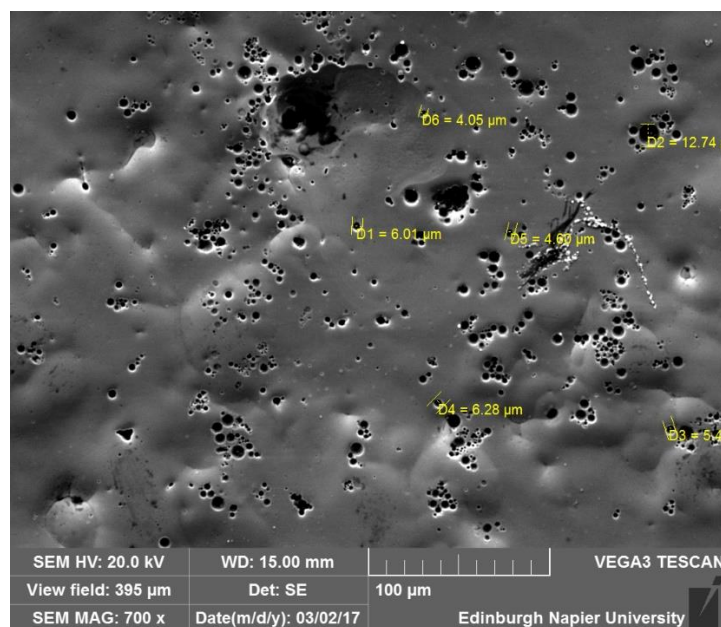


Figure 58: Gelatine microgels adhered to the surface of NiP/gelatine microgel composite coating after 1 hour deposition at 89 °C.

### 5.1.3 Zeta Potential

The zeta potential of non-heat-treated gelatine microgels as well as gelatine microgels after heat treatment were investigated. This showed the isoelectric point, where the particles are most unstable, would be between 7.5–8.5 pH (Figure 59). At solution pH above 10 or below 4.1, the untreated microgels would produce a stable suspension. These pH ranges may be required to achieve suitable depositions at low temperatures.

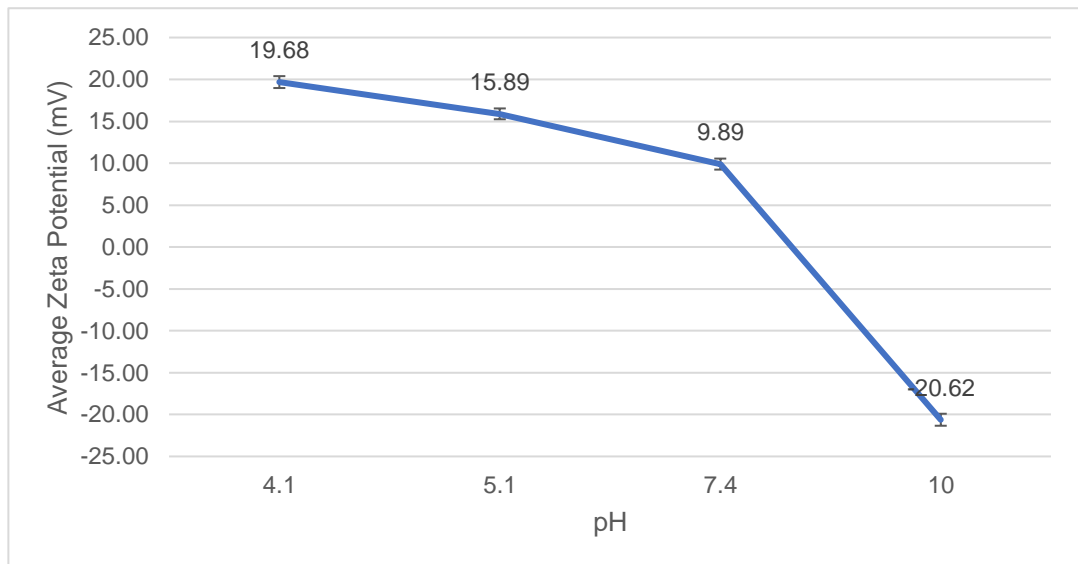


Figure 59: Zeta potential of gelatine microgels in the as received state.

The results for heat-treated microgels showed that the isoelectric point would be in the region of pH 6.0 (Figure 60) and would show low stability at the operating conditions of 1850 (pH 4.9). This would not produce even dispersions within the co-deposition, which confirms that aggregations would be an issue on the surface of the coating. Surfactants would typically be utilised to establish a stable solution, however this could prematurely activate or destroy the microgels. Instead, ultrasonic agitation was employed to thoroughly break up any aggregations and the microgels were added via a solution to prevent overloading the reaction sites and causing large pits due to aggregations.

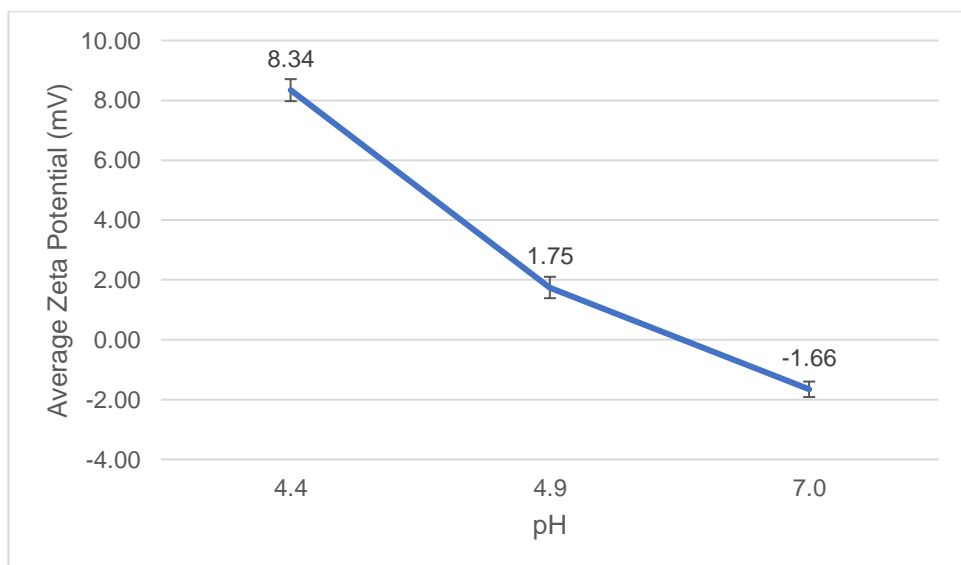
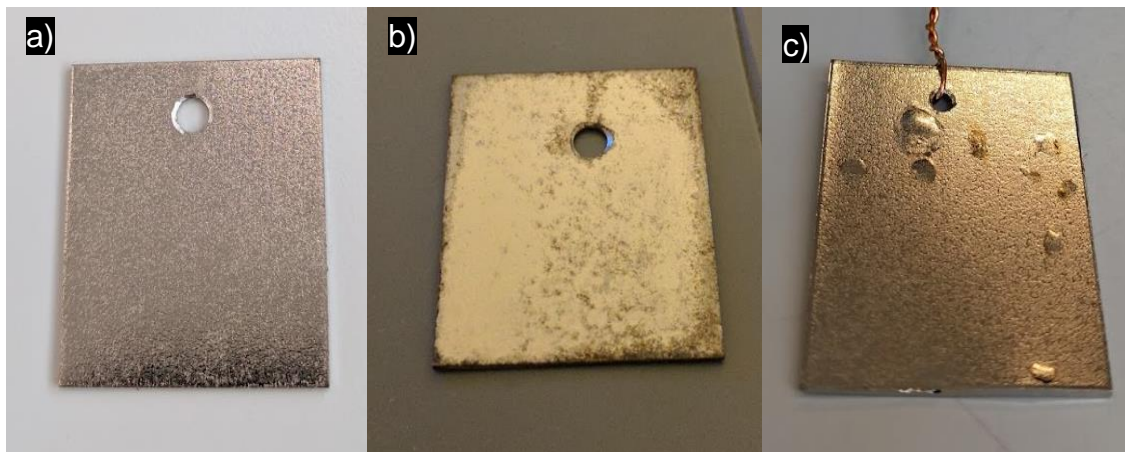


Figure 60: Zeta potential of gelatine microgels after heat treatment, in the ready to be co-deposited state.

## 5.2 Deposition Results

The coatings were examined using visual inspection after the deposition process. If any defects within the coating were observed, the sample was not carried forward for additional testing. Areas in which the coating would fail visual inspection included: blistering or delamination of the coating; sever edge pull back resulting in large uncoated areas; and surface imperfections such as pitting from aggregations of microgels on surface (Figure 61).



*Figure 61: Example of coatings analysed by visual inspection deemed to have a) Passed quality inspection, b) Failed due to surface imperfections and edge peel back, c) Failed due to coating blistering.  
Coupon dimensions = 25 mm x 30 mm.*

Once the coating was deemed to have passed inspection and did not exhibit any visual defects, the samples coating thickness, phosphorus content, and microgel inclusion was analysed and the results are presented in this section.

### 5.2.1 Coating thickness

The results from the non-destructive coating thickness tests showed that deposition rates were impacted negatively by the inclusion of the gelatine microgels. As the concentration of gelatine microgels were increased within the deposition solution, the reaction sites are inhibited, and the deposition rate is reduced (Figure 62). The coating thickness was measured after 1 hour of deposition and shows the plain NiP coating with no microgels performed as described by the manufacturer, with a deposition rate of 20  $\mu\text{m/hr}$ . It was found that by reducing the concentration of gelatine co-deposits to very low levels, the deposition rate was less impeded and successful depositions could take place.

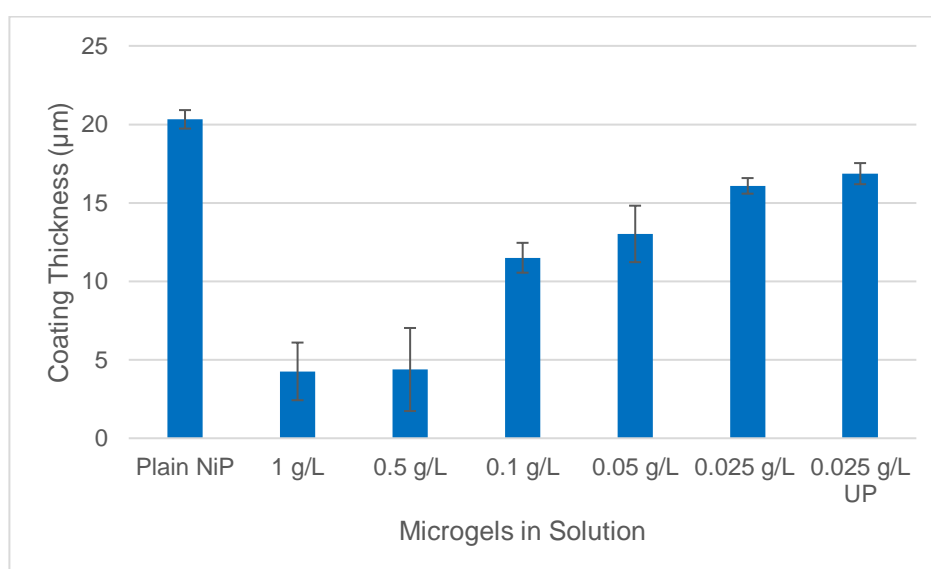


Figure 62: Deposit thickness of coatings produced with varying quantities of gelatine microgel co-deposits. Microgels were mechanically agitated and added in the dry state apart from 0.025 g/L UP in which the microgels were ultrasonically processed before addition to the deposition bath.

The results of the coating thickness cross-sectional analysis performed across six sites for each coating type confirmed the non-destructive electromagnetic induction method produced accurate measurements. A representative image of these cross sections is shown in Figure 63.

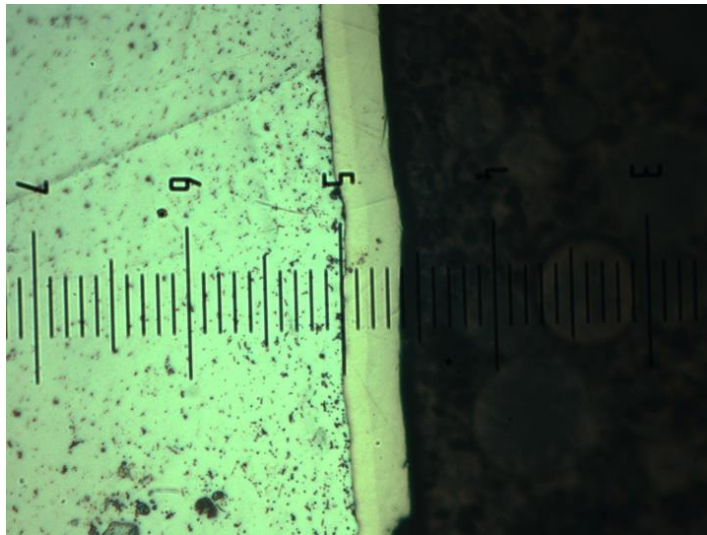


Figure 63: Cross section of NiP+0.025 g/L Gelatine microgels. Each small graticule = 5  $\mu$ m.

### 5.2.2 EDXA Results

The results of the EDXA show the chemical composition of the coating is affected by the inclusion of the gelatine microgels within the deposition solution. Nickel and phosphorus were selected for analysis and all other elements such as carbon and iron were excluded. This provided the ratio of Ni:P which is useful for categorising grain structure. With the inclusion of the gelatine microgels, the phosphorus content of the coatings increased (Figure 64). These coatings now lie in the high phosphorus range, whereas plain NiP is medium phosphorus.

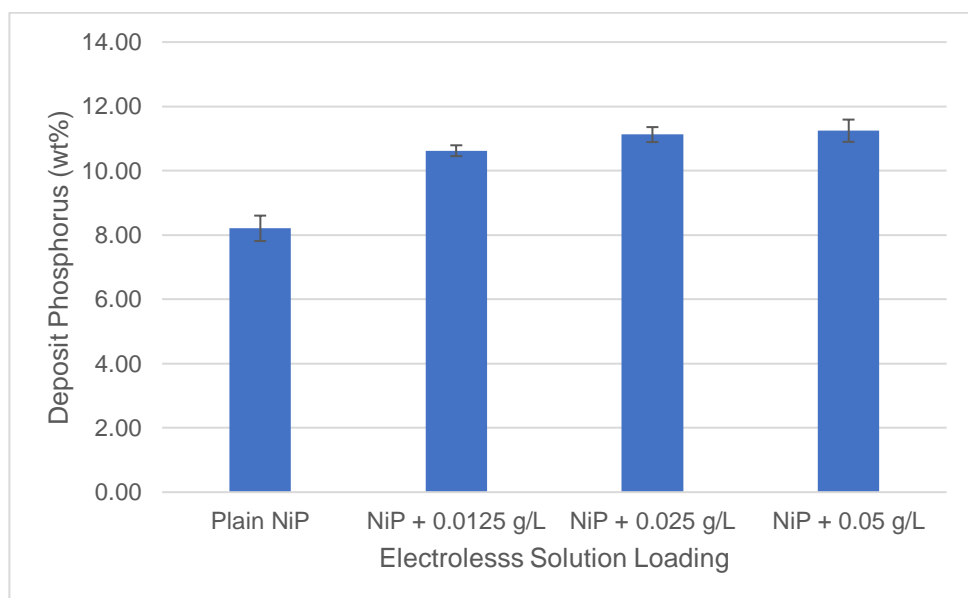


Figure 64: Phosphorus content of NiP coatings with varying quantities of gelatine microgel co-deposits.

### 5.2.3 Glow Discharge Optical Emission Spectroscopy – GDOES

The results from the GDOES confirm that the inclusion of gelatine microgels alters the deposition characteristics and increase the phosphorus content of the coating. As the co-deposit sample was produced with a 5  $\mu\text{m}$  nickel base coat, the Ni:P ratio is that of normal 1850. After the 5  $\mu\text{m}$  base coat, the gelatine microgels are added to the deposition solution, and the phosphorus content spikes, turning to a high phosphorus deposit, confirmed in earlier EDXA comparing plain NiP with NiP/Gelatine co-deposits. This occurs at approximately 15  $\mu\text{m}$  depth of measurement due to measurements recorded from surface–substrate (Figures 65, 66).

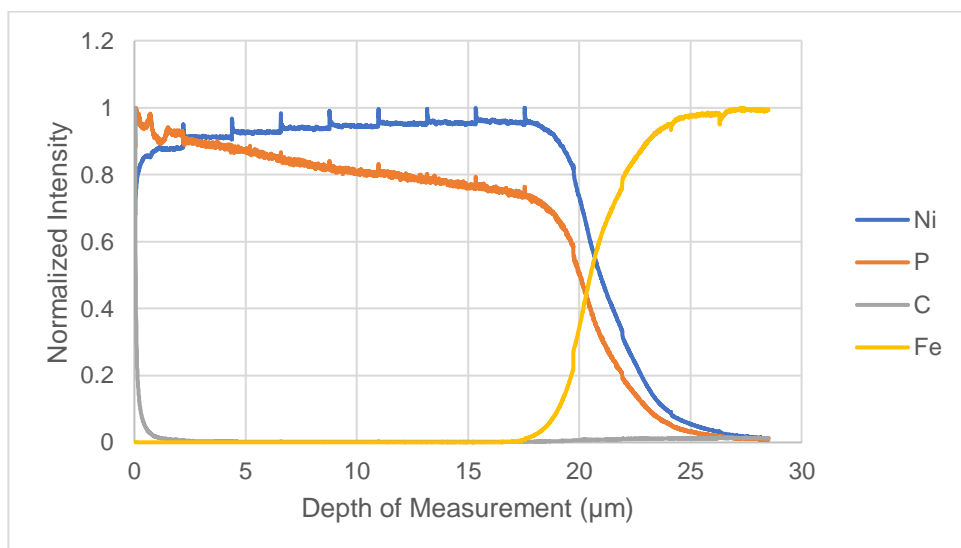


Figure 65: GDOES results for plain NiP only coating.

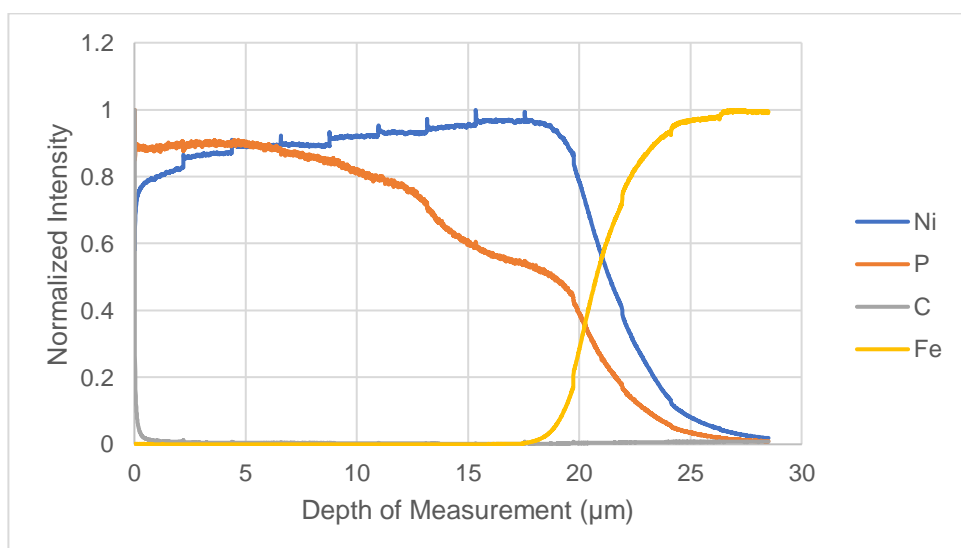


Figure 66: GDOES results for NiP+0.025 g/L gelatine composite coating.

## 5.2.4 Microscopy Analysis

### Fluorescence Microscopy

Fluorescence microscopy confirmed that gelatine microgels would survive the deposition process and were visible on the coatings surface. Images captured using visible white light and ultraviolet light confirmed that the fluorescing particles observed were gelatine microgels (Figure 67).

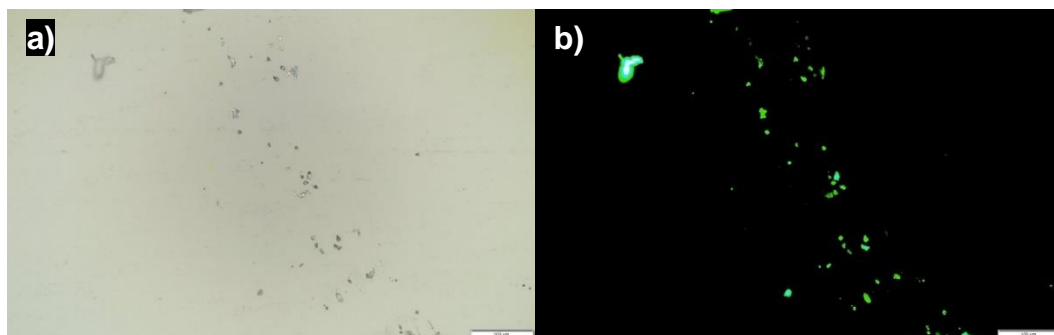


Figure 67: Gelatine microgels imaged using a) RGB colour spectrum using white light, b) fluorescence using ultraviolet light. Images captured at x20 magnification with 100  $\mu\text{m}$  scale bar.

Fluorescing particles match the locations of objects believed to be microgels visible on the coating surface using optical microscopy (see Appendix G). Increasing the solution loading of the microgels resulted with an increase in the observed fluorescing particles (Figure 68).

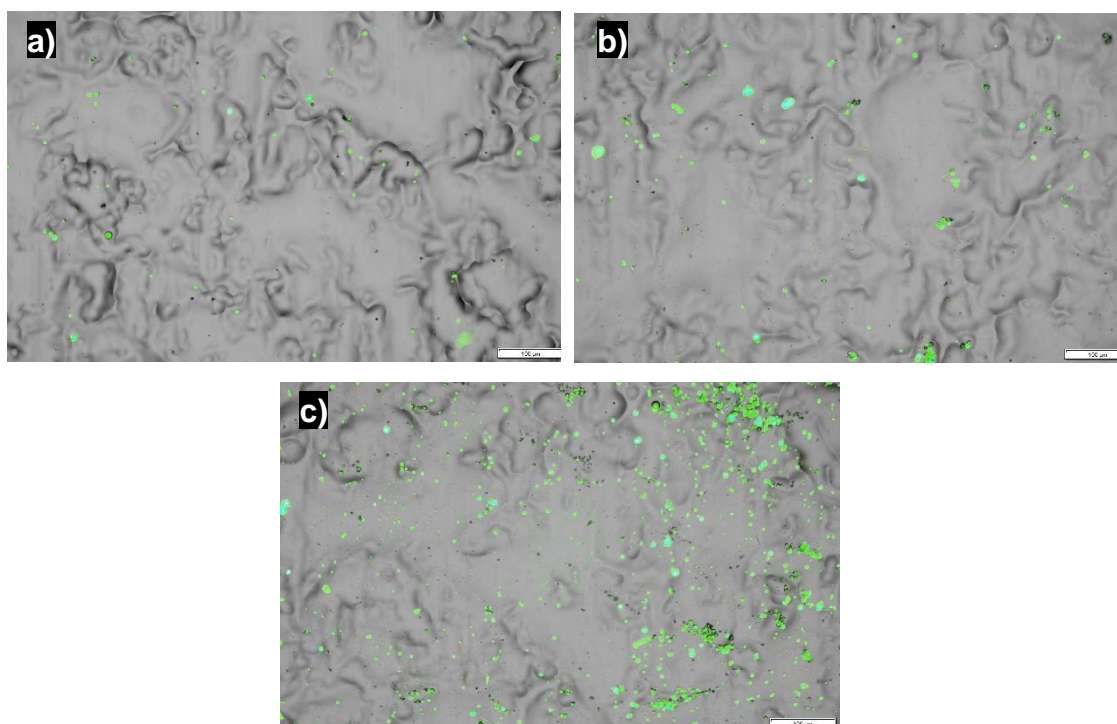


Figure 68: Fluorescent images of a) NiP+0.0125 g/L, b) NiP+0.025 g/L and c) NiP+0.05 g/L gelatine composite coatings.

### Optical Microscopy

Fluorescence imaging showed microgels survive the plating process and were present on the surface of the coating. At higher magnification, optical microscopy shows these microgels on the surface and within defects observed in the coatings. During the deposition process, microgels would aggregate and adhere to the surface of the coating. This blocks the reaction sites where reduction reactions occur, leaving depressions in the coating surface and avenues for corrosive media to permeate (Figure 69).

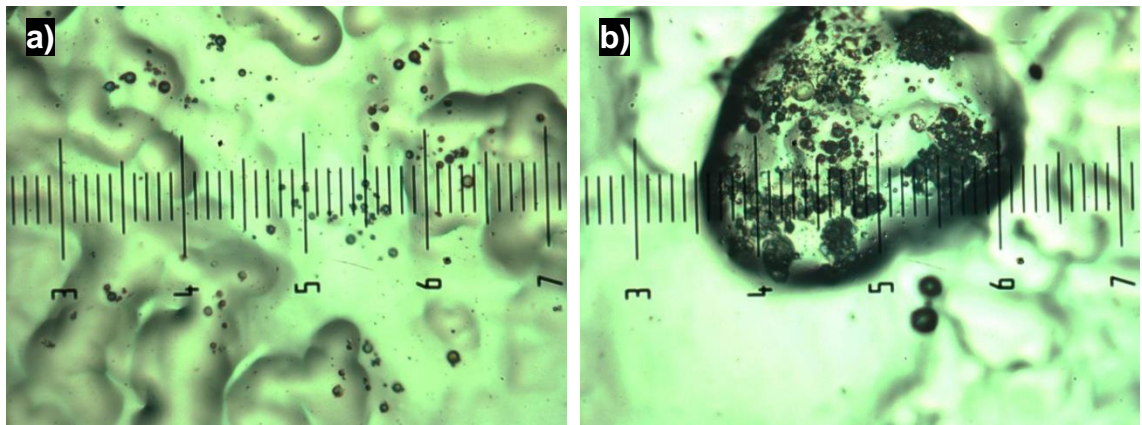


Figure 69: Gelatine microgels observed a) on Surface and b) in coating defect of NiP+0.025 g/L gelatine coating. Each small graticule = 5  $\mu$ m.

Similarly, on cross sectional analysis of a coating with bath loading 0.025 g/L gelatine, microgels were observed within the coatings structure (Figure 70). The inclusions observed are not present in the inner most 5  $\mu$ m of the coating due to the deposition technique of a plain NiP base coat of 5  $\mu$ m. This demonstrates that the technique developed produces coatings in which microgels survived the deposition process and were co-deposited with the NiP coating.

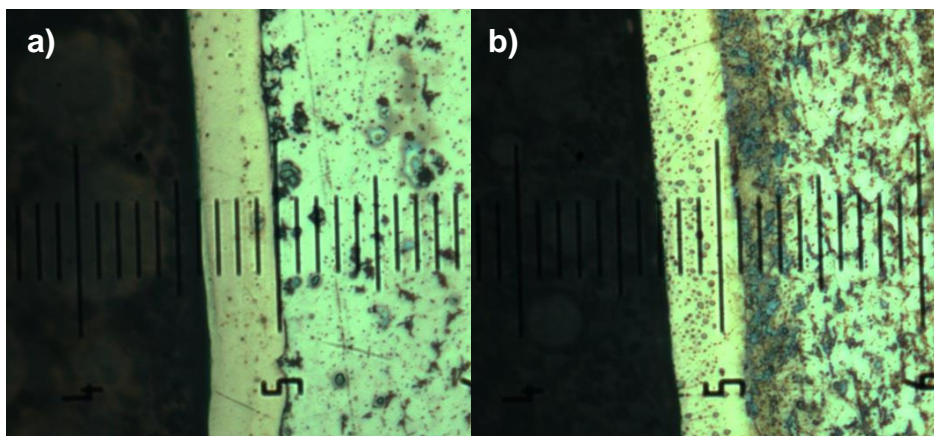


Figure 70: Cross section of NiP+0.025 g/L gelatine coating with a) no acid etch and b) with acid etch. Each small graticule = 5  $\mu$ m.

## 5.3 Corrosion Results

### 5.3.1 Neutral Salt Spray – NSS

The results of this testing showed that coatings with larger co-deposit concentration were more likely to fail, this is potentially due to a more open network leading to barrier coating imperfection. These results proved inconclusive for the level of protection that the gelatine provided as three coatings failed and exhibited corrosion (Figure 71) after just 24 hours, all of which were higher co-deposit concentration coatings. These were two 0.05 g/L and one 0.025 g/L sample.

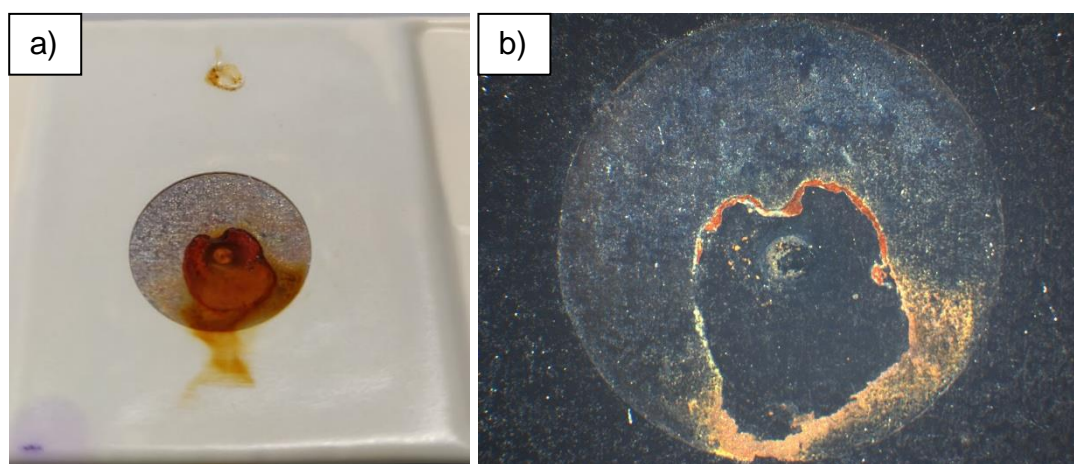


Figure 71: Coating which was deemed to have failed, a) on removal from the NSS chamber, b) after light cleaning. Area of circles = 1 cm<sup>2</sup>.

After 48 hours an additional two coatings exhibited corrosion which were, one plain NiP coating and one 0.025 g/L gelatine coating.

At 72 hours exposure, all coating types had two coatings which had perished, except 0.0125 g/L which had two surviving coatings.

On completion of the test at 96 hours exposure, a single coating from each concentration of gelatine survived (Table 5). These coatings displayed varying levels of discolouration, but no ferrous oxide was observed under visual inspection.

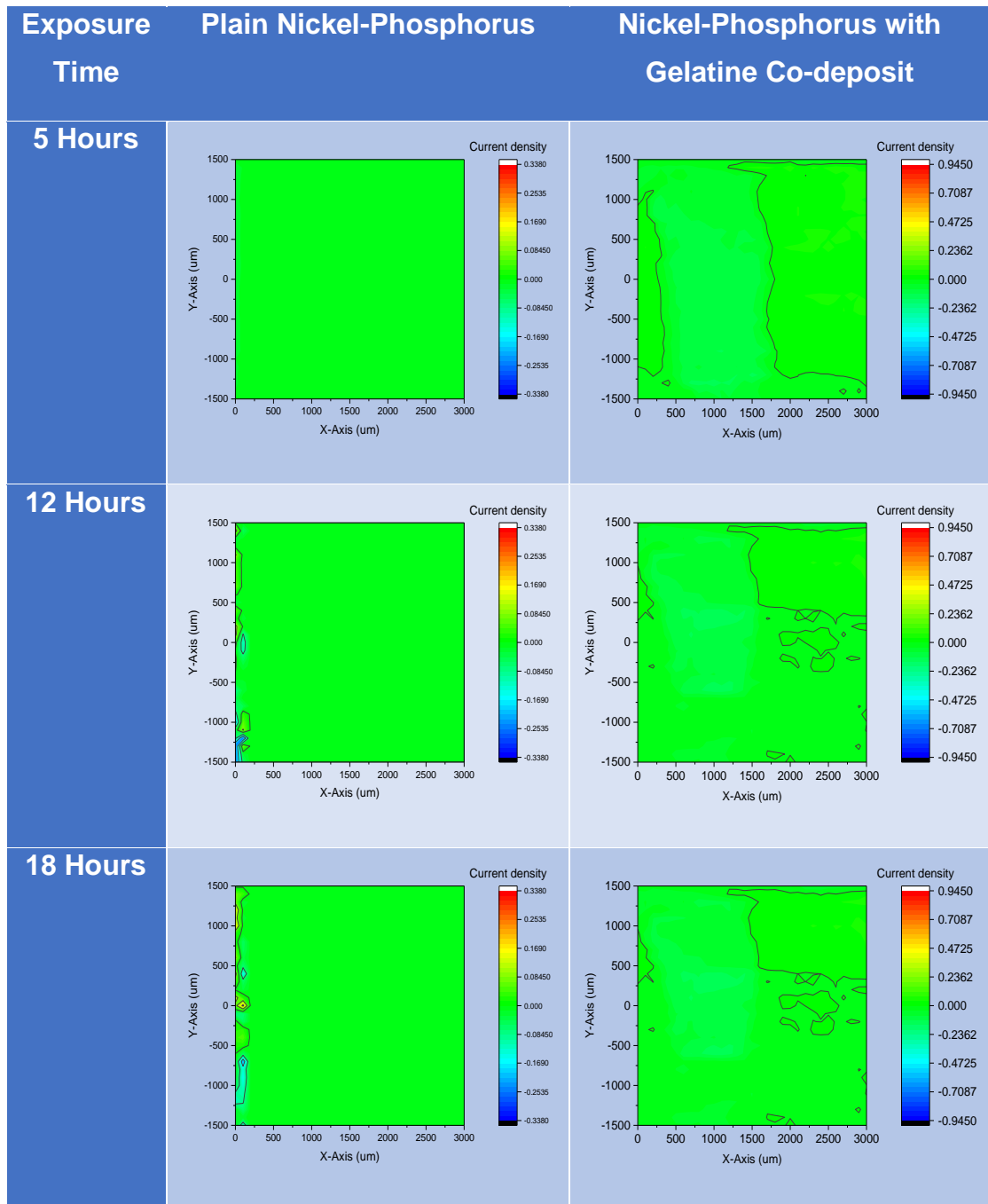
Table 5: Results of visual inspections performed at 24-hour intervals on NSS samples. Samples deemed to have failed if products of corrosion were visible.

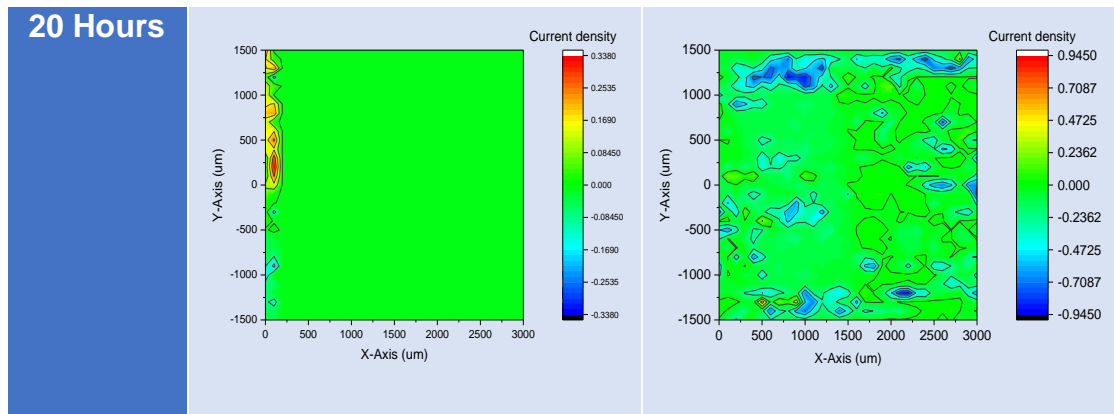
Sample Type	Sample Number	24 Hours	48 Hours	72 Hours	96 Hours
Plain NiP	1	Pass	Pass	Pass	Pass
	2	Pass	Pass	Fail	Fail
	3	Pass	Fail	Fail	Fail
NiP + 0.0125 g/L Gelatine	4	Pass	Pass	Fail	Fail
	5	Pass	Pass	Pass	Fail
	6	Pass	Pass	Pass	Pass
NiP + 0.025 g/L Gelatine	7	Pass	Fail	Fail	Fail
	8	Pass	Pass	Pass	Pass
	9	Fail	Fail	Fail	Fail
NiP + 0.05 g/L Gelatine	10	Fail	Fail	Fail	Fail
	11	Pass	Pass	Pass	Pass
	12	Fail	Fail	Fail	Fail

### 5.3.2 Scanning Vibrating Electrode Technique – SVET

The SVET analysis was performed on in the same location over a time of 20 hours in NaCl solution. The resulting currents measured indicated if anodic or cathodic reaction sites were occurring (Table 6), with the corrosion of Fe producing anodic reactions.

Table 6: SVET scan site results from 5 to 20 hours for plain NiP deposit and for NiP+0.025 g/L gelatine composite coating.





### Plain NiP

After 5 hours of immersion in the NaCl solution, no reactions were measured at the recorded current density. By 12 hours, the appearance of cathodic reaction sites emerged on the left hand edge of the sample scan site. After 18 hours the cathodic reactions became less intense and anodic sites were recorded. By 20 hours immersion, the cathodic sights had retreated further and the anodic sites became more pronounced indicating that corrosion was occurring on the map site left edge.

### NiP with Gelatine Co-deposit

No evidence of anodic current was present during the 20 hours immersion in NaCl. Cathodic currents were recorded across the scan site at 5 hours through 18 hours, however at 20 hours, strong cathodic reactions were recorded across the sample scan site. This implies that the coating provided protection to the substrate during the 20 hour test as no anodic corrosion was detected. Further work is required to determine the cause and impact of these cathodic sites and what impact it will have on the corrosion prevention.

### 5.3.3 Electrochemical Impedance Spectroscopy - EIS

These results represent a single measurement obtained for both plain NiP and NiP+0.025 g/L gelatine microgels. The results of the EIS analysis show an increase in the corrosion protection provided by the NiP/Gelatine coating when compared with plain NiP coating when exposed to a neutral 3.5 wt% NaCl solution.

Comparing the Bode plots (Figures 72, 73), the plain NiP sample is steady up to the 18-hour mark, at which point failure occurs before the next measurement at 24 hours. This is clearly seen in the double hump and reduction in resistance. In contrast, the coating with gelatine microgels, whilst showing a constant decrease in resistance, never fails within the 24-hour timeframe.

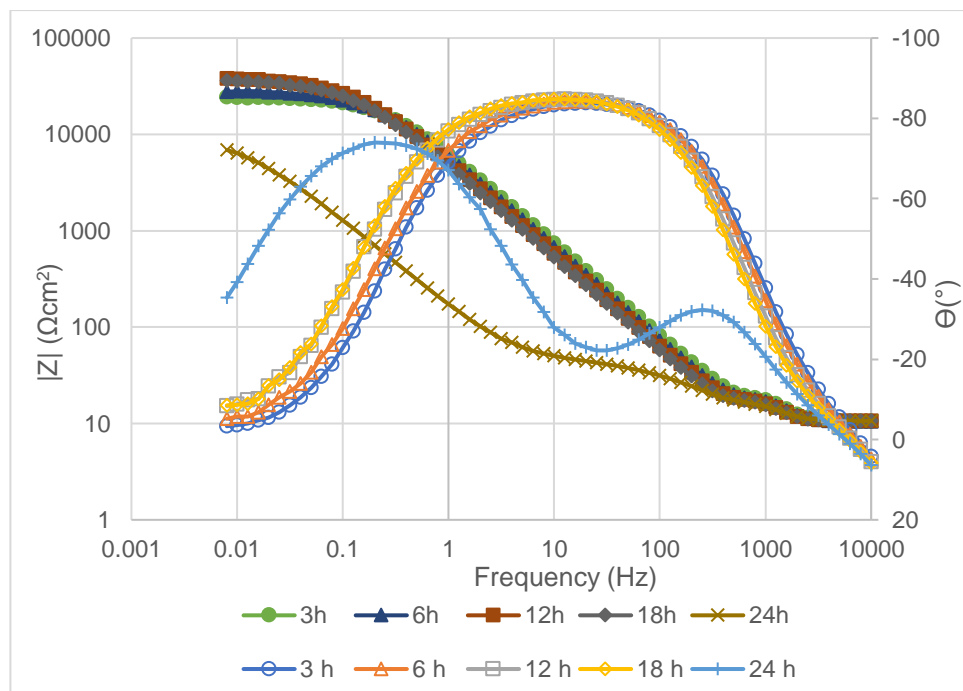


Figure 72: NiP only coating Bode plot demonstrating coating failure as described by the double hump which occurs at 24 hours.

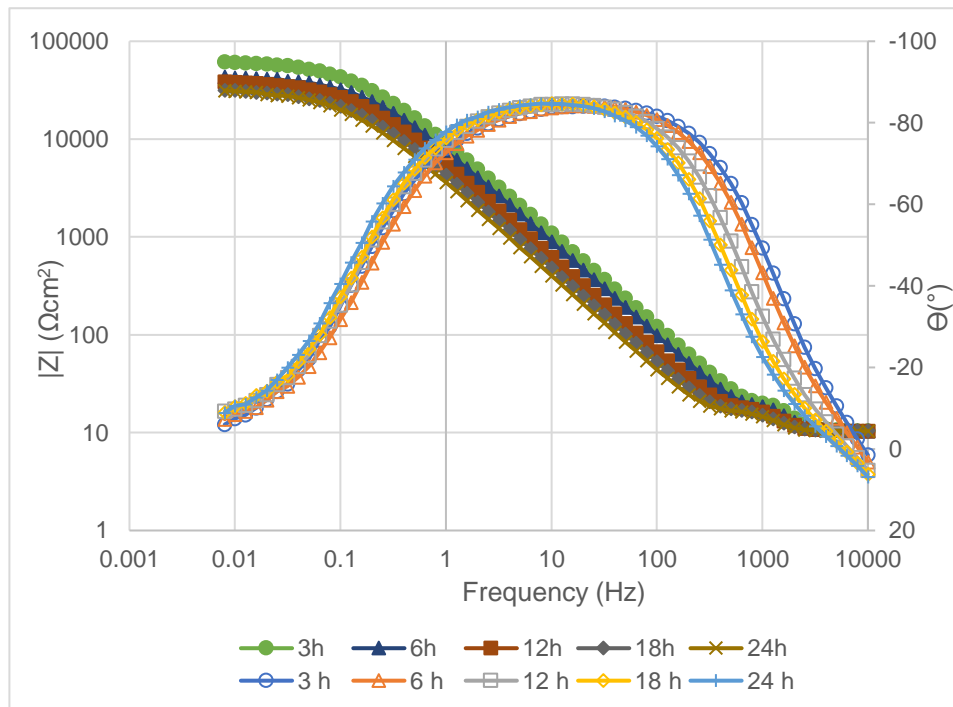


Figure 73: NiP+0.025 g/L gelatine microgel composite coating Bode plot.

When comparing the Nyquist plots showing the resistance of the coating, the increase in resistance up to 18 hours in plain NiP is visible (Figure 74). This is likely the development of an oxide layer, which would correspond with results observed in SVET analysis, before failure at the 24-hour mark. The gelatine co-deposit shows a consistent decrease in resistance (Figure 75) but does not fail like with plain NiP.

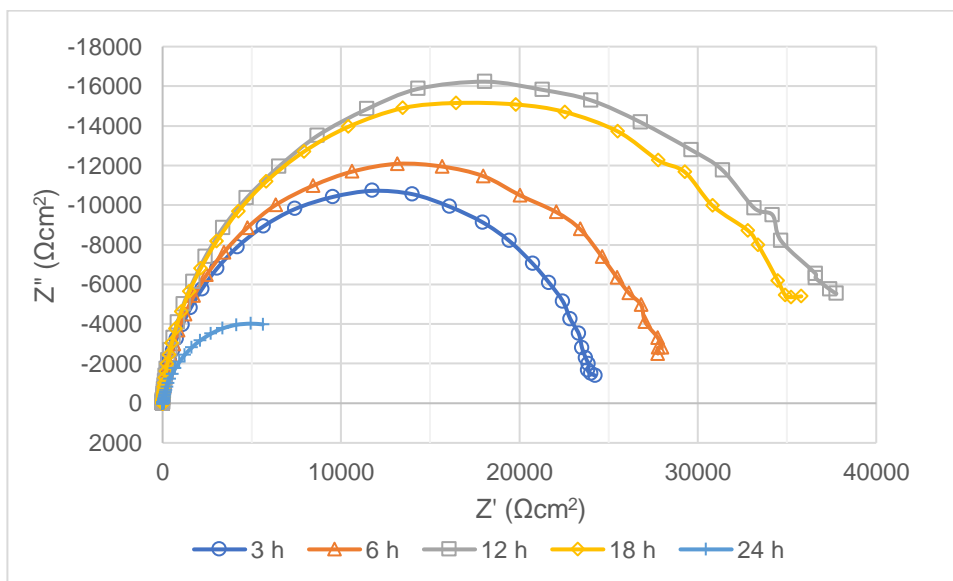


Figure 74: NiP only coating Nyquist plot showing significant drop in resistance at 24-hour plot.

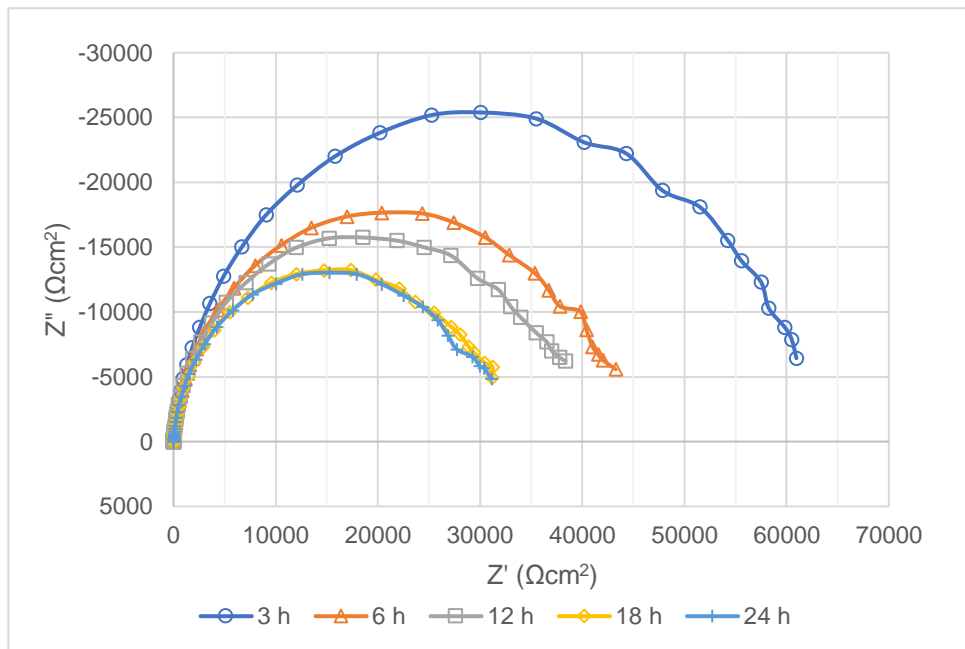


Figure 75: NiP+0.025 g/L gelatine microgel composite coating Nyquist plot.

An accurate fitting was required to determine the coatings resistance to corrosion. This was achieved using the equivalent circuit as described in section 3.4.2 which produced fitting curves that closely match the impedance spectra (Figure 76).

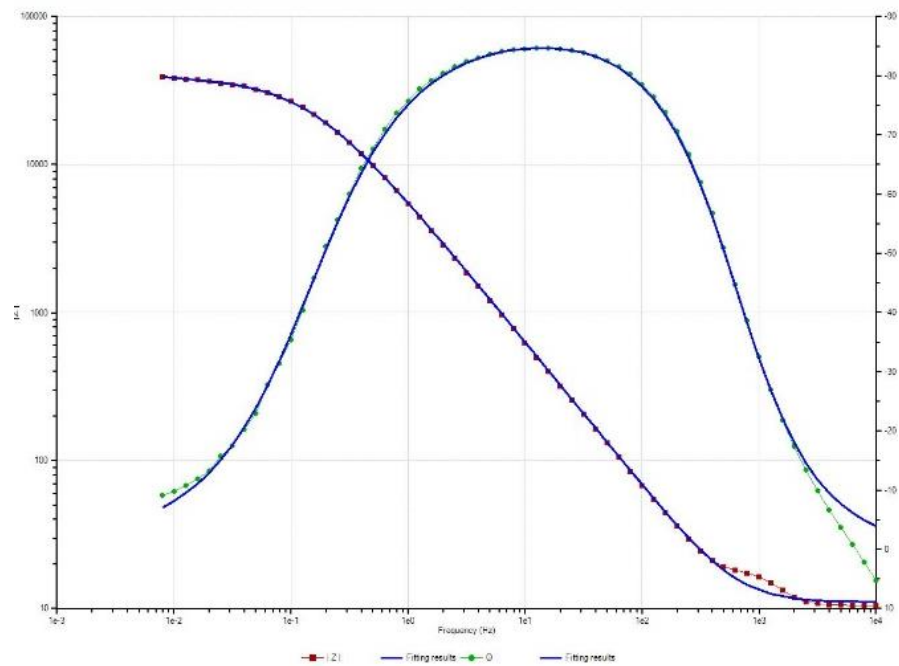


Figure 76: Example of fitting accuracy achieved on NiP+0.025 g/L gelatine microgels composite coating at 12 hours.

For plain NiP (Table 7), the increase observed in the  $R_T$  value over the first 18 hours of the experiment may be explained by the increases in  $R_{coat}$  and  $R_{ct}$ . The increase in  $R_{coat}$  relates to the resistance of the electrolyte in the pores of the coating and discontinuities in the passive layer. Due to exposure the chloride environment, the resulting corrosion products fill these pores, leading to an increase in the barrier properties. The increase in  $R_{ct}$  can also be attributed to the development of a passive oxide film on the coating surface due to corrosion [68]. After 24 hours, the barrier protection provided by the coating is reduced, and corrosion of the substrate is present.

Table 7: NiP only coating fitting results determined from the EIS data and equivalent circuits.

Time (Hrs)	$R_s$ (Ohms)	CPE1 – TDE ( $\mu F$ )	CPE1 – PHIDE	$R_{coat}$ (Ohms)	CPE2 – TDE ( $\mu F$ )	CPE2 – PHIDE	$R_{ct}$ (Ohms)	$R_T$ (Ohms)
3	11.09	21.87	0.98	3524.00	9.13	0.73	20863.00	24398.09
6	11.07	25.11	0.98	7110.30	14.09	0.61	21771.00	28892.37
12	11.18	28.90	0.98	8408.10	12.15	0.687	29754.00	38173.28
18	11.29	31.24	0.98	7570.20	14.66	0.56	30278.00	37859.49
24	10.72	111.52	0.85	36.62	106.45	0.90	9330.60	9377.94

For the NiP + 0.025 g/L gelatine composite coating (Table 8),  $R_{coat}$  and  $R_{ct}$  values do not increase with exposure to the chloride environment, suggesting that there is not a significant build-up of corroded material.  $R_{coat}$  decreases, indicating the development of pitting in on the surface and the decrease in  $R_{ct}$  indicates that the passive oxide layer does not form to the same extent as with plain NiP.

Table 8: NiP+0.025 g/L gelatine composite coating fitting results determined from the EIS data and equivalent circuits.

Time (Hrs)	$R_s$ (Ohms)	CPE1 – TDE ( $\mu F$ )	CPE1 – PHIDE	$R_{coat}$ (Ohms)	CPE2 – TDE ( $\mu F$ )	CPE2 – PHIDE	$R_{ct}$ (Ohms)	$R_T$ (Ohms)
3	10.86	15.68	0.97	11960.00	8.56	0.65	50711.00	62681.86
6	10.90	18.93	0.97	6791.10	10.04	0.59	37235.00	44037.00
12	11.05	27.56	0.97	8927.50	16.60	0.45	33706.00	42644.55
18	11.16	34.55	0.97	7756.80	22.34	0.46	27524.00	35291.96
24	10.34	44.27	0.96	6151.30	13.87	0.49	26396.00	32557.64

The corrosion protection offered by the coatings were taken from the total resistance of the impedance test. This showed that whilst the total resistance of the NiP/gelatine microgel coating decreased at each measured interval, it did not exhibit a severe drop off in performance like that of the plain NiP coating (Figure 77).

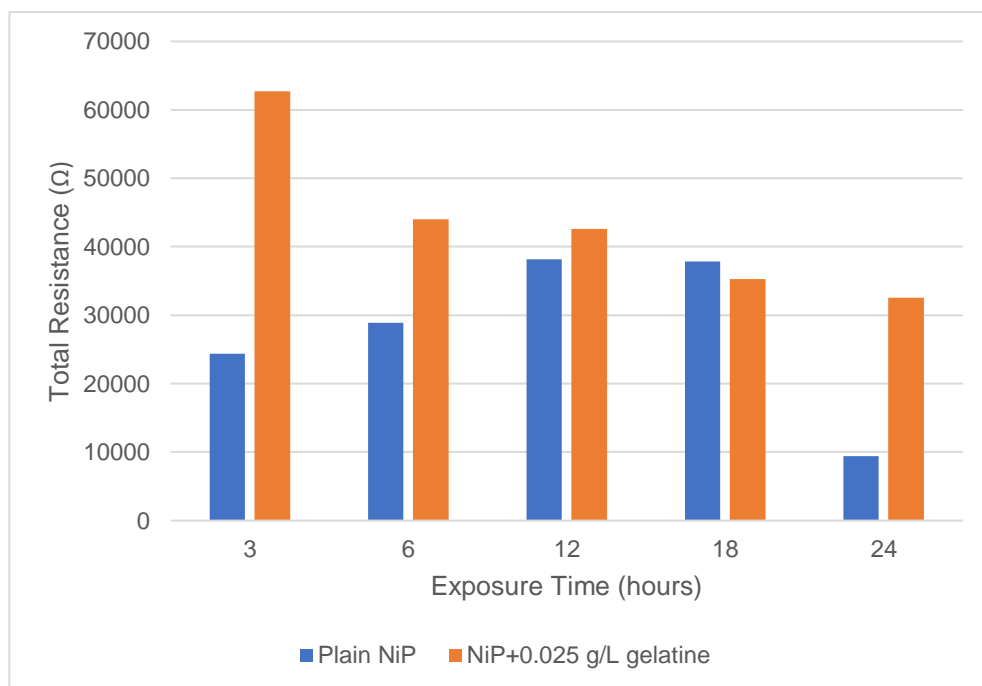


Figure 77: Total resistance calculated from EIS fittings in relation to exposure time for plain NiP and NiP/gelatine composite coatings.

## 5.4 Tribology Results

### 5.4.1 Surface Roughness

The results from surface roughness test show that as microgels are introduced to the coating, the coating roughness decreases (Figure 78). This is likely due to the increase in phosphorus content observed using EDXA (Figure 64). This could be due to the reduction in the “cauliflower heads” due to the increased amorphous structure of the high phosphorus coating resulting in a higher density of atomic packing. Similar trends have been observed by Yung-Chi et al. [69], whereby an increase in phosphorus content within electroless NiP deposits result in a reduction in coating roughness. This effect may be more notable in deposits from other solutions as the 1850 solution used for testing is marketed for use as a bright nickel, thus it exhibits low numbers of cauliflower heads under normal operating conditions (Figure 79).

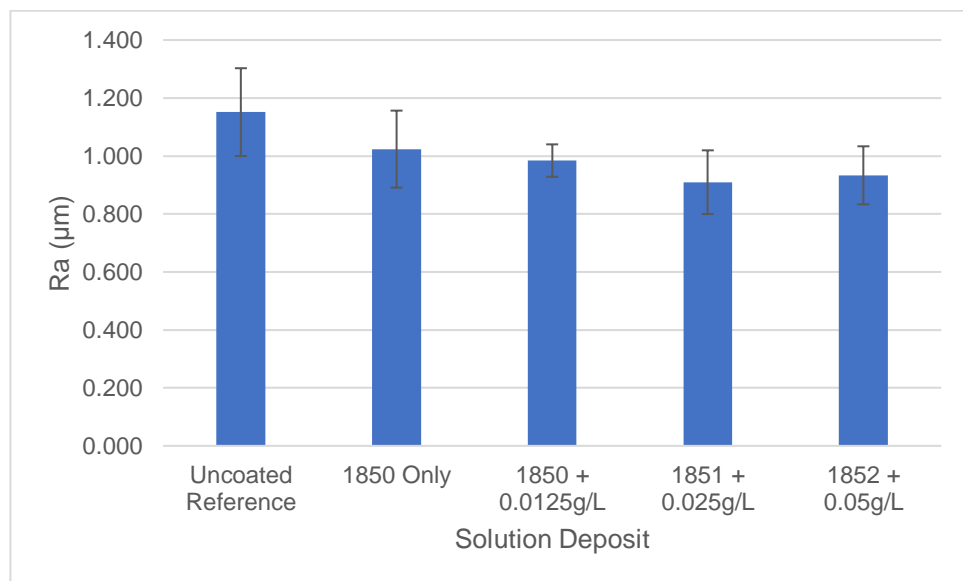


Figure 78: Surface roughness of coatings resulting from NiP/Gelatine co-deposition.

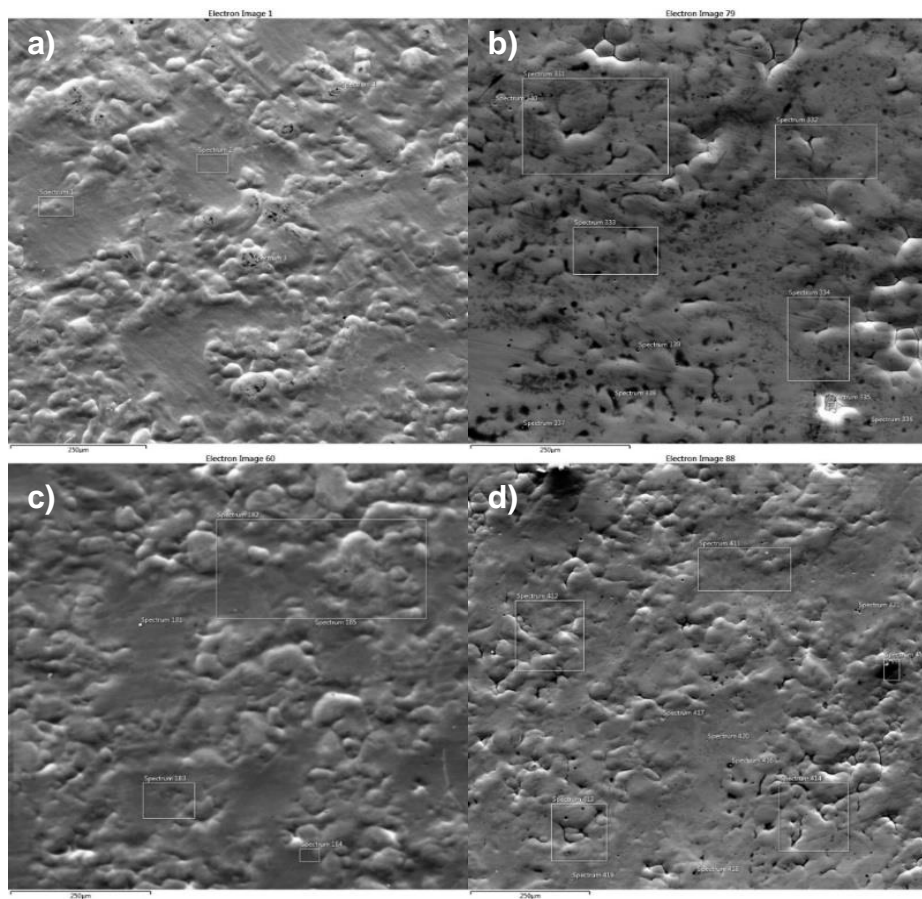


Figure 79: SEM images of a) Plain NiP, b) NiP+0.0125 g/L gelatine microgels, c) NiP+0.025 g/L gelatine microgels, d) NiP+0.05 g/L gelatine microgels. Samples show similar coating morphology with amorphous grain structure.

## 5.4.2 Coating Hardness

With the introduction of gelatine microgels, the coating hardness is reduced in comparison with plain NiP coating (Figure 80). This could be due to the increase in phosphorus content leading to amorphous coating which is less hard due to lack of grain structure. Similar results have been observed by Yan et al. and Sahoo et al. [70] [71], whereby an increase in phosphorus content of NiP coatings increases the amorphous phase. The transition from nanocrystalline to amorphous phase results in a decrease in the surface hardness of the coating.

Alternatively, this may be due to the inclusion of a soft material in the form of gelatine, acting as an effective void within the coating and reducing the hardness due to an effective lowering in density. Similar results have been found when co-depositing PTFE within NiP by Ramalho et al. and Huang et al. [72], [73].

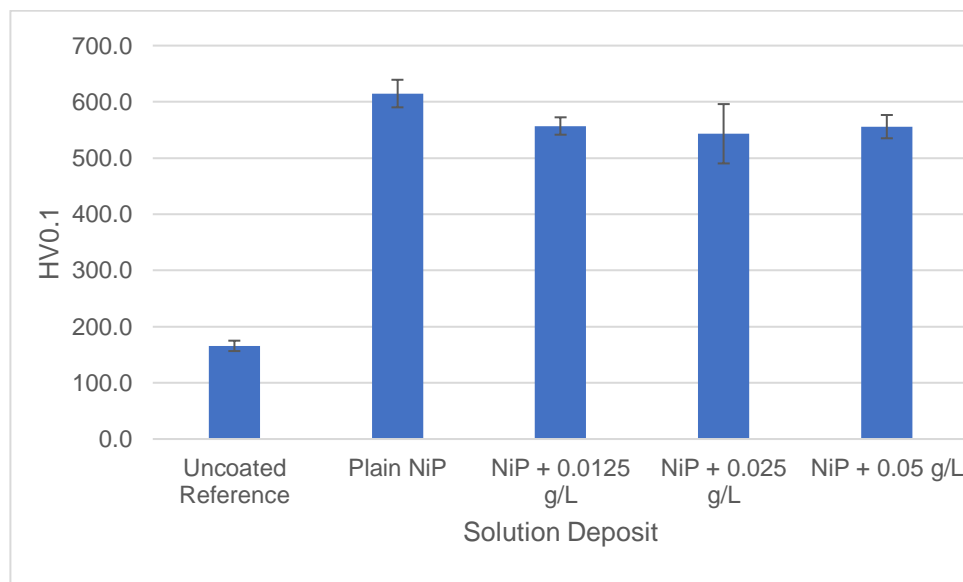


Figure 80: Vickers hardness results for the NiP/gelatine composite coatings in comparison with plain NiP and uncoated steel substrate.

### 5.4.3 Abrasion Resistance

The coatings abrasion resistance is measured as the wear rate of the coating, which is the volume of material removed during the grinding process. These results are then measured and interpreted to determine the size of the crater left during abrasion and hence the rate of wear. Due to the interpretive nature of determining the outer extent of the crater, this introduces opportunities for errors. To counter this, the results from four measuring conditions were averaged to give the general trend of the wear rate (Figure 82). The results show a slight increase in wear rate when compared with plain NiP (Figure 81), which would complement the results showing lower coating hardness. Similar results relating increased phosphorus content to a decrease in wear resistance have been observed by Sahoo et al. [32] and the inverse relationship between Vickers hardness and wear rate has been observed by Jeong et al. [74].

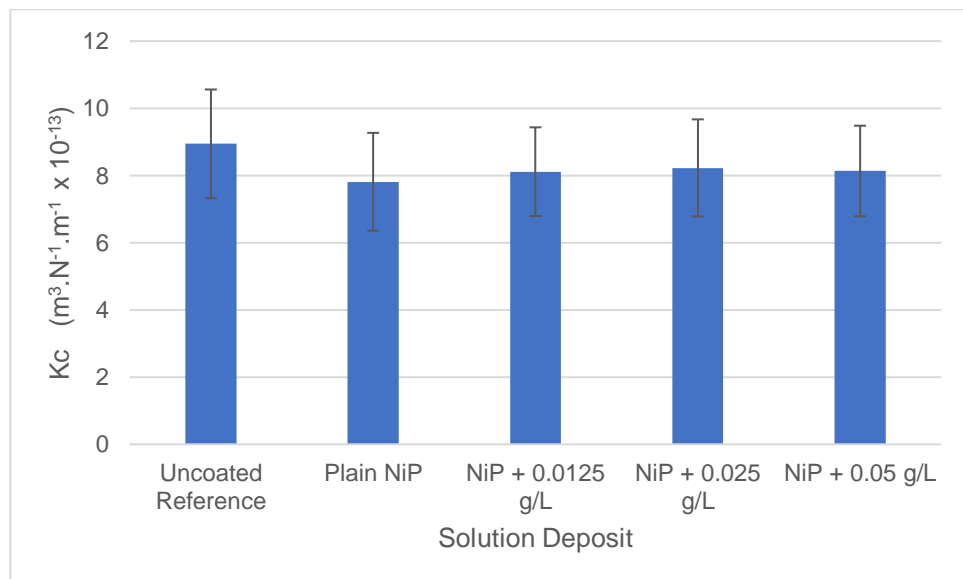


Figure 81: Coatings abrasive wear rate for the NiP/gelatine composite coatings in comparison with plain NiP and uncoated steel substrate.

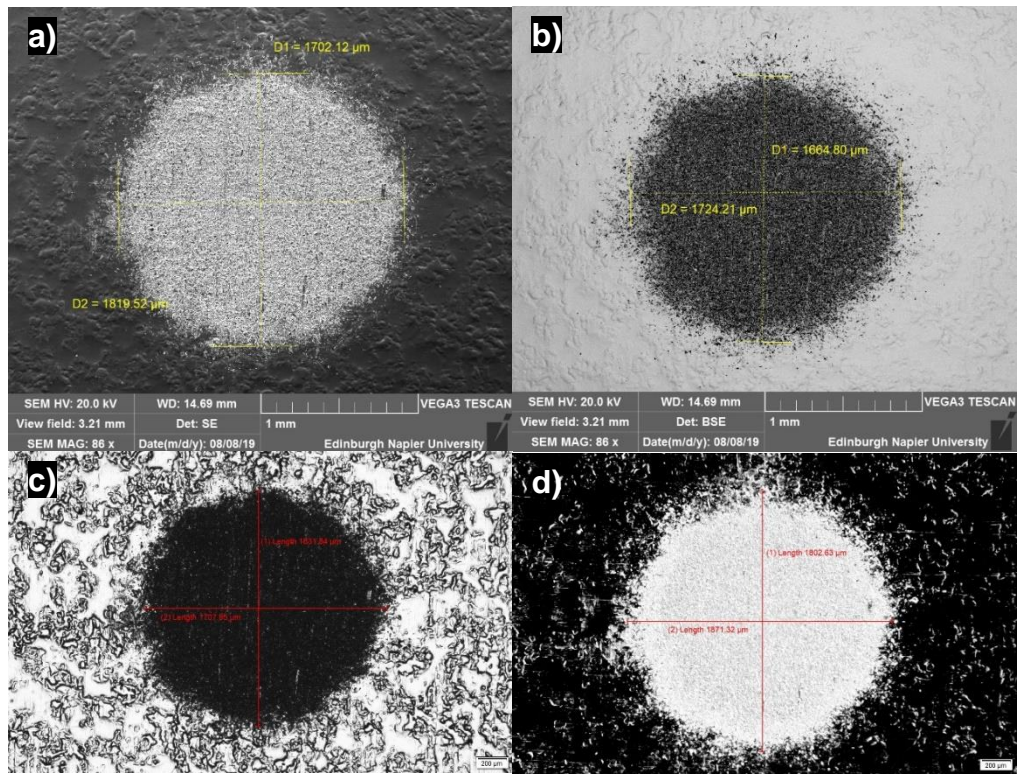


Figure 82: Plain NiP coating wear mark measured using varying imaging techniques: a) SEM imaging using scanning electrode technique, b) SEM imaging using back scatter electrode technique, c) optical microscope with integrated white light illumination, d) optical microscope with integrated white light not present.

## 6 Conclusions

This project has focused on the development of a procedure for successfully producing NiP/microgel composite coatings, along with characterising the impact of the second phase particle within the coating.

Sodium alginate microgels received from Wrocław were analysed and their viability for including in nickel coatings determined. These microgels were capable of loading with active ingredients of ENP deposition solutions for production of self-healing coatings.

The limitation of the microgel structure at elevated temperatures was the main limiting factor for successful deposition. Gelatine microgels once heat treated, proved a viable delivery system that can be incorporated in ENP coatings at temperatures of 89 °C and pH 4.9 for periods of at minimum 1 hour.

The high temperature deposition approach has been proven to be successful with the heat-treated gelatine. Microgels were co-deposited with nickel-phosphorus coatings at deposition rates comparable with standard nickel-phosphorus coatings (approx. 15  $\mu\text{m/hr}$ ).

Both sodium alginate and gelatine microgels are inherently unstable in solutions due to their zeta potential. Agitation methods were utilised with varying success during the study. Magnetic mechanical agitation from the bottom of the deposition was utilised during the plating stage and this produces acceptable coatings and dispersion of the microgels in the deposit. The use of ultrasonic agitation to enhance the microgels in suspension before being introduced gradually to the plating solution shows great promise. This pre-agitation stage should be carried out to increase deposition rates and improve dispersion of the microgel inclusions throughout the deposit.

The coatings mechanical properties were investigated and found to have altered with the inclusion of microgels. A small reduction in coating hardness and wear resistance was observed however it is not confirmed this was due to the microgels and not the change in phosphorus levels which can also affect these properties.

The corrosion protection offered by the inclusion of gelatine microgels proved inconclusive at the quantities tested. Some promise was shown in results of the

SVET and EIS analysis, which showed reduction in the anodic oxidation of these samples. However, the NSS test did not show an increase in the coatings corrosion prevention when compared with plain NiP. Varying the quantity of co-deposit and including corrosion inhibitors within the gelatine microgels may increase the corrosion protection of these coatings.

## 7 Future Work

The results obtained during this study have shown that the inclusion of gelatine microgels is possible within electroless nickel-phosphorus (ENP) coatings. Whilst these results have been promising, further work on the subject should be undertaken. The author suggests some avenues of research that would be beneficial to examine further.

A more expansive EIS study should be performed with coatings of various microgel bath loadings, to determine what impact the microgels have on the barrier coating properties. These microgels should be tailored to include corrosion inhibitors which could increase the corrosion protection offered by the NiP/microgel composite coatings.

The use of surfactants in the deposition process should be explored to determine if this reduces the aggregation of microgels and increases the inclusion rate within the coating.

Additional work on either lower deposition temperature ENP solutions, or deposition with electroplated nickel would be a worthwhile investigation. Other, non-proprietary deposition solutions should be investigated to confirm that the process is repeatable with less robust solutions for other applications.

Further work on microgel size which could have an effect on the surface area in the bath should be undertaken. With increasing or decreasing microgel size, the impact on the electroless nickel reduction sites is unknown and may lead to higher deposition rates.

Due to the minor reduction in tribological mechanical properties identified in this study, the inclusion of a ceramic co-deposit in addition to gelatine microgels, would be useful to maintain or enhance the mechanical properties of the nickel phosphorous deposit. This would assist in determining the suitable applications for the deposition process developed during this project. Additions such as SiC, TiB<sub>2</sub> and Al<sub>2</sub>O<sub>3</sub> that are used to increase mechanical properties would prove a useful addition to the NiP/gelatine composite coating and negate any deleterious effects of the softer gelatine microgels.

## 8 References

- [1] G. Koch, *Cost of corrosion*. Elsevier Ltd, 2017.
- [2] V. Kuklík and J. Kudláček, "Introduction," *Hot-Dip Galvaniz. Steel Struct.*, vol. 1742, pp. xiii–xx, 2016, doi: 10.1016/b978-0-08-100753-2.00019-7.
- [3] B. Roberts, "Paint systems for steel," *Steel Times Int.*, vol. 36, no. 3, pp. 36–37, 2012.
- [4] A. Kumar, L. D. Stephenson, and J. N. Murray, "Self-healing coatings for steel," *Prog. Org. Coatings*, vol. 55, no. 3, pp. 244–253, 2006, doi: 10.1016/j.porgcoat.2005.11.010.
- [5] ASM International, "ASM HANDBOOK: Surface Engineering - Volume 5," vol. 5, 1994.
- [6] M. Samadzadeh, S. H. Boura, M. Peikari, S. M. Kasiriha, and A. Ashrafi, "A review on self-healing coatings based on micro/nanocapsules," *Prog. Org. Coatings*, vol. 68, no. 3, pp. 159–164, 2010, doi: 10.1016/j.porgcoat.2010.01.006.
- [7] A. Stankiewicz, Z. Jagoda, K. Zielinska, and I. Szczygieł, "Gelatin microgels as a potential corrosion inhibitor carriers for self-healing coatings: Preparation and codeposition," *Mater. Corros.*, vol. 66, no. 12, pp. 1391–1396, 2015, doi: 10.1002/maco.201508436.
- [8] B. Aissa, D. Therriault, E. Haddad, and W. Jamroz, "Self-healing materials systems: Overview of major approaches and recent developed technologies," *Adv. Mater. Sci. Eng.*, vol. 2012, 2012, doi: 10.1155/2012/854203.
- [9] E. Rudnik, K. Kokoszka, and J. Łapsa, "Comparative studies on the electroless deposition of Ni-P, Co-P and their composites with SiC particles," *Surf. Coatings Technol.*, vol. 202, no. 12, pp. 2584–2590, 2008, doi: 10.1016/j.surfcoat.2007.09.026.
- [10] I. R. Mafi and C. Dehghanian, "Comparison of the coating properties and corrosion rates in electroless Ni-P/PTFE composites prepared by different types of surfactants," *Appl. Surf. Sci.*, vol. 257, no. 20, pp. 8653–8658, 2011, doi: 10.1016/j.apsusc.2011.05.043.
- [11] R. Turnbull, N. Shearer, and C. Wilson, "Cellulose microfibrils as a pore former in electroless co-deposited anodes for solid oxide fuel cells.," *ECS Trans.*, vol. 78, pp. 1447–1456, 2017.
- [12] M. Paunovic and M. Schlesinger, *Fundamentals of Electrochemical Deposition*, Second. Hoboken: Wiley & Sons Inc., 2006.
- [13] W. Riedel, *Electroless Nickel Plating*. Stevenage: Finishing Publications LTD., 1991.
- [14] G. A. Di Bari, "Electrodeposition of Nickel," *Mod. Electroplat. Fifth Ed.*, pp. 79–114, 2011, doi: 10.1002/9780470602638.ch3.
- [15] G. Schiavone, "Manufacturing integrated MEMS switching devices using electrodeposited NiFe," 2014.

- [16] R. Parkinson, "Properties and Applications of Electroless Nickel," *Nickel Dev. Inst. Publ.*, p. 33, 1997, [Online]. Available: [http://www.nickelinstitute.org/TechnicalLiterature/TechnicalSeries/PropertiesandApplicationsofElectrolessNickel\\_10081\\_.aspx](http://www.nickelinstitute.org/TechnicalLiterature/TechnicalSeries/PropertiesandApplicationsofElectrolessNickel_10081_.aspx).
- [17] X. Yin, L. Hong, B. H. Chen, and T. M. Ko, "Modeling the stability of electroless plating bath - Diffusion of nickel colloidal particles from the plating frontier," *J. Colloid Interface Sci.*, vol. 262, no. 1, pp. 89–96, 2003, doi: 10.1016/S0021-9797(03)00191-7.
- [18] R. C. Agarwala and V. Agarwala, "Electroless alloy / composite coatings : A review," *Sadhana*, vol. 28, no. August, pp. 475–493, 2003, doi: 10.1007/BF02706445.
- [19] I. Baskaran, T. S. N. S. Narayanan, and A. Stephen, "Effect of accelerators and stabilizers on the formation and characteristics of electroless Ni-P deposits," *Mater. Chem. Phys.*, vol. 99, no. 1, pp. 117–126, 2006, doi: 10.1016/j.matchemphys.2005.10.001.
- [20] C. A. Loto, "Electroless Nickel Plating - A Review," *Silicon*, vol. 8, no. 2, pp. 177–186, 2016, doi: 10.1007/s12633-015-9367-7.
- [21] W. Sha, X. Wu, and K. G. Keong, *Electroless Copper and Nickel-Phosphorus Plating*. 2011.
- [22] Doug Vogel, "A Comparison of Electroless and Electrolytic Nickel," *Products Finishing*, 2007. <http://connection.ebscohost.com/c/articles/27494405/comparison-electroless-electrolytic-nickel>.
- [23] H. Ke-Ping and F. Jing-Li, "Acceleration effect of electroless nickel deposition by thiourea," *Int. J. Chem. Kinet.*, vol. 28, no. 4, pp. 259–264, 1996, doi: 10.1002/(SICI)1097-4601(1996)28:4<259::AID-KIN3>3.3.CO;2-N.
- [24] R. Taheri, "Evaluation of Electroless Nickel-Phosphorus ( EN ) Coatings," University of Saskatchewan, 2003.
- [25] A. Wurtz, *Ann. Chim. Phys.*, vol. 3, no. 11, 1844.
- [26] P. Breteau, *Bull. Soc. Chim.*, p. 9, 1911.
- [27] F. A. Roux, "U.S. patent 1,207,218," 1916.
- [28] a. Brenner and G. E. Riddell, "Nickel plating on steel by chemical reduction," *J. Res. Natl. Bur. Stand. (1934)*, vol. 37, no. 1, pp. 31–34, 1946, doi: 10.6028/jres.037.019.
- [29] G. O. Mallory and J. B. Hajdu, "Electroless Plating: Fundamentals And Applications," pp. 1–532, 1990.
- [30] S. Yae, K. Ito, T. Hamada, N. Fukumuro, and H. Matsuda, "Electroless deposition of pure nickel films from a simple solution consisting of nickel acetate and hydrazine," *Plat. Surf. Finish.*, vol. 92, no. 4, pp. 58–62, 2005.
- [31] W. (National U. of S. Ke, "Development of lead-free electroless nickel plating systems and metal thin films on silicone and nafion membranes," 2008.

- [32] P. Sahoo and S. K. Das, "Tribology of electroless nickel coatings - A review," *Mater. Des.*, vol. 32, no. 4, pp. 1760–1775, 2011, doi: 10.1016/j.matdes.2010.11.013.
- [33] A. Stankiewicz, I. Szczygieł, and B. Szczygieł, "Summary of existing models of the Ni-P coating electroless deposition process," *Int. J. Chem. Kinet.*, vol. 45, no. 11, pp. 755–762, 2013, doi: 10.1002/kin.20810.
- [34] G. Gutzeit, "Catalytic nickel deposition from aqueous solution.," *Plating*, vol. 46, pp. 1158–1164, 1959.
- [35] P. Hersch, "Transactions of the Institute of Metal Finishing," vol. 33, pp. 417–420, 1955.
- [36] G. Salvago and P. L. Cavallotti, "Characteristics of the chemical reduction of nickel alloys with hypophosphite," *Plating*, vol. 59, pp. 665–671, 1972.
- [37] J. Sudagar, J. Lian, and W. Sha, "Electroless nickel, alloy, composite and nano coatings - A critical review," *J. Alloys Compd.*, vol. 571, pp. 183–204, 2013, doi: 10.1016/j.jallcom.2013.03.107.
- [38] G. O. Mallory, "The fundamental aspects of electroless nickel plating," *Fundam. Asp. electroless nickel Plat.*, pp. 1–56, 1990, [Online]. Available: <http://scholar.google.com/scholar?hl=en&btnG=Search&q=intitle:The+Fundamental+Aspects+Of+Electroless+Nickel+Plating#0>.
- [39] C. de Minjer and A. Brenner, ".,," *Plating*, vol. 44, no. 63, 1960.
- [40] G. Zhou, C. Y. Chen, L. Li, Z. Tao, W. He, and C. P. Wong, "Effect of MnSO<sub>4</sub> on the Deposition of Electroless Nickel Phosphorus and its Mechanism," *Electrochim. Acta*, vol. 127, pp. 276–282, 2014, doi: 10.1016/j.electacta.2014.02.044.
- [41] W. J. Cheong, B. L. Luan, and D. W. Shoesmith, "The effects of stabilizers on the bath stability of electroless Ni deposition and the deposit," *Appl. Surf. Sci.*, vol. 229, no. 1–4, pp. 282–300, 2004, doi: 10.1016/j.apsusc.2004.02.003.
- [42] H. Keping and J. L. Fang, "Stabilization effect of electroless nickel plating by thiourea," *Met. Finish.*, vol. 95, no. February, pp. 73–75, 1997, doi: 10.1016/S0026-0576(97)81818-1.
- [43] M. Der Ger and B. J. Hwang, "Effect of surfactants on codeposition of PTFE particles with electroless Ni-P coating," *Mater. Chem. Phys.*, vol. 76, no. 1, pp. 38–45, 2002, doi: 10.1016/S0254-0584(01)00513-2.
- [44] B.-H. Chen, L. Hong, Y. Ma, and T.-M. Ko, "Effects of surfactants in an electroless nickel-plating bath on the properties of Ni-P alloy deposits," *Ind. Eng. Chem. Res.*, vol. 41, no. 11, pp. 2668–2678, 2002, doi: 10.1021/ie0105831.
- [45] A. A. Aal, A. Shaaban, and Z. A. Hamid, "Nanocrystalline soft ferromagnetic Ni-Co-P thin film on Al alloy by low temperature electroless deposition," *Appl. Surf. Sci.*, vol. 254, no. 7, pp. 1966–1971, 2008, doi: 10.1016/j.apsusc.2007.08.017.

- [46] C. Baldwin and T. E. Such, "The Plating Rates and Physical Properties of Electroless Nickel/Phosphorus Alloy Deposits," *Trans. IMF*, vol. 46, no. 2, p. 73, 1968, doi: 10.1080/00202967.1968.11870052.
- [47] M. Schwartz, *Proc. AES*, vol. 47, no. 176, 1960.
- [48] B. Hu *et al.*, "Effect of bath pH and stabilizer on electroless nickel plating of magnesium alloys," *Surf. Coatings Technol.*, vol. 228, pp. 84–91, 2013, doi: 10.1016/j.surfcoat.2013.04.011.
- [49] Y. S. Park, T. H. Kim, M. H. Lee, and S. C. Kwon, "Study on the effect of ultrasonic waves on the characteristics of electroless nickel deposits from an acid bath," *Surf. Coatings Technol.*, vol. 153, no. 2–3, pp. 245–251, 2002, doi: 10.1016/S0257-8972(01)01683-8.
- [50] A. J. Copley, T. J. Mason, and V. Saez, "Review of effect of ultrasound on electroless plating process," *Trans. Inst. Met. Finish.*, vol. 89, no. 6, pp. 303–309, 2011, doi: 10.1179/174591911X13170500147670.
- [51] I. Tudela, Y. Zhang, M. Pal, I. Kerr, and A. J. Copley, "Ultrasound-assisted electrodeposition of composite coatings with particles," *Surf. Coatings Technol.*, vol. 259, no. PC, pp. 363–373, 2014, doi: 10.1016/j.surfcoat.2014.06.023.
- [52] M. Y. Abyaneh, A. Sterritt, and T. J. Mason, "Effects of Ultrasonic Irradiation on the Kinetics of Formation, Structure, and Hardness of Electroless Nickel Deposits," *J. Electrochem. Soc.*, vol. 154, no. 9, p. D467, 2007, doi: 10.1149/1.2754075.
- [53] A. J. Copley and V. Saez, "The use of ultrasound to enable low temperature electroless plating (PowerPoint)," *Circuit World*, vol. 38, no. 1, pp. 12–15, 2012, doi: 10.1108/03056121211195003.
- [54] A. J. Copley and V. Saez, "The use of ultrasound to enable low temperature electroless plating," *Circuit World*, vol. 38, no. 1, pp. 12–15, 2012, doi: 10.1108/03056121211195003.
- [55] Z. Jagoda, A. Stankiewicz, K. Zielińska, and I. Szczygieł, "Gelatin e microgels as a potential corrosion inhibitor carriers – preparation and codeposition with Ni-P coating To obtain the possible smallest gelatine microgel Proof of Concept," vol. 28, no. 2012, p. 10837, 2015.
- [56] T. H. Tran *et al.*, "Regenerative Nano-Hybrid Coating Tailored for Autonomous Corrosion Protection," *Adv. Mater.*, pp. 3825–3830, 2015, doi: 10.1002/adma.201501044.
- [57] W. Xiong *et al.*, "A novel capsule-based self-recovery system with a chloride ion trigger," *Sci. Rep.*, vol. 5, p. 10866, 2015, doi: 10.1038/srep10866.
- [58] Malvern, *Zetasizer nano series user manual*, no. 11. 2013.
- [59] Nanocomposix, "Zeta Potential Measurements." <https://nanocomposix.com/pages/zeta-potential-measurements#target>.

- [60] A. P. V. Ferreyra Maillard, J. C. Espeche, P. Maturana, A. C. Cutro, and A. Hollmann, "Zeta potential beyond materials science: Applications to bacterial systems and to the development of novel antimicrobials," *Biochim. Biophys. Acta - Biomembr.*, vol. 1863, no. 6, 2021, doi: 10.1016/j.bbamem.2021.183597.
- [61] N. Nwosu, "Optimisation of Electroless Co-deposited Solid Oxide Fuel Cell Electrodes by," Edinburgh Napier University, 2013.
- [62] K. Haruna, I. B. Obot, N. K. Ankah, A. A. Sorour, and T. A. Saleh, "Gelatin: A green corrosion inhibitor for carbon steel in oil well acidizing environment," *J. Mol. Liq.*, vol. 264, pp. 515–525, 2018, doi: 10.1016/j.molliq.2018.05.058.
- [63] I. Mukherjee and M. Rosolen, "Thermal transitions of gelatin evaluated using DSC sample pans of various seal integrities," *J. Therm. Anal. Calorim.*, vol. 114, no. 3, pp. 1161–1166, 2013, doi: 10.1007/s10973-013-3166-4.
- [64] S. Fakirov, E. Cagiao, M. J. Balta Calleja, F. D. Sapundjieva, and E. Vassileva, "Melting of Gelatin Crystals below Glass Transition Temperature: A Direct Crystal-Glass Transition as Revealed by microhardness," *Int. J. Polym. Mater. Polym. Biomater.*, vol. 43, pp. 195–206, 1999.
- [65] A. Stankiewicz, J. Winiarski, K. Zielinska, and M. Barker, "Electroless Ni-P \ alginate microgels coatings with self-healing properties," in *Proceedings of EuroCorr*, 2017, pp. 1–5.
- [66] Inam-UI-Haque, S. Ahmad, and A. Khan, "Electroless nickel plating on ABS plastics from nickel chloride and nickel sulphate baths," *Jour. Chem. Soc. Pak.*, vol. 27, no. 3. 2005.
- [67] A. Brenner and G. Riddell, "Deposition of nickel and cobalt by chemical reduction," *J. Res. Natl. Bur. Stand. (1934).*, vol. 39, no. November, p. 385, 1947, doi: 10.6028/jres.039.024.
- [68] A. Stankiewicz, J. Winiarski, M. Stankiewicz, I. Szczygieł, and B. Szczygieł, "Corrosion resistance evaluation of Ni-P/nano-ZrO<sub>2</sub> composite coatings by electrochemical impedance spectroscopy and machine vision method," *Mater. Corros.*, vol. 66, no. 7, pp. 643–648, 2015, doi: 10.1002/maco.201407831.
- [69] L. Yung-Chi, D. Jenq-Gong, and C. Bi-Shiou, "Wettability of Electroplated Ni-P in Under Bump Metallurgy with Sn-Ag-Cu Solder," *J. Electron. Mater.*, vol. 35, no. 1, 2006.
- [70] M. Yan, H. G. Ying, and T. Y. Ma, "Surface & Coatings Technology Improved microhardness and wear resistance of the as-deposited electroless Ni – P coating," *Surf. Coat. Technol.*, vol. 202, pp. 5909–5913, 2008, doi: 10.1016/j.surfcoat.2008.06.180.
- [71] S. K. Das and P. Sahoo, "Tribological characteristics of electroless Ni-B coating and optimization of coating parameters using Taguchi based grey relational analysis," *Materials and Design*, vol. 32, no. 4. pp. 2228–2238, 2011, doi: 10.1016/j.matdes.2010.11.028.

- [72] A. Ramalho and J. C. Miranda, "Friction and wear of electroless NiP and NiP + PTFE coatings," *Wear*, vol. 259, no. 7–12, pp. 828–834, 2005, doi: 10.1016/j.wear.2005.02.052.
- [73] Y. S. Huang, X. T. Zeng, I. Annergren, and F. M. Liu, "Development of electroless NiP – PTFE – SiC composite coating," *Surf. Coat. Technol.*, vol. 167, no. 02, pp. 207–211, 2003, doi: 10.1016/S0257-8972(02)00899-X.
- [74] D. H. Jeong, U. Erb, K. T. Aust, and G. Palumbo, "The relationship between hardness and abrasive wear resistance of electrodeposited nanocrystalline Ni-P coatings," *Scripta Materialia*, vol. 48, no. 8, pp. 1067–1072, 2003, doi: 10.1016/S1359-6462(02)00633-4.

## 9 Appendices

### 9.1 Appendix A – EDXA report of sodium alginate microgels

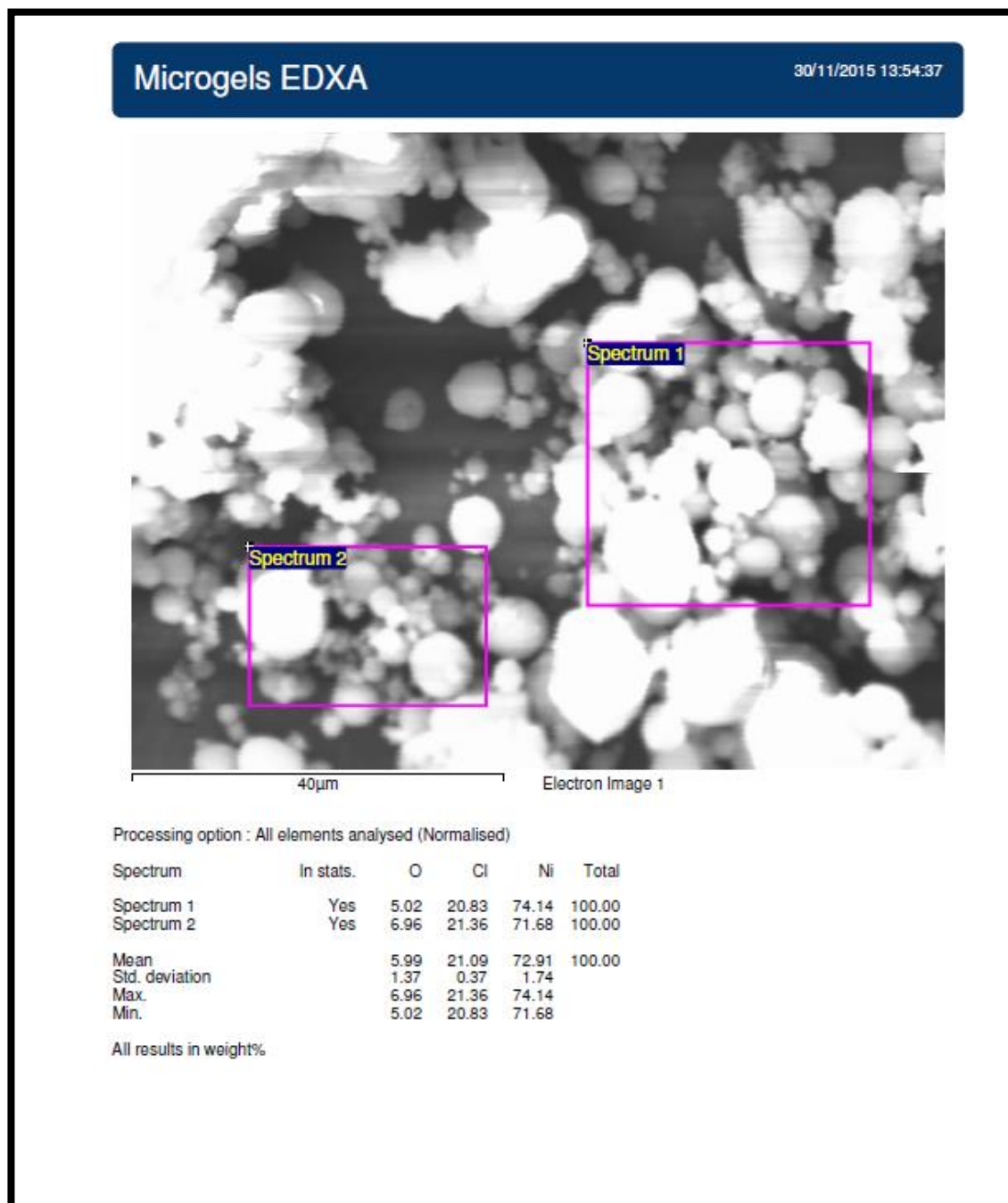


Figure 83: EDXA report for sodium alginate microgels as received prior to immersion in deionised water.

Table 9: Results of EDXA performed on sodium alginate microgels 1 before and after immersion in deionised water.

Microgel Type	Site	Spectrum	Element	Weight %	±	Atomic %	
Microgels 1 (Synthetic) - Dry	1	1	Oxygen	9.10	0.55	23.89	
			Chlorine	23.56	0.32	27.92	
			Nickel	67.35	0.51	48.20	
		2	Oxygen	13.98	0.58	33.00	
			Chlorine	27.70	0.32	29.50	
			Nickel	58.32	0.48	37.50	
	2	1	Oxygen	5.02	0.49	14.51	
			Chlorine	20.83	0.34	27.15	
			Nickel	74.14	0.50	58.34	
		2	Oxygen	6.96	0.64	19.27	
			Chlorine	21.36	0.38	26.67	
			Nickel	71.68	0.61	54.06	
	3	1	Oxygen	11.80	0.56	28.99	
			Chlorine	27.17	0.33	30.13	
			Nickel	61.03	0.49	40.88	
		2	Oxygen	15.61	0.56	36.34	
			Chlorine	24.28	0.31	25.51	
			Nickel	60.11	0.49	38.14	
	Average			Oxygen	10.41	na	26.00
				Chlorine	24.15	na	27.81
				Nickel	65.44	na	46.19
Microgels 1 (Synthetic) - After Hydration	1	1	Oxygen	30.66	0.54	61.60	
			Chlorine	1.22	0.19	1.11	
			Nickel	68.12	0.54	37.29	
		2	Oxygen	5.97	0.49	18.78	
			Chlorine	1.12	0.22	1.59	
			Nickel	92.91	0.52	79.63	
	2	1	Oxygen	4.11	0.46	13.57	
			Chlorine	0.39	0.15	0.58	
			Nickel	95.50	0.48	85.85	
		2	Oxygen	17.34	0.55	43.26	
			Chlorine	1.19	0.19	1.34	
			Nickel	81.47	0.57	55.40	
	3	1	Oxygen	0.75	0.33	2.71	
			Chlorine	0.07	0.06	0.12	
			Nickel	99.17	0.33	97.17	
		2	Oxygen	1.12	0.29	3.98	
			Chlorine	0.22	0.12	0.36	
			Nickel	98.66	0.31	95.66	
	Average			Oxygen	9.99	na	23.98
				Chlorine	0.70	na	0.85
				Nickel	89.31	na	75.17

## 9.2 Appendix B – Zeta Potential Measurements

Table 10: Results from Zeta potential for sodium alginate, as received gelatine and heat-treated gelatine with outliers removed.

Record	Type	Sample Name	Measurement Date and Time	ZP (mV)	Outlier	Q1	Q3	IQR	Upper Bound	Lower Bound
1	Zeta	3g/l Alginate in Water 1	28/07/2016 10:15	13.8	FALSE	12.25	13.3	1.05	14.875	10.675
2	Zeta	3g/l Alginate in Water 2	28/07/2016 10:17	13.7	FALSE					
3	Zeta	3g/l Alginate in Water 3	28/07/2016 10:18	13.3	FALSE					
4	Zeta	3g/l Alginate in Water 4	28/07/2016 10:19	13.1	FALSE					
5	Zeta	3g/l Alginate in Water 5	28/07/2016 10:19	13.7	FALSE					
6	Zeta	3g/l Alginate in Water run 21	28/07/2016 10:26	13	FALSE					
7	Zeta	3g/l Alginate in Water run 22	28/07/2016 10:28	13.1	FALSE					
8	Zeta	3g/l Alginate in Water run 23	28/07/2016 10:28	13.2	FALSE					
9	Zeta	3g/l Alginate in Water run 24	28/07/2016 10:29	12.3	FALSE					
10	Zeta	3g/l Alginate in Water run 25	28/07/2016 10:30	13.3	FALSE					
11	Zeta	3g/l Alginate in Water run 21	28/07/2016 10:37	12.9	FALSE					
12	Zeta	3g/l Alginate in Water run 22	28/07/2016 10:39	12.6	FALSE					
13	Zeta	3g/l Alginate in Water run 23	28/07/2016 10:40	12.9	FALSE					
14	Zeta	3g/l Alginate in Water run 24	28/07/2016 10:41	13.7	FALSE					
15	Zeta	3g/l Alginate in Water run 25	28/07/2016 10:41	12.9	FALSE					
16	Zeta	3g/l Alginate in Water run 21	28/07/2016 10:46	11.2	FALSE					
17	Zeta	3g/l Alginate in Water run 22	28/07/2016 10:48	11.6	FALSE					
18	Zeta	3g/l Alginate in Water run 23	28/07/2016 10:49	11.6	FALSE					
19	Zeta	3g/l Alginate in Water run 24	28/07/2016 10:49	12.1	FALSE					
20	Zeta	3g/l Alginate in Water run 25	28/07/2016 10:50	11.9	FALSE					
102	Zeta	3g/l gelatin microgels pH4.1 10 micron filter 1 1	29/07/2016 12:16	19.2	FALSE	19.2	20.2	1	21.7	17.7
103	Zeta	3g/l gelatin microgels pH4.1 10 micron filter 1 2	29/07/2016 12:18	20.2	FALSE					
104	Zeta	3g/l gelatin microgels pH4.1 10 micron filter 1 3	29/07/2016 12:19	19.7	FALSE					
105	Zeta	3g/l gelatin microgels pH4.1 10 micron filter 1 4	29/07/2016 12:20	19.2	FALSE					
106	Zeta	3g/l gelatin microgels pH4.1 10 micron filter 1 5	29/07/2016 12:20	19.2	FALSE					
107	Zeta	3g/l gelatin microgels pH4.1 10 micron filter 1 1	29/07/2016 12:23	20.3	FALSE					
108	Zeta	3g/l gelatin microgels pH4.1 10 micron filter 1 2	29/07/2016 12:25	20.2	FALSE					
109	Zeta	3g/l gelatin microgels pH4.1 10 micron filter 1 3	29/07/2016 12:25	21.2	FALSE					
110	Zeta	3g/l gelatin microgels pH4.1 10 micron filter 1 4	29/07/2016 12:26	19.6	FALSE					
111	Zeta	3g/l gelatin microgels pH4.1 10 micron filter 1 5	29/07/2016 12:27	20.2	FALSE					
112	Zeta	3g/l gelatin microgels pH4.1 10 micron filter 1 1	29/07/2016 12:29	19.3	FALSE					
113	Zeta	3g/l gelatin microgels pH4.1 10 micron filter 1 2	29/07/2016 12:31	19.5	FALSE					
114	Zeta	3g/l gelatin microgels pH4.1 10 micron filter 1 3	29/07/2016 12:31	20.5	FALSE					
115	Zeta	3g/l gelatin microgels pH4.1 10 micron filter 1 4	29/07/2016 12:32	19.1	FALSE					
116	Zeta	3g/l gelatin microgels pH4.1 10 micron filter 1 5	29/07/2016 12:33	20.4	FALSE					
117	Zeta	3g/l gelatin microgels pH4.1 10 micron filter 1 1	29/07/2016 12:35	19.4	FALSE					
118	Zeta	3g/l gelatin microgels pH4.1 10 micron filter 1 2	29/07/2016 12:37	20	FALSE					
119	Zeta	3g/l gelatin microgels pH4.1 10 micron filter 1 3	29/07/2016 12:38	20.4	FALSE					
120	Zeta	3g/l gelatin microgels pH4.1 10 micron filter 1 4	29/07/2016 12:38	20	FALSE					
121	Zeta	3g/l gelatin microgels pH4.1 10 micron filter 1 5	29/07/2016 12:39	19.7	FALSE					
122	Zeta	3g/l gelatin microgels pH4.1 10 micron filter 1 1	29/07/2016 12:41	19.3	FALSE					
123	Zeta	3g/l gelatin microgels pH4.1 10 micron filter 1 2	29/07/2016 12:43	19.2	FALSE					
124	Zeta	3g/l gelatin microgels pH4.1 10 micron filter 1 3	29/07/2016 12:44	18.9	FALSE					
125	Zeta	3g/l gelatin microgels pH4.1 10 micron filter 1 4	29/07/2016 12:45	17.7	FALSE					
26	Zeta	3g/l gelatin microgels pH5.11 10 micron filter 1	29/07/2016 10:16	16	FALSE	15.45	16.25	0.8	17.45	14.25
27	Zeta	3g/l gelatin microgels pH5.11 10 micron filter 2	29/07/2016 10:19	15.2	FALSE					
28	Zeta	3g/l gelatin microgels pH5.11 10 micron filter 3	29/07/2016 10:19	15.1	FALSE					
29	Zeta	3g/l gelatin microgels pH5.11 10 micron filter 4	29/07/2016 10:20	15.9	FALSE					
30	Zeta	3g/l gelatin microgels pH5.11 10 micron filter 5	29/07/2016 10:21	14.9	FALSE					
31	Zeta	3g/l gelatin microgels pH5.11 10 micron filter 1	29/07/2016 10:24	16.5	FALSE					
32	Zeta	3g/l gelatin microgels pH5.11 10 micron filter 2	29/07/2016 10:26	15.6	FALSE					
33	Zeta	3g/l gelatin microgels pH5.11 10 micron filter 3	29/07/2016 10:27	15.8	FALSE					
34	Zeta	3g/l gelatin microgels pH5.11 10 micron filter 4	29/07/2016 10:27	15.9	FALSE					
35	Zeta	3g/l gelatin microgels pH5.11 10 micron filter 5	29/07/2016 10:28	15.9	FALSE					
36	Zeta	3g/l gelatin microgels pH5.11 10 micron filter 1	29/07/2016 10:31	16.9	FALSE					
37	Zeta	3g/l gelatin microgels pH5.11 10 micron filter 2	29/07/2016 10:33	16.6	FALSE					
38	Zeta	3g/l gelatin microgels pH5.11 10 micron filter 3	29/07/2016 10:34	15.6	FALSE					
39	Zeta	3g/l gelatin microgels pH5.11 10 micron filter 4	29/07/2016 10:34	15.4	FALSE					
40	Zeta	3g/l gelatin microgels pH5.11 10 micron filter 5	29/07/2016 10:35	14.9	FALSE					
41	Zeta	3g/l gelatin microgels pH5.11 10 micron filter 1	29/07/2016 10:38	15.9	FALSE					
42	Zeta	3g/l gelatin microgels pH5.11 10 micron filter 2	29/07/2016 10:40	16.3	FALSE					
43	Zeta	3g/l gelatin microgels pH5.11 10 micron filter 3	29/07/2016 10:41	15.8	FALSE					
44	Zeta	3g/l gelatin microgels pH5.11 10 micron filter 4	29/07/2016 10:41	14.9	FALSE					
45	Zeta	3g/l gelatin microgels pH5.11 10 micron filter 5	29/07/2016 10:42	15.7	FALSE					
46	Zeta	3g/l gelatin microgels pH5.11 10 micron filter 1	29/07/2016 10:44	15.4	FALSE					
47	Zeta	3g/l gelatin microgels pH5.11 10 micron filter 2	29/07/2016 10:46	17	FALSE					
48	Zeta	3g/l gelatin microgels pH5.11 10 micron filter 3	29/07/2016 10:47	17.1	FALSE					
49	Zeta	3g/l gelatin microgels pH5.11 10 micron filter 4	29/07/2016 10:48	16.8	FALSE					
50	Zeta	3g/l gelatin microgels pH5.11 10 micron filter 5	29/07/2016 10:48	16.1	FALSE					
51	Zeta	3g/l gelatin microgels pH5.11 10 micron filter 1	29/07/2016 10:16	16	FALSE					
77	Zeta	3g/l gelatin microgels pH7.4 10 micron filter 1	29/07/2016 11:18	11.3	FALSE	9.37	10.5	1.13	12.195	7.675
78	Zeta	3g/l gelatin microgels pH7.4 10 micron filter 1	29/07/2016 11:20	10.9	FALSE					
79	Zeta	3g/l gelatin microgels pH7.4 10 micron filter 1	29/07/2016 11:21	10.9	FALSE					
80	Zeta	3g/l gelatin microgels pH7.4 10 micron filter 1	29/07/2016 11:21	10.8	FALSE					
81	Zeta	3g/l gelatin microgels pH7.4 10 micron filter 1	29/07/2016 11:22	10.6	FALSE					
82	Zeta	3g/l gelatin microgels pH7.4 10 micron filter 1	29/07/2016 11:24	9.15	FALSE					
83	Zeta	3g/l gelatin microgels pH7.4 10 micron filter 1	29/07/2016 11:26	9.31	FALSE					
84	Zeta	3g/l gelatin microgels pH7.4 10 micron filter 1	29/07/2016 11:27	9.54	FALSE					
85	Zeta	3g/l gelatin microgels pH7.4 10 micron filter 1	29/07/2016 11:28	9.86	FALSE					
86	Zeta	3g/l gelatin microgels pH7.4 10 micron filter 1	29/07/2016 11:28	9.91	FALSE					
87	Zeta	3g/l gelatin microgels pH7.4 10 micron filter 1	29/07/2016 11:31	9.66	FALSE					
88	Zeta	3g/l gelatin microgels pH7.4 10 micron filter 1	29/07/2016 11:33	9.77	FALSE					
89	Zeta	3g/l gelatin microgels pH7.4 10 micron filter 1	29/07/2016 11:33	10.5	FALSE					
90	Zeta	3g/l gelatin microgels pH7.4 10 micron filter 1	29/07/2016 11:34	9.39	FALSE					
91	Zeta	3g/l gelatin microgels pH7.4 10 micron filter 1	29/07/2016 11:35	9.37	FALSE					
92	Zeta	3g/l gelatin microgels pH7.4 10 micron filter 1	29/07/2016 11:37	9.26	FALSE					
93	Zeta	3g/l gelatin microgels pH7.4 10 micron filter 1	29/07/2016 11:39	9.25	FALSE					
94	Zeta	3g/l gelatin microgels pH7.4 10 micron filter 1	29/07/2016 11:40	9.73	FALSE					
95	Zeta	3g/l gelatin microgels pH7.4 10 micron filter 1	29/07/2016 11:40	10.1	FALSE					
96	Zeta	3g/l gelatin microgels pH7.4 10 micron filter 1	29/07/2016 11:41	9.91	FALSE					
97	Zeta	3g/l gelatin microgels pH7.4 10 micron filter 1	29/07/2016 11:43	9.29	FALSE					
98	Zeta	3g/l gelatin microgels pH7.4 10 micron filter 1	29/07/2016 11:45	8.78	FALSE					
99	Zeta	3g/l gelatin microgels pH7.4 10 micron filter 1	29/07/2016 11:46	10.5	FALSE					
100	Zeta	3g/l gelatin microgels pH7.4 10 micron filter 1	29/07/2016 11:47	9.47	FALSE					
101	Zeta	3g/l gelatin microgels pH7.4 10 micron filter 1	29/07/2016 11:47	10.1	FALSE					

Table 11: Zeta potential results continued.

138 Zeta	3g/l Gelatin Microgels pH10 - 10 micron filter 1	23/08/2016 10:53	-19.9	FALSE	-21.2	-20	1.2	-18.2	-23
139 Zeta	3g/l Gelatin Microgels pH10 - 10 micron filter 2	23/08/2016 10:55	-21.2	FALSE					
140 Zeta	3g/l Gelatin Microgels pH10 - 10 micron filter 3	23/08/2016 10:56	-21.5	FALSE					
141 Zeta	3g/l Gelatin Microgels pH10 - 10 micron filter 4	23/08/2016 10:56	-21.5	FALSE					
142 Zeta	3g/l Gelatin Microgels pH10 - 10 micron filter 5	23/08/2016 10:57	-21.1	FALSE					
143 Zeta	3g/l Gelatin Microgels pH10 - 10 micron filter 1	23/08/2016 11:00	-20.2	FALSE					
144 Zeta	3g/l Gelatin Microgels pH10 - 10 micron filter 2	23/08/2016 11:02	-21.3	FALSE					
145 Zeta	3g/l Gelatin Microgels pH10 - 10 micron filter 3	23/08/2016 11:03	-20	FALSE					
146 Zeta	3g/l Gelatin Microgels pH10 - 10 micron filter 4	23/08/2016 11:03	-22.3	FALSE					
147 Zeta	3g/l Gelatin Microgels pH10 - 10 micron filter 5	23/08/2016 11:04	-20.5	FALSE					
148 Zeta	3g/l Gelatin Microgels pH10 - 10 micron filter 1	23/08/2016 11:08	-21.3	FALSE					
149 Zeta	3g/l Gelatin Microgels pH10 - 10 micron filter 2	23/08/2016 11:10	-21	FALSE					
150 Zeta	3g/l Gelatin Microgels pH10 - 10 micron filter 3	23/08/2016 11:10	-20.3	FALSE					
151 Zeta	3g/l Gelatin Microgels pH10 - 10 micron filter 4	23/08/2016 11:11	-21.7	FALSE					
152 Zeta	3g/l Gelatin Microgels pH10 - 10 micron filter 5	23/08/2016 11:12	-20.3	FALSE					
153 Zeta	3g/l Gelatin Microgels pH10 - 10 micron filter 1	23/08/2016 11:14	-20.3	FALSE					
154 Zeta	3g/l Gelatin Microgels pH10 - 10 micron filter 2	23/08/2016 11:16	-20.5	FALSE					
155 Zeta	3g/l Gelatin Microgels pH10 - 10 micron filter 3	23/08/2016 11:16	-19.9	FALSE					
156 Zeta	3g/l Gelatin Microgels pH10 - 10 micron filter 4	23/08/2016 11:17	-20.5	FALSE					
157 Zeta	3g/l Gelatin Microgels pH10 - 10 micron filter 5	23/08/2016 11:18	-20.6	FALSE					
158 Zeta	3g/l Gelatin Microgels pH10 - 10 micron filter 1	23/08/2016 11:21	-19.8	FALSE					
159 Zeta	3g/l Gelatin Microgels pH10 - 10 micron filter 2	23/08/2016 11:23	-19.3	FALSE					
160 Zeta	3g/l Gelatin Microgels pH10 - 10 micron filter 3	23/08/2016 11:24	-20.5	FALSE					
161 Zeta	3g/l Gelatin Microgels pH10 - 10 micron filter 4	23/08/2016 11:25	-20	FALSE					
162 Zeta	3g/l Gelatin Microgels pH10 - 10 micron filter 5	23/08/2016 11:25	-20	FALSE					
77 Zeta	Gelatine HT pH4.38 2.2g/L Alginate SOP 1	11/02/2018 19:36	7.88	FALSE	8.0425	8.545	0.5025	9.29875	7.28875
78 Zeta	Gelatine HT pH4.38 2.2g/L Alginate SOP 2	11/02/2018 19:38	8.44	FALSE					
79 Zeta	Gelatine HT pH4.38 2.2g/L Alginate SOP 3	11/02/2018 19:39	8.07	FALSE					
80 Zeta	Gelatine HT pH4.38 2.2g/L Alginate SOP 4	11/02/2018 19:40	8.2	FALSE					
81 Zeta	Gelatine HT pH4.38 2.2g/L Alginate SOP 5	11/02/2018 19:40	8.72	FALSE					
82 Zeta	Gelatine HT pH4.38 2.2g/L Alginate SOP 1	11/02/2018 19:42	8.62	FALSE					
83 Zeta	Gelatine HT pH4.38 2.2g/L Alginate SOP 2	11/02/2018 19:44	8.78	FALSE					
84 Zeta	Gelatine HT pH4.38 2.2g/L Alginate SOP 3	11/02/2018 19:45	8.5	FALSE					
85 Zeta	Gelatine HT pH4.38 2.2g/L Alginate SOP 4	11/02/2018 19:45	8.22	FALSE					
86 Zeta	Gelatine HT pH4.38 2.2g/L Alginate SOP 5	11/02/2018 19:46	9.21	FALSE					
87 Zeta	Gelatine HT pH4.38 2.2g/L Alginate SOP 1	11/02/2018 19:47	8.12	FALSE					
88 Zeta	Gelatine HT pH4.38 2.2g/L Alginate SOP 2	11/02/2018 19:49	7.96	FALSE					
89 Zeta	Gelatine HT pH4.38 2.2g/L Alginate SOP 3	11/02/2018 19:50	7.84	FALSE					
91 Zeta	Gelatine HT pH4.38 2.2g/L Alginate SOP 5	11/02/2018 19:51	7.89	FALSE					
92 Zeta	Gelatine HT pH4.38 2.2g/L Alginate SOP 1	11/02/2018 19:52	8.38	FALSE					
93 Zeta	Gelatine HT pH4.38 2.2g/L Alginate SOP 2	11/02/2018 19:54	8.28	FALSE					
94 Zeta	Gelatine HT pH4.38 2.2g/L Alginate SOP 3	11/02/2018 19:55	7.87	FALSE					
95 Zeta	Gelatine HT pH4.38 2.2g/L Alginate SOP 4	11/02/2018 19:56	8.42	FALSE					
96 Zeta	Gelatine HT pH4.38 2.2g/L Alginate SOP 5	11/02/2018 19:56	7.87	FALSE					
102 Zeta	Gelatine HT pH4.38 2.2g/L Alginate SOP 1	11/02/2018 19:58	8.36	FALSE					
103 Zeta	Gelatine HT pH4.38 2.2g/L Alginate SOP 2	11/02/2018 20:00	8.42	FALSE					
104 Zeta	Gelatine HT pH4.38 2.2g/L Alginate SOP 3	11/02/2018 20:01	8.52	FALSE					
105 Zeta	Gelatine HT pH4.38 2.2g/L Alginate SOP 4	11/02/2018 20:01	8.77	FALSE					
106 Zeta	Gelatine HT pH4.38 2.2g/L Alginate SOP 5	11/02/2018 20:02	8.86	FALSE					
36 Zeta	Gelatine HT pH4.87 3g/L filter 11 micron 1 Alginate SoP 1	11/02/2018 18:25	1.42	FALSE	1.46	1.81	0.35	2.335	0.935
37 Zeta	Gelatine HT pH4.87 3g/L filter 11 micron 1 Alginate SoP 2	11/02/2018 18:27	1.73	FALSE					
38 Zeta	Gelatine HT pH4.87 3g/L filter 11 micron 1 Alginate SoP 3	11/02/2018 18:27	1.81	FALSE					
39 Zeta	Gelatine HT pH4.87 3g/L filter 11 micron 1 Alginate SoP 4	11/02/2018 18:29	2.31	FALSE					
40 Zeta	Gelatine HT pH4.87 3g/L filter 11 micron 1 Alginate SoP 5	11/02/2018 18:30	1.46	FALSE					
42 Zeta	Gelatine HT pH4.87 3g/L filter 11 micron Alginate SoP retest	11/02/2018 18:39	1.83	FALSE	1.545	1.86	0.315	2.3325	1.0725
43 Zeta	Gelatine HT pH4.87 3g/L filter 11 micron Alginate SoP retest	11/02/2018 18:41	1.95	FALSE					
45 Zeta	Gelatine HT pH4.87 3g/L filter 11 micron Alginate SoP retest	11/02/2018 18:47	1.41	FALSE					
46 Zeta	Gelatine HT pH4.87 3g/L filter 11 micron Alginate SoP retest	11/02/2018 18:52	1.59	FALSE					
1 Zeta	Gelatine HT pH7 6g/L 11micron filter syringe 1	09/02/2018 19:10	-1.88	FALSE	-1.88	-1.51	0.37	-0.955	-2.435
2 Zeta	Gelatine HT pH7 6g/L 11micron filter syringe 2	09/02/2018 19:12	-1.97	FALSE					
3 Zeta	Gelatine HT pH7 6g/L 11micron filter syringe 3	09/02/2018 19:12	-1.51	FALSE					
4 Zeta	Gelatine HT pH7 6g/L 11micron filter syringe 4	09/02/2018 19:13	-1.56	FALSE					
5 Zeta	Gelatine HT pH7 6g/L 11micron filter syringe 5	09/02/2018 19:13	-1.36	FALSE					
6 Zeta	Gelatine HT pH7 6g/L 11micron filter syringe 1	09/02/2018 19:10	-1.88	FALSE					
7 Zeta	Gelatine HT pH7 6g/L 11micron filter syringe 2	09/02/2018 19:12	-1.97	FALSE					
8 Zeta	Gelatine HT pH7 6g/L 11micron filter syringe 3	09/02/2018 19:12	-1.51	FALSE					
9 Zeta	Gelatine HT pH7 6g/L 11micron filter syringe 4	09/02/2018 19:13	-1.56	FALSE					
10 Zeta	Gelatine HT pH7 6g/L 11micron filter syringe 5	09/02/2018 19:13	-1.36	FALSE					
11 Zeta	Gelatine HT pH7 6g/L 11micron filter syringe 1	09/02/2018 19:10	-1.88	FALSE					
12 Zeta	Gelatine HT pH7 6g/L 11micron filter syringe 2	09/02/2018 19:12	-1.97	FALSE					
13 Zeta	Gelatine HT pH7 6g/L 11micron filter syringe 3	09/02/2018 19:12	-1.51	FALSE					
14 Zeta	Gelatine HT pH7 6g/L 11micron filter syringe 4	09/02/2018 19:13	-1.56	FALSE					
15 Zeta	Gelatine HT pH7 6g/L 11micron filter syringe 5	09/02/2018 19:13	-1.36	FALSE					
16 Zeta	Gelatine HT pH7 6g/L 11micron filter syringe 1	09/02/2018 19:10	-1.88	FALSE					
17 Zeta	Gelatine HT pH7 6g/L 11micron filter syringe 2	09/02/2018 19:12	-1.97	FALSE					
18 Zeta	Gelatine HT pH7 6g/L 11micron filter syringe 3	09/02/2018 19:12	-1.51	FALSE					
19 Zeta	Gelatine HT pH7 6g/L 11micron filter syringe 4	09/02/2018 19:13	-1.56	FALSE					
20 Zeta	Gelatine HT pH7 6g/L 11micron filter syringe 5	09/02/2018 19:13	-1.36	FALSE					
21 Zeta	Gelatine HT pH7 6g/L 11micron filter syringe 1	09/02/2018 19:10	-1.88	FALSE					
22 Zeta	Gelatine HT pH7 6g/L 11micron filter syringe 2	09/02/2018 19:12	-1.97	FALSE					
23 Zeta	Gelatine HT pH7 6g/L 11micron filter syringe 3	09/02/2018 19:12	-1.51	FALSE					
24 Zeta	Gelatine HT pH7 6g/L 11micron filter syringe 4	09/02/2018 19:13	-1.56	FALSE					
25 Zeta	Gelatine HT pH7 6g/L 11micron filter syringe 5	09/02/2018 19:13	-1.36	FALSE					
26 Zeta	Gelatine HT pH7 6g/L 11micron filter syringe 1	09/02/2018 19:10	-1.88	FALSE					
27 Zeta	Gelatine HT pH7 6g/L 11micron filter syringe 2	09/02/2018 19:12	-1.97	FALSE					
28 Zeta	Gelatine HT pH7 6g/L 11micron filter syringe 3	09/02/2018 19:12	-1.51	FALSE					
29 Zeta	Gelatine HT pH7 6g/L 11micron filter syringe 4	09/02/2018 19:13	-1.56	FALSE					
30 Zeta	Gelatine HT pH7 6g/L 11micron filter syringe 5	09/02/2018 19:13	-1.36	FALSE					

### 9.3 Appendix C – 1850 Variables

Table 12: Coating thickness of varying temperatures of 1850.

Sample	Face	Position					Average Thickness (µm)
		1	2	3	4	5	
70°C	1	0.2	0.8	0.4	0.1	0.1	0.30
	2	0.5	0.4	0.2	0.1	0.2	
75°C	1	3.6	2.3	2.3	2.2	2.1	2.50
	2	2.4	3.1	2.8	2.3	1.9	
80°C	1	3.7	3.5	3.5	4.0	3.6	3.93
	2	4.2	4.4	4.2	4.3	3.9	
89°C	1	11.4	10.5	9.9	10.2	10.3	10.10
	2	10.3	9.8	8.7	10.3	9.6	

Table 13: Coating thickness of varying solution pH of 1850.

Sample	Face	Position					Average Thickness (µm)
		1	2	3	4	5	
pH 3.9	1	6.2	6.8	6.5	7.0	6.3	6.57
	2	6.4	7.0	6.1	6.9	6.5	
pH 5.9	1	12.3	12.7	11.8	11.9	12.5	12.62
	2	13.6	13.1	12.2	13.0	13.1	
pH 7.0	1	15.9	16.6	16.3	15.7	14.9	15.68
	2	15.5	16.5	14.1	15.5	15.8	
pH 8.0	1	20.1	19.4	19.2	19.4	19.1	19.67
	2	20.2	21.1	18.8	19.3	20.1	

Table 14: Coating thickness of 1850 produced with ultrasonic agitation.

Sample	Face	Position					Average Thickness (µm)
		1	2	3	4	5	
80°C - Sonification	1	8.5	8.6	7.3	5.2	6.1	7.11
	2	8.1	7.2	8.5	6.5	5.1	

## 9.4 Appendix D – Pyrophosphate Low Temperature Solution

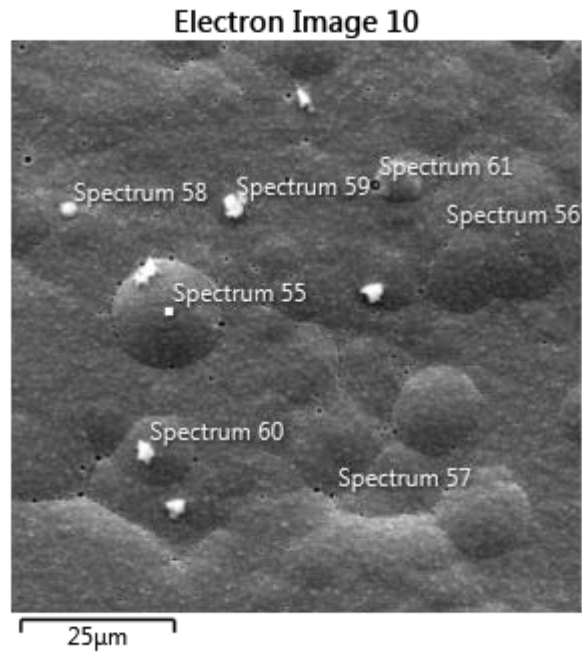


Figure 84: Pyrophosphate solution coating showing pores.

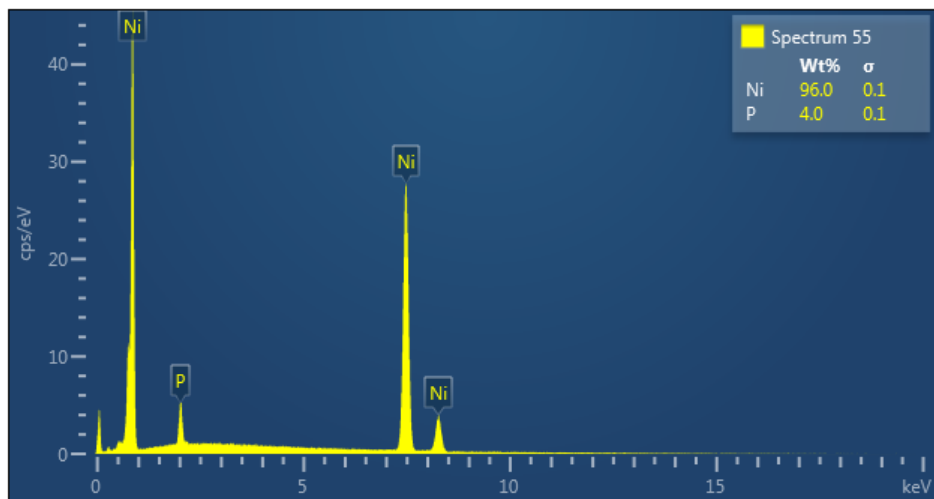


Figure 85: Spectrum of coating showing low phosphorus content.

Table 15: Ni:P ratio as wt% for pyrophosphate deposit.

Element	Wt%	Wt% Sigma
P	4.01	0.11
Ni	95.99	0.11
Total:	100.00	

## 9.5 Appendix E – Gelatine Microgel Analysis

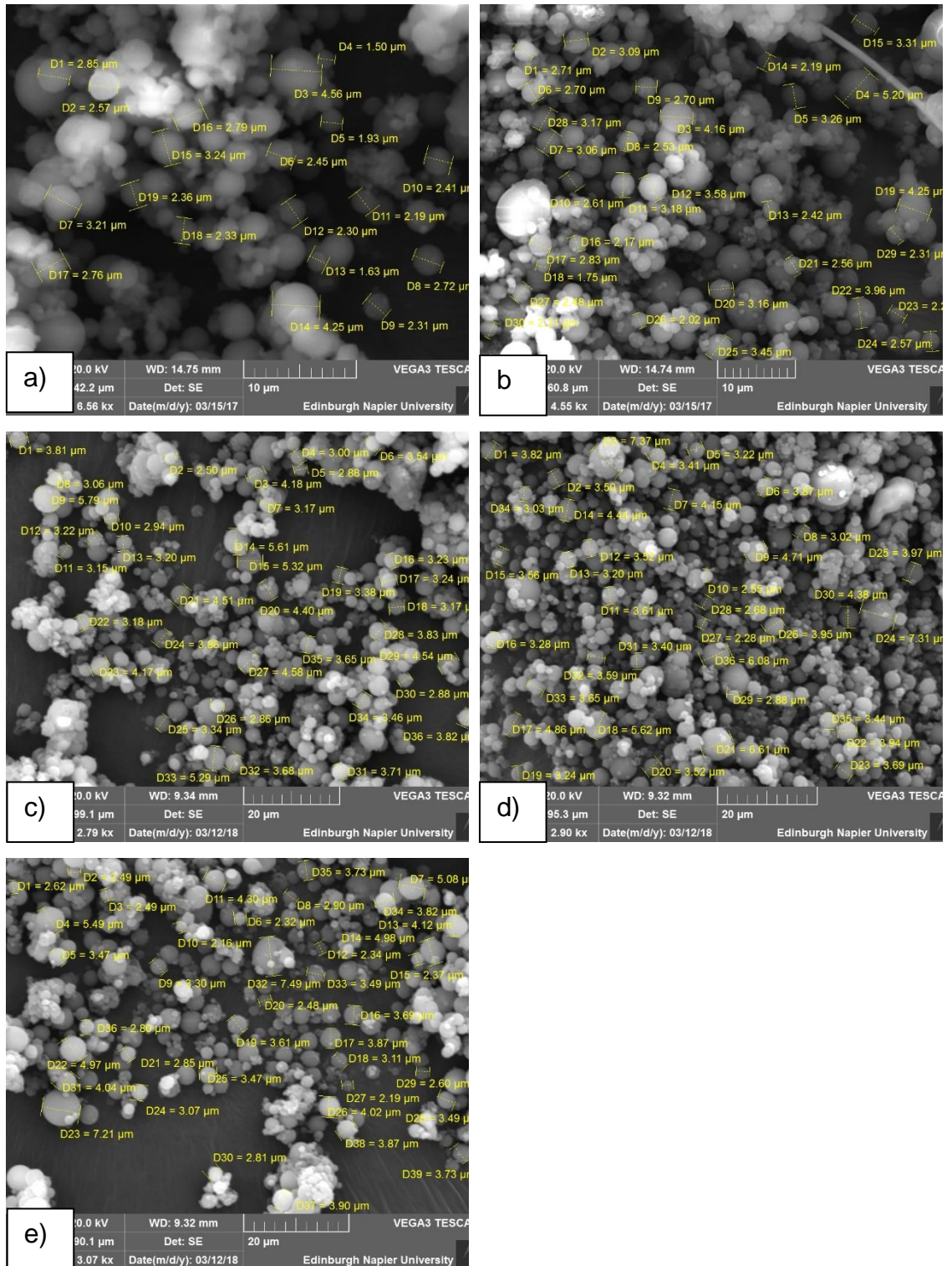


Figure 86: Microgel size analysis using SEM imaging. Image a) and b) are as received gelatine microgels, image c),d) & e) are post heat treatment.

## 9.6 Appendix F – Phosphorus content in NiP/gelatine composite coatings.

Table 16: EDXA results for NiP/gelatine composite coatings relating to the phosphorus content by wt%.

Sample	Scan	Spectrum	Ni	P	%P Adjust	Average %P	Coating Average %P
Plain NiP	76	306	88.5	8.2	8.48	8.41	8.21
		308	88.5	8.1	8.39		
		309	88.8	8.1	8.36		
	77	313	88.5	8.3	8.57	8.34	
		314	88.6	7.7	8.00		
		319	88.1	8.0	8.32		
		321	87.7	8.1	8.46		
	78	322	89.2	7.9	8.14	7.92	
		324	89.2	8.1	8.32		
		326	88.5	7.8	8.10		
		328	89.8	6.9	7.14		
	NiP + 0.0125 g/L	79	331	85.8	10.2	10.63	
332			86.3	9.9	10.29		
333			86.2	10.4	10.77		
334			86.6	10.3	10.63		
80		341	86.9	10.4	10.69	10.64	
		342	85.9	10.4	10.80		
		343	86.0	10.0	10.42		
		344	86.1	10.4	10.78		
		345	75.5	9.2	10.86		
81		346	83.8	9.6	10.28	10.63	
		351	86.9	10.4	10.69		
		352	86.7	10.2	10.53		
		354	86.7	10.3	10.62		
		356	86.7	10.2	10.53		
		358	86.3	10.4	10.75		
NiP + 0.025 g/L	82/85	359	85.2	10.2	10.69	11.27	11.12
		360	85.9	10.2	10.61		
		389	85.8	10.9	11.27		
		390	86.6	10.7	11.00		
	83/86	393	86.1	11.1	11.42	11.15	
		394	85.4	11.0	11.41		
		395	86.3	10.8	11.12		
		396	86.1	10.7	11.05		
	84/87	400	86.3	10.8	11.12	11.02	
		402	85.6	10.9	11.30		
403		86.0	10.9	11.25			
405		86.4	10.9	11.20			
406		86.5	10.5	10.82			
407		87.1	10.3	10.57			
NiP + 0.05 g/L	85/88	408	86.8	10.6	10.88	11.33	11.24
		409	85.9	10.7	11.08		
		410	86.1	11.0	11.33		
		411	85.7	11.1	11.47		
		412	85.9	10.9	11.26		
	86/89	413	85.4	11.1	11.50	11.43	
		414	85.7	10.8	11.19		
		415	70.2	8.9	11.25		
		422	85.7	11.2	11.56		
87/90	423	85.7	11.5	11.83	11.07		
	426	86.6	10.8	11.09			
	429	86.0	10.9	11.25			
	430	86.4	10.3	10.65			
	431	86.4	10.2	10.56			
	432	86.0	10.5	10.88			
	433	86.0	10.9	11.25			
87/90	434	86.0	11.2	11.52	11.03		
	444	82.3	10.2	11.03			
	445	88.4	11.6	11.60			

## 9.7 Appendix G – Fluorescence Microscopy Images

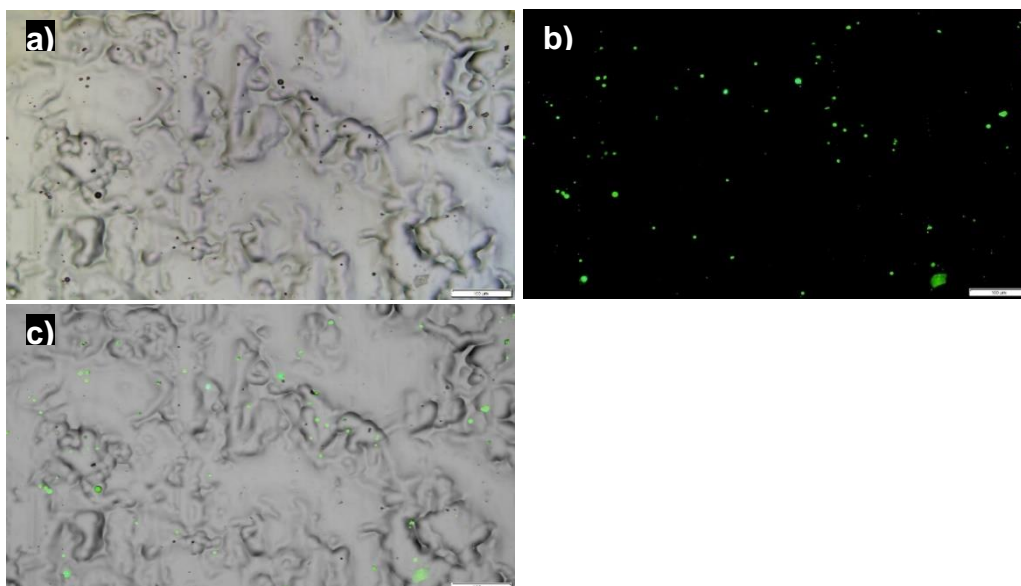


Figure 87: NiP+0.0125 g/L gelatine microgels deposit surface imaged using a) RGB colour spectrum using white light, b) fluorescence using ultraviolet light, c) composite image of combined RGB and fluorescence imaging. Images captured at x20 magnification with 100  $\mu\text{m}$  scale bar.

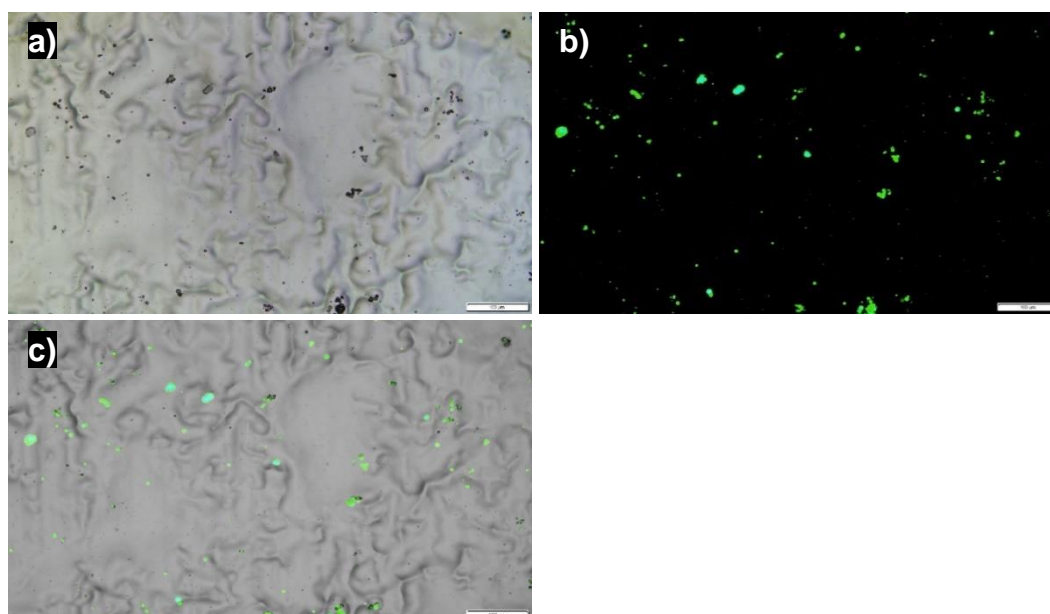
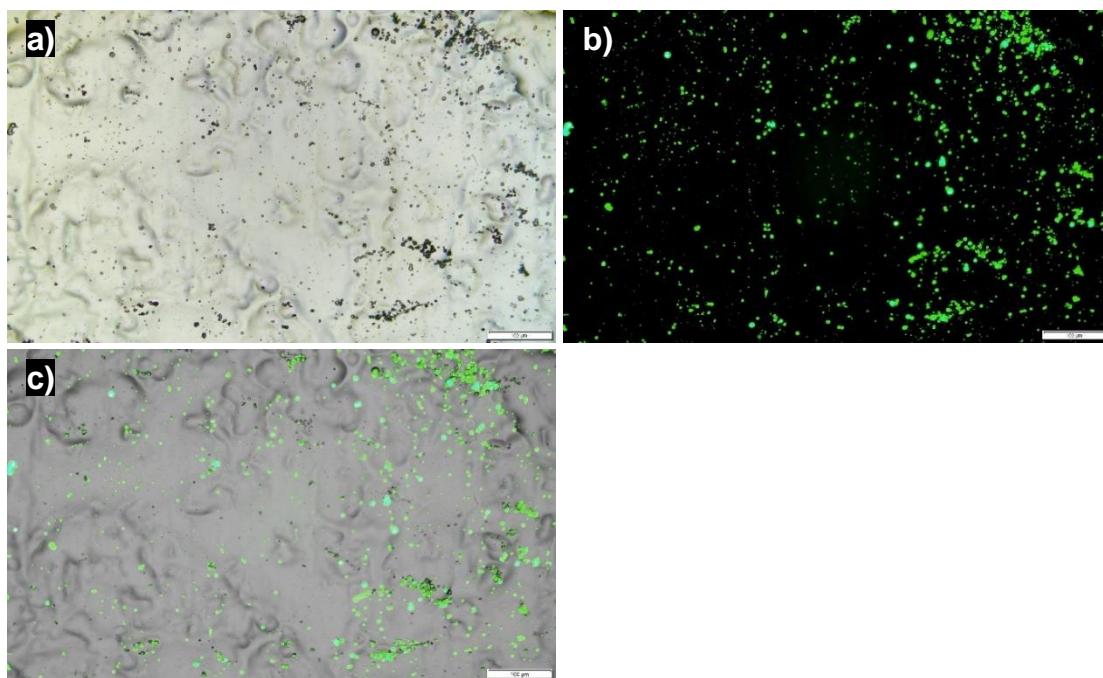


Figure 88: NiP+0.025 g/L gelatine microgels deposit surface imaged using a) RGB colour spectrum using white light, b) fluorescence using ultraviolet light, c) composite image of combined RGB and fluorescence imaging. Images captured at x20 magnification with 100  $\mu\text{m}$  scale bar.

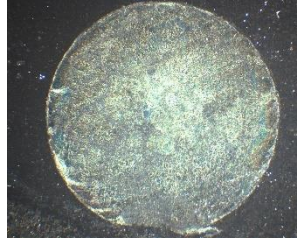
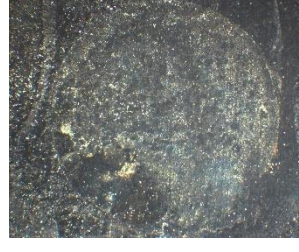
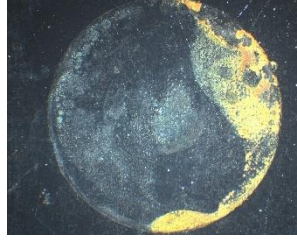
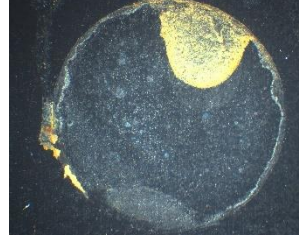
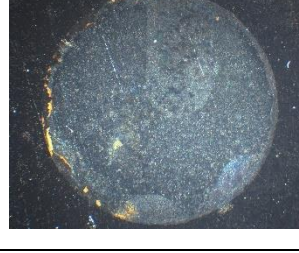


*Figure 89: NiP+0.0125 g/L gelatine microgels deposit surface imaged using a) RGB colour spectrum using white light, b) fluorescence using ultraviolet light, c) composite image of combined RGB and fluorescence imaging. Images captured at x20 magnification with 100  $\mu\text{m}$  scale bar.*

## 9.8 Appendix H – NSS Samples

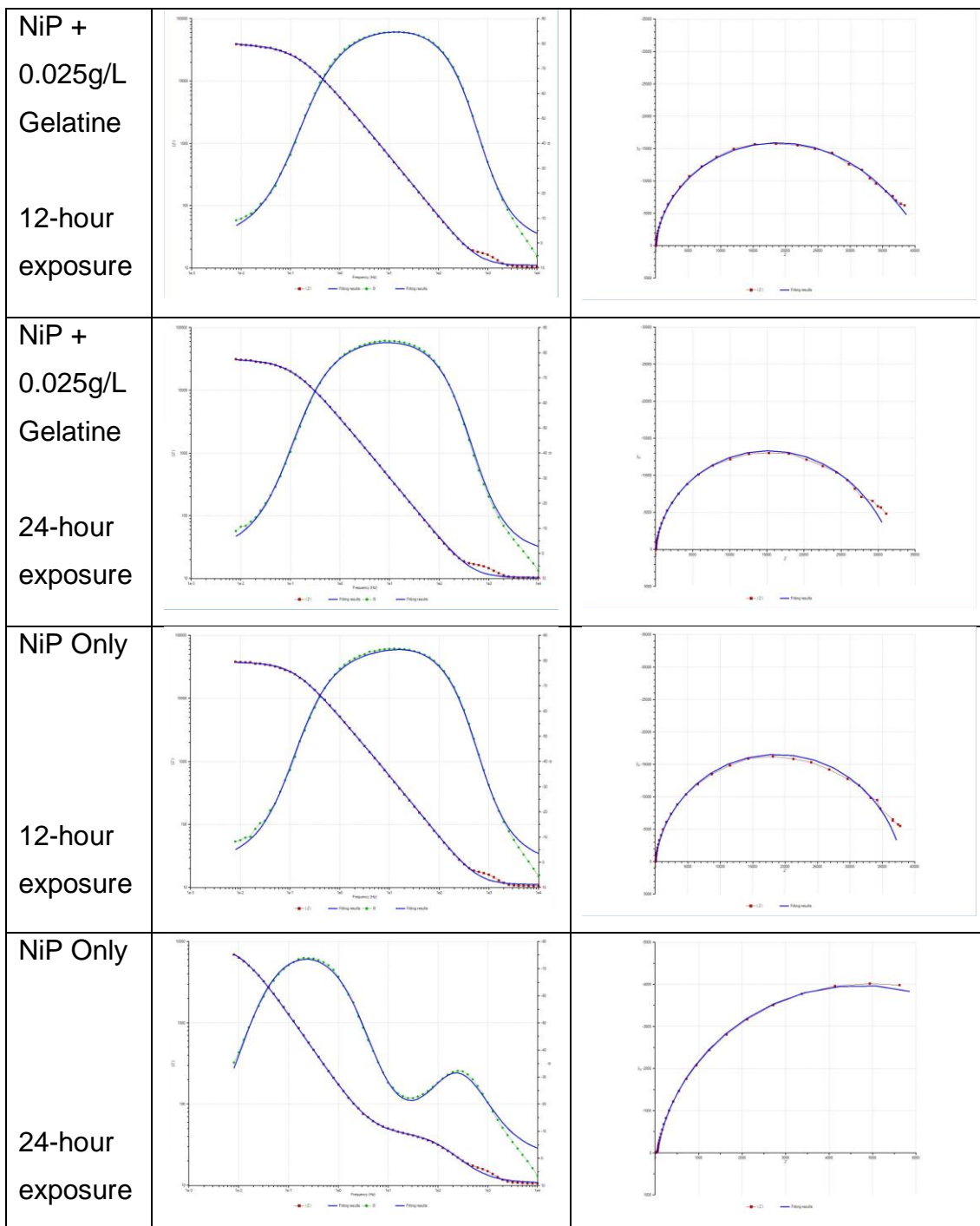
Table 17: NSS samples after test and lightly cleaned under running water using brush with no abrasive.

Area of circle = 1cm<sup>2</sup>.

Plain NiP only			
NiP+0.0125 g/L Gelatine			
NiP+0.025 g/L Gelatine			
NiP+0.05 g/L Gelatine			

## 9.9 Appendix I – EIS Fitting

Table 18: EIS equivalent circuit at 12 hours and 24 hours exposure for Plain NiP coating and NiP/gelatine composite coating.



## 9.10 Appendix J – Surface Roughness Data

Table 19: Surface roughness measurements in x and y-axis orientations.

Coating	Sample	Ra Values					
		X1	X2	X3	Y1	Y2	Y3
Reference	Ref 1	1.372	1.054	1.205	0.986	1.133	1.140
	Ref 2	1.044	1.013	0.988	1.134	1.149	0.982
	Ref 3	1.096	1.132	1.392	1.522	1.108	1.272
1850 Only	1	0.998	0.850	0.968	1.169	1.065	1.003
	2	1.082	1.196	1.243	1.021	1.151	1.003
	3	1.107	0.958	0.953	0.735	1.099	0.824
1850 + 0.0125 g/L	4	0.965	0.985	1.023	0.929	0.878	0.930
	5	1.022	1.021	0.845	1.009	1.032	0.982
	6	1.007	1.003	1.050	1.043	1.005	0.985
1850 + 0.025 g/L	7	0.877	1.088	1.069	0.992	0.868	0.817
	8	0.927	0.875	0.817	1.193	0.884	0.798
	9	0.881	0.916	0.831	0.891	0.777	0.870
1850 + 0.05 g/L	10	0.965	0.797	0.739	1.019	1.004	1.022
	11	0.874	0.889	0.952	0.956	0.854	0.881
	12	1.014	0.869	1.000	1.149	0.824	0.992

Table 20: Average surface roughness per sample.

Coating	Sample	Ra Values		
		X-axis	Y-axis	Average
<b>Reference</b>	Ref 1	1.210	1.086	1.148
	Ref 2	1.015	1.088	1.052
	Ref 3	1.207	1.301	1.254
<b>1850 Only</b>	1	0.939	1.079	1.009
	2	1.174	1.058	1.116
	3	1.006	0.886	0.946
<b>1850 + 0.0125 g/L</b>	4	0.991	0.912	0.952
	5	0.963	1.008	0.985
	6	1.020	1.011	1.016
<b>1850 + 0.025 g/L</b>	7	1.011	0.892	0.952
	8	0.873	0.958	0.916
	9	0.876	0.846	0.861
<b>1850 + 0.05 g/L</b>	10	0.834	1.015	0.924
	11	0.905	0.897	0.901
	12	0.961	0.988	0.975

## 9.11 Appendix K – Coating Hardness results

Table 21: Detailed coating hardness results for NiP/Gelatine composite coatings.

Coatings	Sample	D1(μm)	D2(μm)	HARDNESS (HV0.1)	CONVERSION (HK)	Standard Deviation	Coating Average (HV0.1)
Uncoated Reference	1	32.99	34.08	164.9	179.9	9.3	165.7
		33.33	31.89	174.4	190.6		
		32.13	32.13	179.6	195.6		
	2	34.23	34.24	158.2	172.2		
		33.71	33.71	163.2	177.5		
		34.08	33.10	164.4	179.1		
	3	34.93	34.05	155.9	169.9		
		34.29	35.10	154.1	168.1		
		32.16	32.63	176.7	192.7		
Plain NiP	1	17.08	17.41	623.6	660.9	24.5	614.7
		16.28	17.13	664.5	701.1		
		17.92	17.96	576.2	611.2		
	2	17.29	17.81	602.1	637.7		
		17.52	17.52	604.1	639.9		
		17.34	17.91	597	632.1		
	3	16.90	17.61	622.8	660.1		
		16.88	17.55	625.7	663		
		17.23	17.47	616	653.1		
NiP + 0.0125 g/L	1	18.23	18.17	559.8	593.8	15.5	556.9
		18.26	18.33	554	587.2		
		17.57	18.59	567.3	601.9		
	2	17.88	18.06	574.3	609.2		
		17.78	18.12	575.5	610.5		
		18.35	18.17	556.2	589.7		
	3	18.99	18.54	526.6	556.5		
		18.45	18.54	542.1	573.8		
		17.87	18.64	556.5	590.1		
NiP + 0.025 g/L	1	17.88	17.30	599.3	634.6	52.8	543.1
		18.48	18.69	536.9	567.9		
		19.19	19.07	506.7	535.4		
	2	20.69	20.69	433.2	450.9		
		17.35	18.24	585.6	620.7		
		19.10	18.50	524.7	554.5		
	3	17.34	17.82	600	635.4		
		18.17	18.21	560.5	594.5		
		18.79	18.23	541.2	572.8		
NiP + 0.05 g/L	1	17.68	18.48	567.3	601.9	20.7	555.8
		18.54	18.83	531.2	561.5		
		18.79	18.64	529.4	559.5		
	2	18.03	18.40	558.9	592.8		
		17.88	18.54	559.2	593.1		
		18.52	18.69	535.7	566.5		
	3	17.63	18.24	576.5	611.5		
		18.34	18.23	554.6	587.9		
		17.51	17.96	589.6	624.7		

## 9.12 Appendix L – Abrasion Resistance Results

Table 22: Abrasion resistance detailed results. This shows the difference in the wear rate for each inspection lighting environment.

Coating	Sample	Wear Mark	Kc (m <sup>3</sup> .N <sup>-1</sup> .m <sup>-1</sup> x 10 <sup>-13</sup> )			
			Optical Microscope		Scanning Electron Microscope	
			Light On	Light Off	Scanning Electrode	Back Scatter Electrode
Reference	R1	Left	8.88	9.54	8.99	6.48
		Middle	8.80	9.91	8.03	7.22
		Right	10.94	12.31	8.76	7.44
Plain NiP	M1	Left	6.68	10.71	7.64	5.69
		Middle	6.89	10.03	8.18	6.59
		Right	6.36	9.52	7.17	5.61
	M2	Left	6.95	9.87	8.74	6.70
		Left Middle	6.71	10.48	8.72	7.09
		Right	6.61	10.52	8.14	6.73
	M3	Left	6.61	8.97	8.09	6.63
		Left Middle	6.58	9.52	8.28	6.89
		Right	6.61	9.67	8.17	7.00
NiP + 0.0125 g/L	M4	Left	6.77	9.97	8.86	6.98
		Middle	7.15	10.27	8.93	7.35
		Right	6.81	9.75	8.24	7.03
	M5	Left	6.68	9.99	8.26	6.70
		Middle	6.93	10.21	8.62	6.81
		Right	7.01	10.03	8.61	7.21
	M6	Left	6.75	9.23	8.68	7.10
		Middle	6.66	9.95	8.86	6.82
		Right	6.74	10.11	9.07	6.97
NiP + 0.025 g/L	M7	Left	7.36	11.29	9.23	6.77
		Middle	5.94	9.71	8.45	6.82
		Right	6.55	10.23	8.86	7.25
	M8	Left	7.18	10.31	8.54	7.13
		Middle	7.43	10.21	8.77	7.45
		Right	6.69	9.95	8.14	7.02
	M9	Left	6.27	9.85	8.89	6.79
		Middle	7.04	10.36	8.90	7.20
		Right	7.20	10.38	8.68	7.32
NiP + 0.05 g/L	M10	Left	7.42	9.54	8.05	6.96
		Middle	6.61	9.67	7.90	6.73
		Right	6.53	9.29	7.50	6.39
	M11	Left	6.58	10.01	7.87	6.28
		Middle	7.29	10.46	8.61	6.77
		Right	7.96	10.92	9.26	7.78
	M12	Left	7.06	9.87	8.42	6.92
		Middle	7.09	10.09	8.24	7.65
		Right	7.34	10.71	8.94	8.19